Enhancement of palladium activity in wet-lean methane combustion

by

Hanieh Nassiri

A thesis submitted in partial fulfillment of the requirements for the degree of

Doctor of Philosophy

in

Chemical Engineering

Department of Chemical and Materials Engineering
University of Alberta

Abstract

The beneficial feature of the application of natural gas in the automotive industry is the lowest carbon content of any fossil fuel, which results in the lowest CO_2 emissions. On the other hand, the concern of atmospheric pollution due to methane emissions from natural-gas vehicles (NGV) engines evokes the stringent regulations of vehicular pollution from NGVs, and specific considerations in designing the catalytic converters with expensive and scarce noble metal catalysts. Pd is conventionally used for the catalytic combustion of methane but its activity is inhibited by water, and a considerable work needs to be done to increase its stability. Adding a co-metal like Pt in order to produce a bimetallic alloy catalyst or adding a metal-oxide promoter is desirable to stabilize the catalytic conversion. However, the chemical states of Pd in bimetallic catalysts is expected to be completely different from that of the mono Pd under the reaction conditions. Therefore, an in situ X-ray absorption spectroscopy (XAS) study can also be a viable investigation to shed light on the effect of Pt on Pd/PdO_x distribution in bimetallic Pd-Pt catalysts under reaction conditions at low temperatures (200-550ºC) with or without the presence of water as a catalytic poison. Furthermore, loss of activity can be avoided by choosing a SnO_2 promoter as a non-noble metal oxide support material with a low metal-oxygen bond.

This thesis develops an understanding of the effect of the addition of Pt in bimetallic $Pd-Pt/Al_2O_3$ catalysts and also the benefits of using SnO_2 as a support for Pd-based catalysts encountering the effect of water in a low-temperature methane combustion reaction.

The synthesis method of controlled-size nanoparticles via a colloidal solution technique and evaluating the effect of different synthesis parameters helps to control interactions between catalytic phases in bimetallic catalysts, and also assures the existence of intrinsic bimetallicity to

get desired activity and stability in order to study the structure-property relationship and understand not only the role of Pt as a secondary catalytic phase, but also SnO_2 as a metal-oxide promoter in methane combustion reactions. Besides, in situ XAS studies demonstrate the effect of Pt on the state of the active Pd surface under low-temperature, dry and wet lean methane combustion conditions. Pt addition promotes Pd reduction even in a reactive oxidizing environment with a significantly lower activity in a dry condition as compared with the oxidized Pd. However, the presence of water leads to the increased fraction of metallic Pd due to the lack of surface oxygen, resulting in Pt atoms available for methane dissociation, which does not occur in the dry methane-lean feed in which oxygen poisons Pt.

Evaluation of the effect of the Pd:Pt ratio on the stability of the bimetallic Pd-Pt/Al_2O_3 catalysts during and after 40-hour in-situ hydrothermal ageing at 400-550ºC with 5% water in a low-temperature lean methane combustion revealed that the ratio of Pd/Pt had the governing effect, not the catalyst preparation method. The Pd:Pt 1:1 (atomic) ratio catalyst was found to provide the most optimal combination of activity and stability. Significant structural changes also occurred in-situ regardless of the preparation method.

Finally, as a potential replacement of Pt in catalytic converters for NGVs, the beneficial role of SnO_2 as a metal oxide support was also studied. SnO_2 enhanced the activity of PdO sites by providing oxygen, and overrode the Pt-promoting role in bimetallic Pd-Pt/Al_2O_3 catalysts.

Preface

The literature review related to the present research work is in Chapter 1.

Chapter 2 of the thesis has been submitted to the MethodsX journal as "Effect of the solvent and metal precursor on the structure of PVP-protected Pd and Pt nanoparticles" H. Nassiri, N. Semagina MethodsX (2017). Nanoparticles syntheses and TEM characterizations and analyses, manuscript preparation, and writing were all conducted by the author under the supervision and final approval of Dr. Natalia Semagina.

Chapter 3 of the thesis has been published as "Platinum Inhibits Low-Temperature Dry Lean Methane Combustion via Palladium Reduction in Pd-Pt/Al_2O_3: An In Situ X-ray Absorption Study." H. Nassiri, K.-E. Lee, Y. Hu, R.E. Hayes, R.W.J. Scott, N. Semagina, ChemPhysChem. 18 (2017) 238-244. The paper is reprinted with the permission of co-authors. The reaction setup for methane oxidation was originally designed and built by Dr. Long Wu and Dr. Robert E. Hayes. The lab view program to communicate with the reaction setup was written by Les Dean. The NAA analysis was performed by Dr. John Duke at the University of Alberta. The in situ EXAFS was performed by Dr. Kee-Eun Lee under the supervision of Dr. Yongfeng Hu at Canadian Light Source and Dr. Robert W.J. Scott at the University of Saskatchewan. Part of the ex situ EXAFS was performed by the author under the technical support of Dr. Ning Chen at Canadian Light Source and Dr. Robert W.J. Scott. EXAFS data modeling was done by Dr. Kee-Eun Lee and Dr. Robert W.J. Scott. The author performed all the syntheses, catalytic reactions, analyses and other characterizations. Manuscript preparation and writing were conducted by the author under the supervision and final approval of Dr. Natalia Semagina, Dr. Robert E. Hayes, and Dr. Robert W.J. Scott.

Chapter 4 of the thesis has been published as "Water shifts PdO-catalyzed lean methane combustion to Pt-catalyzed rich combustion in Pd-Pt catalysts: In situ X-ray absorption spectroscopy." H. Nassiri, K.-E. Lee, Y. Hu, R.E. Hayes, R.W.J. Scott, N. Semagina, J. Catal. 352 (2017) 649-656. The paper is reprinted with the permission of co-authors. The reaction setup for methane oxidation was originally designed and built by Dr. Long Wu and Dr. Robert E. Hayes. The lab view program to communicate with the reaction setup was written by Les Dean. The NAA analysis was performed by Dr. John Duke at the University of Alberta. The in situ EXAFS was

performed by Dr. Kee-Eun Lee under the supervision of Dr. Yongfeng Hu at Canadian Light Source and Dr. Robert W.J. Scott at the University of Saskatchewan. Part of the ex situ EXAFS was performed by the author under the technical support of Dr. Ning Chen at the Canadian Light Source and Dr. Robert W.J. Scott. EXAFS data modeling was done by Dr. Kee-Eun Lee and Dr. Robert W.J. Scott. The author performed all the syntheses, catalytic reactions, analyses and other characterizations. The literature review and preparation of the first draft of the manuscript were conducted by the author. Dr. Natalia Semagina performed the final manuscript writing. The work is conducted under the supervision and final approval of Dr. Natalia Semagina, Dr. Robert E. Hayes, and Dr. Robert W.J. Scott.

Chapter 5 of the thesis has been submitted to the Chemical Engineering Science journal as "Stability of Pd-Pt catalysts in low-temperature wet methane combustion: metal ratio and particle reconstruction" H. Nassiri, R.E. Hayes, N. Semagina, Chem. Eng. Sci. (2017). The reaction setup for methane oxidation was originally designed and built by Dr. Long Wu and Dr. Robert E. Hayes. The lab view program to communicate with the reaction setup was written by Les Dean. The NAA analysis was performed by Dr. John Duke at the University of Alberta. HRTEM and TEM-EDX mapping were performed by Dr. Peng Li and Dr. Jing Shen at the University of Alberta Nanofabrication and Characterization Facility (nanoFAB). The author performed all the syntheses, catalytic reactions, analyses and other characterizations. Manuscript preparation and writing were conducted by the author under the supervision and final approval of Dr. Natalia Semagina and Dr. Robert E. Hayes.

Chapter 6 of the thesis is under submission as "Tin dioxide as a potential replacement of Pt in wet lean methane combustion catalysts" H. Nassiri, R.E. Hayes, N. Semagina (2018). The reaction setup for methane oxidation was originally designed and built by Dr. Long Wu and Dr. Robert E. Hayes. The lab view program to communicate with the reaction setup was written by Les Dean. The NAA analysis was performed by Dr. John Duke at the University of Alberta and Becquerel Laboratories Inc.; Maxxam Analytics, Ontario. HRTEM and TEM-EDX mapping were performed by Dr. Jing Shen at the University of Alberta Nanofabrication and Characterization Facility (nanoFAB). SEM analysis was performed by Dr. Shihong Xu at the University of Alberta Nanofabrication and Characterization Facility (nanoFAB). Dr. Shihong Xu and Dr. Anqiang He performed XPS analyses at the University of Alberta Nanofabrication and Characterization

Facility (nanoFAB). The author performed all the syntheses, catalytic reactions, analyses and other characterizations. Manuscript preparation and writing were conducted by the author under the supervision and final approval of Dr. Natalia Semagina and Dr. Robert E. Hayes.

Dr. Natalia Semagina, my supervisor, provided discussions and feedback on experimental results, and comments and revisions for all writing work including the present thesis. Dr. Robert E. Hayes, my co-supervisor, and Dr. Robert W. J. Scott provided discussions and feedback on methane oxidation and EXAFS analysis, respectively. The rest of the research work such as the literature review, catalyst synthesis, some of the catalyst characterizations, the catalytic reaction experiments, data collection and analysis, and interpretation of the experimental results were all conducted by Hanieh Nassiri in the Department of Chemical and Materials Engineering at the University of Alberta.

The research project of the present thesis is funded by the Natural Sciences and Engineering Research Council of Canada (NSERC).

To my loving ones…

My husband, Ali and my son, Elvin

Acknowledgments

First, I would like to sincerely thank my supervisor, Dr. Natalia Semagina. It has been a great honor to be her PhD student. I appreciate all her time, effort, advice, ideas, patience, knowledge, experience, and contributions throughout my PhD program. She made this journey very productive, enthusiastic, and stimulating even during the tough times of my life. She will always be in my mind as a resourceful, understanding, and considerate professor in chemical engineering.

I would also like to genuinely thank my co-supervisor, Dr. Robert Hayes, for his invaluable knowledge, constant support, and guidance on methane combustion reactions. His valuable feedback and helpful comments throughout these years have helped completion of this project.

The XAS analysis part of this project would not have been possible without the collaboration of Dr. Robert Scott from the University of Saskatchewan and Dr. Kee-Eun Lee from Canadian Light Source. I truly appreciate the time, knowledge, and skills they put through this experiment.

I am particularly indebted to Dr. John Duke, who did the majority of this thesis' NAA analyses with his meticulous attention for the accuracy of data.

For this thesis, I would like to thank my defense committee members: Dr. Natalia Semagina (Supervisor), Dr. Robert Hayes (Co-supervisor), Dr. Hao Zhang (Supervisory committee), Dr. Arno de Klerk (Internal Examiner), and Dr. Jafar Soltan (External Examiner) for their time, interest, valuable questions, and helpful comments. I would also like to thank the other two members of my candidacy defense committee: Dr. Dominic Sauvageau and Dr. Thomas Etsell, for their time and insightful questions on the early stage of the research.

I would like to express my gratitude to Dr. Dimitre Karpuzov, Dr. Shihong Xu, Dr. Anqiang He, and Peng Li at the University of Alberta for performing XPS, HRTEM-EDX, and SEM analyses, and their guidance on data analysis processes. Also, thanks go to Dr. Xuejun Sun and Priscilla Gao, Department of Oncology, Cross Cancer Institute, University of Alberta, for training and assisting on TEM analysis.

I thank Walter Boddez and Les Dean in the CME instrument shop for the fixing and maintenance of the reaction setup whenever I encountered a problem. I also thank the staff at the CME machine shop: Clark Bicknell, Herb Green, James McKinnon, Dave Parlin, and Robert Smith, who all did

projects for me at some point. I must also thank Kevin Heidebrecht, who helped with shipping and deliveries. I truly appreciate graduate administrative assistants Lily Laser and Mia Law for their kindness, help, and support from when I started utill the end.

I gratefully acknowledge the funding source of my project: The Natural Sciences and Engineering Research Council of Canada (NSERC).

My time at the University of Alberta was made enjoyable in large part due to my colleagues, who all became a part of my life: Dr. Jing Shen, who not only helped me a lot with tremendous teaching and training while she was doing her PhD in the group but who also did lots of fantastic TEM characterizations during her post-doctoral fellowship. Dr. Allen Reule, who I am very grateful for his kindness, consideration, and willingness to help me in the lab especially with the Autochem instrument. Dr. Hessam Ziaei-azad, who was the first PhD student of the group and kindly helped me in the first couple of months when I had just started. I was always so grateful to have someone like them in the lab as both colleagues and friends.

Lastly, I would like to deeply thank my family for all their love and encouragement, especially my mother Effat, for all her blessing and moral support in all my pursuits. Also my brother Nima, for encouraging me to go forward and cheering me up. And most of all, I wish to give my heartfelt thanks to my loving, supportive, encouraging, and patient husband Ali, whose all faithful and continual support of my academic endeavors over the past several years enabled me to complete this thesis. Thank you, Honey, for also being understanding and cooperative to extend your support in taking care of our little son during my hectic work schedule. Finally, there is my little one, Elvin, who was so well-behaved and never once fussed about me not being able to spend time with him. Thank you for being such a darling. I hope I have been a good mother and that I have not lost too much.

Thank you all for everything you have done to assist me in the most ambitious endeavor of my career thus far.

Hanieh Nassiri
University of Alberta
March 2018

Table of Contents

List of Tables

List of Figures

Nomenclature

C_M	Methane concentration
C_{WP}	Weisz-Prater criterion
D_{AB}	Bulk diffusivity
D_{eff}	Effective diffusivity
D_K	Knudsen diffusivity
D_p	Particle diameter
d_{pore}	Catalyst pore diameter
D_{pore}	Diffusivity in a pore
E	Activation energy
E_0	Energy shift parameter
F_{Mo}	Initial methane molar flow rate
h	Heat transfer coefficient
k	Reaction rate constant
k_c	Mass transfer coefficient
k_{eff}	Effective thermal conductivity
k_t	Thermal conductivity
M	Molecular mass
n	Reaction order
Nu	Nusselt number
P	Pressure
Pr	Prandtl number
R	Particle radius
Re	Reynolds number
R_{gas}	Universal gas constant
$-r_M$	Reaction rate
S	Catalyst surface area
Sc	Schmidt number
Sh	Sherwood number
T	Temperature

U	Free-stream velocity
W	Catalyst weight
X	Conversion
ΔH^0_{298}	Standard enthalpy of formation at 298 K
$-\Delta H_{ads}$	Enthalpy of adsorption
$-\Delta H_{rx}$	Heat of reaction
ΔT_{max}	Maximum internal temperature rise
μ	Dynamic viscosity
σ^2	Disorder parameter
τ	Tortuosity
υ_i	Diffusion volume
ϕ_p	Particle porosity
β	Prater number
ρ	Density

Abbreviations

A/F	Air to Fuel ratio
BET	Brunauer-Emmett-Teller
C	Core
CFEG	Cold Field Emission Gun
CN	Coordination Number
C-S	Core-Shell
DFT	Density Functional Theory
DRIFTS	Diffuse Reflectance Infrared Fourier Transform Spectroscopy
EDX	Energy-dispersive X-ray spectroscopy
EG	Ethylene Glycol
EPR	Electron Paramagnetic Resonance
ER	Eley-Rideal

EtOH	Ethanol
ET-SE	Evehart-Thornley Secondary Electron
EXAFS	Extended X-ray Absorption Spectroscopy
FID	Flame Ionization Detector
FTIR	Fourier-Transform Infrared Spectroscopy
HRTEM	High-Resolution Transmission Electron Microscopy
HTA	Hydrothermal Aging
HTL	Heat Transfer Limitation
HXMA	Hard X-ray MicroAnalysis
I-E	Ignition-Extinction
IR	Infrared
LH	Langmuir-Hinshelwood
LHHW	Langmuir-Hinshelwood Hougen-Watson
MC	Mixed Colloids
MS	Mixed Supports
MTL	Mass Transfer Limitation
MVK	Mars-van Krevelen
NAA	Neutron Activation Analysis
NGV	Natural Gas Vehicle
PGMs	Platinum Group Metals
PVP	Poly (N-vinyl-2-pyrrolidone)
RDS	Rate-Determining Step
S	Shell
SEM	Secondary Electron Microscopy
SMSI	Strong Metal Support Interaction
TCD	Thermal Conductivity Detector
TDS	Thermal Desorption Spectroscopy
TEM	Transmission Electron Microscopy
TOF	Turnover Frequency
TPD	Temperature-Programmed Desorption
TPO	Temperature-Programmed Oxidation

TPR	Temperature-Programmed Reduction
TWC	Three-Way Catalytic Converter
UHC	Unburned Hydrocarbon
UPS	Ultraviolet Photoelectron Spectroscopy
XANES	X-ray Absorption Near Edge Structure
XAS	X-ray Absorption Spectroscopy
XPS	X-ray Photoelectron Spectroscopy

Chapter 1. Introduction

1.1 NGV's emission control

Dealing with a worldwide increase in energy demand has been a controversial issue over the past 20 years. Natural gas, a mixture of methane (80-90%) and C_2-C_4 alkanes (5-15%), provides an attractive source of energy since it is in abundant supply on Earth but remains less exploited than petroleum [1]. In particular, the rapid production of shale gas in recent years has brought attention to the economy of natural gas. Natural gas is applicable in power plant combustors and the automotive industry. On the other hand, there is the concern of atmospheric pollution due to pollutants emission from combustion reaction. However, natural gas has the lowest carbon content of any fossil fuel, resulting in the lowest CO_2 emissions when burned.

Methane, the main component of natural gas, is the smallest hydrocarbon. It has high stability due to its tetrahedron shape, an almost spherical electron cloud, and weak polarization in the C-H bonds. The dissociation energy of the first CH_3-H bond is comparably high [2], so high reaction temperatures are required to activate the molecule. Therefore, the abatement of unburned methane, which has 23 times more global-warming potential than CO_2 from the combustion reaction, evokes the development of catalytic technologies for environmentally friendly processes [3].

The advantages of catalytic combustion in heat and power production make it a suitable alternative to conventional flame combustion: lower operating temperature, a complete oxidation reaction, stable combustion of lean fuel/air mixtures, no formation of thermal NO_x, low levels of CO, and unburned hydrocarbons (UHC). Low-temperature catalytic combustion is used in the temperature range 300-500ºC. A typical scheme is as follows: Exhaust gases from the chemical processes are preheated in heat exchangers and then passed over a combustion catalyst. The heat generated is recovered fully and the clean exhaust gas is vented out. Another increasing application for low-temperature catalytic combustion is abatement of gaseous emissions from natural gas vehicles (NGV), in which a compression ignition engine fuelled with natural gas is operated at lean conditions, improving the fuel efficiency meanwhile reducing the emissions of pollutants by passing the exiting gases through a catalytic converter in the exhaust [4]. Heat from combustion generated in the engine is transferred to the exhaust piping. Finally, a temperature is reached within

the catalyst that initiates the catalytic reactions. The light-off temperature and the reaction rate kinetically depend on the nature of the catalytic system. Catalytic deactivation with time due to the various factors causes the increase in the gaseous emissions and time to replace the catalytic converter. Use of catalytic converters to abate NO_x emissions and oxidize UHC and CO in the engine exhausts is a regulatory framework to lower the environmental impact of greenhouse gases emissions.

A catalytic converter has gone through many processes and a remarkable evolution for the past 30 years. A granular ceramic bed had been used in early converters, with the gas passing between the packed spheres. Due to the difficulty of keeping the spheres in place, a ceramic or metallic monolith was used, which offers various advantages such as high conversion efficiencies at high gaseous throughput, smaller volumes, high volumetric flow rates, low back pressure and pressure drop, lower mass and greater ease of packaging, and good thermal shock resistance [5]. The monolith is a porous ceramic or metallic honeycomb structure consisting of a large number of parallel channels made of an inert substrate coating with a washcoat and active catalysts. The contact area between the catalytic layer and the reactant fluid inside the channels is very large, and the straight and parallel channels prevent obstruction of passing flow. The washcoat is a mixture of mainly alumina and gives a further irregular and larger surface area. The washcoat may also contain oxygen storage promoters and stabilizers.

To prepare an active monolith, layer-by-layer deposition or dipping methods are used so that a layer of washcoat is first deposited on the ceramic or metal honeycomb substrate, and then catalysts are deposited on the washcoat. Or, the monolith is dipped into a washcoat and the metal catalyst components' slurry and the excess of the deposited material is removed using high-pressure air or by applying a vacuum, and then the monolith is calcined to obtain the finished catalyst. The monolith's structure is comprised of many shapes, including square, triangular, hexagonal, and sinusoidal. The geometrical characteristics play a key role in distribution of temperature and reactant species throughout the device to determine the efficiency of the converter [5, 6]. The conversion efficiencies of a catalytic converter is strictly related to the Air to Fuel ratio (A/F), therefore, there should be an efficient control of the A/F by measuring the amount of air and fuel injection to get the optimum performance from the catalytic converter. In a gasoline or diesel engine, a higher A/F ratio than stoichiometry (fuel-lean condition) provides an excess amount of

oxygen and a lower level of CO and NO_x, leaving the exhaust. On the other hand, a lower A/F ratio than stoichiometry (fuel-rich condition) provides a higher concentration of CO and UHC in the exhaust [7]. The methane emission difference should be considered in catalytic converters of NGVs as methane is emitted 40% more from NGV engines than from gasoline and diesel engines [8]. Therefore, a conventional catalytic converter is not efficient for meeting the stringent regulations of vehicular pollutions from NGVs. The high stability of methane to get oxidized and the high concentration of oxidation products like H_2O that makes faster deactivation of the catalyst caused specific considerations when designing catalytic converters with expensive and rare noble metal catalysts. Two principal approaches for decreasing CH_4 emissions from internal combustion engines are:

1. Optimization of the combustion process by fuel or motor engine modification.
2. Abatement of exhaust gas emissions by catalytic oxidation in a catalytic converter.

This thesis is primarily concerned with the second approach: The design of catalysts for the oxidation of methane used in the exhaust of NGVs.

1.2 Catalytic methane combustion

Metal oxides and noble metals are used extensively as combustion catalysts. These catalysts can be either supported or unsupported. Supported catalysts are usually preferred because of much better utilization of the metal, which is present as small particles on the support surface. A large fraction of catalytic metal is at the surface, and the supported catalysts have much higher thermal stability. This support may also play a role in the oxidation reactions, providing oxygen storage capability. Conventional γ-Al_2O_3 has been widely used as a support. Other than alumina, so many metal oxides, mixed-oxides support, and their combinations have been used, including ZrO_2, TiO_2, MgO, CeO_2, Fe_2O_3, SiO_2, SnO_2, CuO, NiO, Mn_3O4, etc. [9]. In general, an ideal catalyst for the catalytic combustion should have high and stable activity, high thermal stability, nontoxicity and high resistance to the poisons, and low cost. Unfortunately, no catalyst fulfills all of these characteristics. However, this list can be used to judge the performance of the catalysts and choose the appropriate catalyst for a specific application. Among the noble metals, Pd and its combination with Pt are used for the catalytic combustion of methane. The activity of these noble metals is

generally higher than that of metal oxide catalysts. The applications of other noble metals are limited for the purpose of the catalytic combustion because they have lower activity and oxidize more easily in comparison with Pd and Pt.

1.3 Catalytic active phases

Pd and Pt show different reactivity towards oxygen depending on the temperature and partial pressure of oxygen [9-14], metal support [12, 15], and nanoparticle size [10, 16]. Therefore, under the reaction conditions, in addition to metallic Pd and Pt, oxide species such as PdO, PdO_2, PtO, PtO_2, and Pt_3O_4 may be present [17-20]. At oxygen partial pressure of 21 kPa, Pd easily transforms to PdO at temperatures lower than 800ºC, however PtO_2 (which is very unstable) can hardly be generated below 600ºC. Because of the greater stability of PdO in comparison with PtO_2, PdO is generally known as the active phase in the case of Pd-based catalysts. In the case of Pt-based catalysts the active phase is metallic Pt. The activity of PdO is greater than that of Pt, which will result in higher conversions for the PdO catalyst in lean conditions.

However, topics such as whether Pd or PdO are more active are still a matter of debate [21-26]. Loss of activity with formation of metallic Pd under reducing reaction conditions was reported by Farrauto et al. [21]. Grunwaldt et al. [27] observed higher activity with the pre-reduced Pd/ZrO_2 catalyst compared to the oxidized catalyst and also detected the presence of metallic Pd at 500-550ºC by using in situ EXAFS. Below 500ºC, only the formation of Pd oxide was detected on a Pd/Al_2O_3 catalyst using an operando Raman study [28], which is consistent with thermodynamic expectations and the kinetic investigation of Pd/ZrO_2 catalysts by Fujimoto et al. [25], who reported requirement of the coexistence of $Pd\text{-}PdO_x$ by a Mars-van Krevelen (MVK) mechanism for the reaction. Thus, knowledge of the required chemical state of Pd under reaction conditions which can be obtained through an in situ analysis like an in situ EXAFS is necessary to design an efficient and stable NGV combustion catalyst.

1.4 Inhibitory effect of water

It should be noted that various parameters such as metal loading, precursors' materials, preparation methods, promoters, support, and pretreatments can greatly affect the activity and performance of the noble-metal-combustion catalysts. Generally, the performance of Pt-based catalysts is more stable, and it is a relatively simple catalyst mainly because of the fact that its phase behavior is much simpler than a Pd-based catalyst, which undergoes complex phase transformations during the reaction, i.e. with changes in temperature [29-31]. Therefore, considerable work has been done on Pd to increase and stabilize its activity by changing the aforementioned parameters because deactivation of the catalyst with time on stream is an inevitable issue in catalytic reactions.

In addition to mechanical factors like fouling, thermal and chemical factors are also responsible for deactivation of a catalyst. Volatilization of components, surface segregation and restructuring, alloying or de-alloying, sintering, coke formation, and adsorption of a catalytic poison species driven from thermal and chemical catalytic deactivation causes loss or blockage of catalyst active centers and/or change in the metal surface and catalyst structure [32, 33]. The catalytic poison species, which can be an impurity in the feed stream or a reactant, by-product, or product of the reaction, are adsorbed on the active sites and by blockage of the surface area of the catalyst inhibiting the reaction.

Water as a product of the reaction is one of the most important catalytic poisons of the methane combustion reaction. The inhibitory effect of water, either in the feed stream or generated by the combustion reaction on Pd-based catalysts, has attracted many studies on methane combustion reactions [12, 34-43]. Water affects both activity and stability of the catalyst and the cause of inhibition has been suggested to be the formation of inactive hydroxyl groups on the catalytic surface, which block active PdO sites for methane dissociation. Fujimoto et al. [25] believe that adsorption-desorption of water would be as follows:

$$2OH^{*} \Leftrightarrow H_2O\,(g) + O^{*} + \square^{*} \qquad (1)$$

Where $\square^{*}$ is the active site.

Therefore, the higher H_2O concentration, the more hydroxyl groups block active sites and inhibit the reaction by deactivation of the catalyst. Although formation of inactive $Pd(OH)_2$ has been accepted as a cause of deactivation by water, Ciuparu et al. [44] and Schwartz et al. [45] proposed

another deactivation mechanism by using in situ FTIR and isotopic labeling experiments to monitor formation of hydroxyl groups on the surface of the catalyst. They proposed that below 450ºC, presence of water retards the catalytic activity by lowering the oxygen mobility on the support and therefore, causes dihydroxylation at the surface. Hence, higher oxygen mobility on the support results in less inhibition by water. Gholami et al. [43] summarized that the inhibition effect of water not only depends on H_2O concentration, but also catalyst formulation, catalyst time-on-stream history, and reaction temperature. It has indicated that the effect of water could be partially or completely reversible by removal of water from the feed stream or by an increase in temperature [31, 40, 41, 46]. However, the retarding effect is very negligible above 450ºC [13, 35, 42-44]. Compared to the monometallic Pd catalyst, the activation loss of the Pd-Pt bimetallic catalyst is less severe in the presence of extra water in the feed because of the interaction between Pt and Pd and their synergistic effects [40, 46, 47]. Complete activity recovery upon removal of water is also another positive effect from the addition of a small amount of Pt to the Pd catalyst [40]. Therefore, adding a co-metal to produce a bimetallic alloy catalyst or as a promoter is desirable to stabilize the catalytic conversion [48].

1.5 Bimetallic Pd-Pt catalyst

The beneficial addition of small amounts of Pt to a Pd system to increase low-temperature activity and also to improve the thermal durability [47, 49-51] is shown in the combustion of methane and also lower hydrocarbons like propane and propene [52]. The effect of Pt on the performance of Pd catalysts is still strongly debated and can be explained in terms of electronic and geometric effects, synergistic effect, and/or presence of mixed sites [48, 53]. Enhancement of catalytic activity and sintering stability by addition of Pt to a Pd catalyst has been shown in many studies [47, 48, 52, 54-57]. However, some studies contradict each other in terms of activity enhancement or suppression [58-60], which is a common problem in catalysis over bimetallic catalysts, where different catalyst supports and preparation conditions result in different structure modes, chemical states of Pd and Pt and their distribution in the catalytic system, and therefore different catalytic behavior in methane combustion reactions [52]. Studies of different co-metals on bimetallic Pd catalysts with 5 wt.% metal loadings and constant molar amount of precious metals as a 1:1 ratio by Persson et al. [48] showed that Pt is the most promising metal for getting stable high activity,

as Pd and Pt are in close interaction and Pt forms an alloy with Pd. The formation of a spinel structure with the alumina support or formation of separate particles from Pd particles rather than formation of an alloy make other co-metals ineffective for the reaction [48] (Table 1.1). Therefore, alloy formation along with higher PdO content and lower formation of inactive hydroxyl groups from water production in the reaction are the reasons for having a more active and stable catalyst with Pt rather than other co-metals. Persson et al. [17] studied different ratios of 5 wt.% Pd-Pt bimetallic catalysts and showed that considering both good activity and stability, Pd-Pt 2:1 and 1:1 ratios are the best compositions because of the close proximity of Pd and PdO particles in the alloys. Investigation of the water effect by in situ DRIFTS [40] on the aforementioned Pd-Pt 2:1 and 1:1 revealed a lower concentration of hydroxyl groups on these two catalysts as the reason behind good stability in the reaction.

A study of the ratios' effect by Lapisardi et al. [47] on 2 wt.% Pd-Pt catalysts concluded good interaction between the two metals achieved by molar ratios of Pd/Pt higher than 2 which resulted in higher activity. Yamamoto et al. [54] found that the optimum ratio is Pd-Pt 3:1, which leads to a lower degree of sintering of Pd and PdO crystallites, and also causes the highest activity and stability. Recently, Goodman et al. [60] investigated the effect of different molar ratios of Pd-Pt synthesized through a controlled particle size route, showing a Pd-rich 4:1 catalyst with no deactivation after hydrothermal ageing (HTA) with 4.2% water in the feed. The reason was related to the close proximity of the Pd-Pt alloy with PdO segregation induced by HTA, which causes formation of active and stable methane combustion sites.

The chemical states of Pd in bimetallic catalysts are expected to be completely different from those of the mono Pd under the reaction conditions. In bimetallic catalysts, the formation of the mixed-oxide phases of $Pd_xPt_{1-x}O_y$ was shown via DFT calculations by Dianat et al. [20]: The addition of Pt to Pd was suggested in order to stabilize the higher oxidation state of Pd. They also found that because of the charge transfer from Pd to Pt atoms, the oxygen-binding energy in the Pd-Pt catalysts is higher on Pd-rich surfaces [61]. An in situ EXAFS study could also be a viable investigation to shed light on the effect of Pt on Pd/PdO_x distribution in bimetallic Pd-Pt catalysts under the reaction condition at low temperatures (200-550ºC) with or without the presence of water as a catalytic poison.

Table 1.1 Interaction of co-metals with Pd catalyst on alumina support. Reprinted from [48] with permission from Elsevier.

Catalyst type	Catalyst (Pd-M)	Description of interaction
$PdO//MAl_2O_4/Al_2O_3$	PdCo	20-40 nm PdO particles on cobalt spinel-alumina
(Spinel formation with support)	PdNi	20-40 nm PdO particles on nickle spinel-alumina
	PdRh	1-5 nm PdO particles and <2 nm Rh_2O_3 particles on alumina
$PdO/MO//Al_2O_3$	PdIr	80-600 nm PdO and 80-200 nm IrO_2 crystals on alumina
(Formation of separate particles)	PdCu	34-50 nm PdO particles and 1-5 nm CuO particles on alumina
	PdAg	34-50 nm PdO particles and 1-5 nm Ag_2O particles on alumina
$Pd-M//Al_2O_3$	PdPt	Pd-Pt alloy with particle size of 35 nm on alumina
(Alloy formation)	PdAu	Pd-Au alloy with particle size of 190 nm on alumina

1.6 Support material

The performance of Pd-based catalysts is also strictly related to the nature of the support through Pd crystallite size and morphology [62-64], Pd dispersion on the support [65, 66], and Pd-support interaction effects [66-68]. Since the rate of catalytic deactivation, water inhibition effect through hydroxyl coverage on the surface [45], and kinetics of surface dihydroxylation [38] are strongly dependent on the nature of the support, loss of activity due to formation of inactive $Pd(OH)_2$ and sintering of Pd particles may be avoided by choosing other types of support materials rather than adding an expensive and rare second noble metal like Pt. It is also reported that the oxygen adsorption property of Pd and stability of Pd oxide are influenced by the support materials [69]. Depending on the metal and oxide support, the so-called strong metal-support interaction (SMSI) is the specific reason occurring at the interface of active metal(s) and the support causing perturbation of the electronic and chemical interactions between metal(s) and support. The SMSI results in strong stabilization/destabilization of metal particles on the support or surface transport of adsorbates through the boundary by spillover or reverse spillover effects [70-73].

The effect of different supports on the activity of precious metal catalysts should be investigated, as the particle size of a catalyst and the crystal phase of the support affects the core level-binding energy of Pd (Pd $3d_{5/2}$) and therefore, the catalytic activity and metal-support interactions [74].

Alumina has been widely used as support for Pd catalysts in the methane combustion reaction. The catalytic performance of the Pd catalyst supported on various metal oxides (MO_x; M = Al, Ga, In, Nb, Si, Sn, Ti, Y, Zr, Ni) was studied for the methane combustion reaction by a few research groups and the highest activity was achieved by Pd/Al_2O_3-36NiO and Pd/SnO_2 [66, 75-81]. SnO_2 is an n-type oxide and is widely used in semiconductor and gas sensor technology [82-84]. It is also employed as a support of Pd and Pt catalysts in the CO oxidation reaction, as SnO_2 is known to enhance catalytic performance in the combustion of CO because of the beneficial effect of CO spillover [65, 83, 85-88]. For the methane combustion reaction, Roth et al. [79] did not observe any beneficial effect to using SnO_2 support for mono Pd, which could be the reason for using a chlorine-containing precursor for making a mono Pd catalyst, which is known to have a strong inhibitory effect. Widjaja et al. [66] tried making a mixed-oxides support of SnO_2-MO_x (M= Al, Ce, Fe, Mn, Ni, Zr) with a 1:1 ratio for 1 wt.% Pd catalyst, but it led to lower activity. They claimed the high exposure of Pd-active centers as a result of making egg-shell structures around SnO_2 fragments, the interaction of Pd and SnO_2, the adsorption state of oxygen on Pd/SnO_2, and the slow reduction rate of Pd on SnO_2 as a result of SMSI were all reasons for the higher activity of Pd/SnO_2 which did not occur in the mixed-oxides structure. Eguchi et al. [76] and Kikuchi et al. [78] studied the water inhibition effect on Pd/SnO_2 in which the activity dropped with increasing the water concentration from 0 to 20%, but Pd/SnO_2 still kept a good $T_{30\%}$ of 365ºC compared to Pd/Al_2O_3 with a $T_{30\%}$ of 510ºC at 20% water. On the other hand, Gholami [80] observed better performance with Pd/Al_2O_3 rather than Pd/SnO_2 at higher temperatures than 550ºC because of the higher sintering of Pd particles on SnO_2.

1.7 Size-controlled nanoparticles and structure sensitivity

Previous studies of heterogeneous catalysts were done using single-crystal metal catalysts in a high vacuum or with supported catalysts in real conditions. Because of the pressure and materials gaps the single-crystal studies are rarely transferable to reality [89]. On the other hand, the supported catalysts were prepared by a support impregnation with metal precursors followed by calcination and reduction steps in which the preparation conditions allowed altering the metal nanoparticle size, but precise control of a real structure and size was not achievable. Since bimetallic particles may form a random alloy, cluster-in-cluster, core/shell, and inverted core/shell structures (Figure

1.1) [90], electronic and geometric properties of the surface atoms will also be strongly affected by the structure mode. Such properties underlie the chemisorption strength and catalytic reaction mode of the participants. Thus, by changing precisely the atom position and its surroundings, one can control catalytic properties on an atomic level. Recent success in colloidal chemistry techniques allows for easy preparation of a desirable bimetallic particle [91, 92], and bridging the pressure and materials gap by providing well-defined real nanoparticles that can operate in real conditions. Intrinsic bimetallicity in making Pd-Pt bimetallic catalysts may not be obtained by the industrial way of making catalysts.

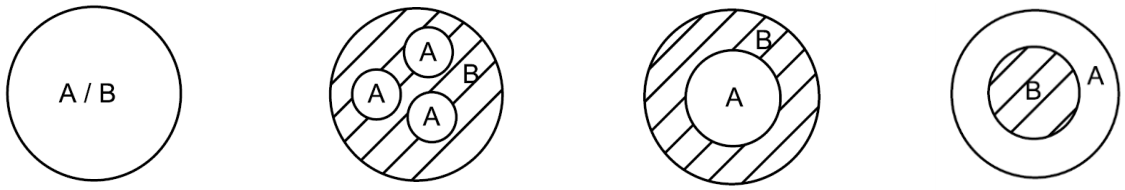

random alloy **cluster-in-cluster** **core/shell** **inverted core/shell**

Figure 1.1 Various Structures of bimetallic nanoparticles. Reprinted from [90] with permission from Taylor & Francis Group.

Another issue in size-controlled metal nanoparticles in catalysis is the traditional concept, which believed that the decrease in nanoparticle size led to a higher surface-to-volume ratio and a higher reaction rate. But, there are numerous reactions which occur on quite large nanoparticles (> 3 nm) and these reactions have much higher rates and selectivities than on smaller particles [93]. The surface configuration is the reason for this phenomenon, i.e. the decrease of edge and vertice atoms compared to terrace atoms with the particle size increase (Figure 1.2) [94]. Such atoms possess different electronic and geometric properties, affecting the chemisorption strength and mode of reaction substrates. For example, if a reactant adsorbs too strongly on the edge atoms of nanoparticles and does not react, chemisorption on the terrace atoms favors the reaction then the reaction rates on larger particles with higher proportions of terrace atoms are higher [93].

Therefore, with the size increase, the reactions demanding large ensembles of atoms as active sites are affected most. In methane combustion, increasing Pd nanoparticle size for particles <15 nm leads to a 65-fold increase in turnover frequency (TOF) with the Pd/ZrO_2 catalyst [46], which has been attributed to the change in oxygen-binding energy. The linear increase in TOF also happened

with the size increase of Pd from 1 to 20 nm in another study with Pd/Al_2O_3 [95] and is not only attributed to the decreased Pd-O bond strength for larger particles, but also to the decreased negative influence of support by stabilization of small PdO particles against the redox transformation. A similar trend has been reported for Pt in one study [9], however, in another study it showed that the increase in TOF just happened with the 1-3 nm size increase and remained constant above 3 nm (Figure 1.3) [95].

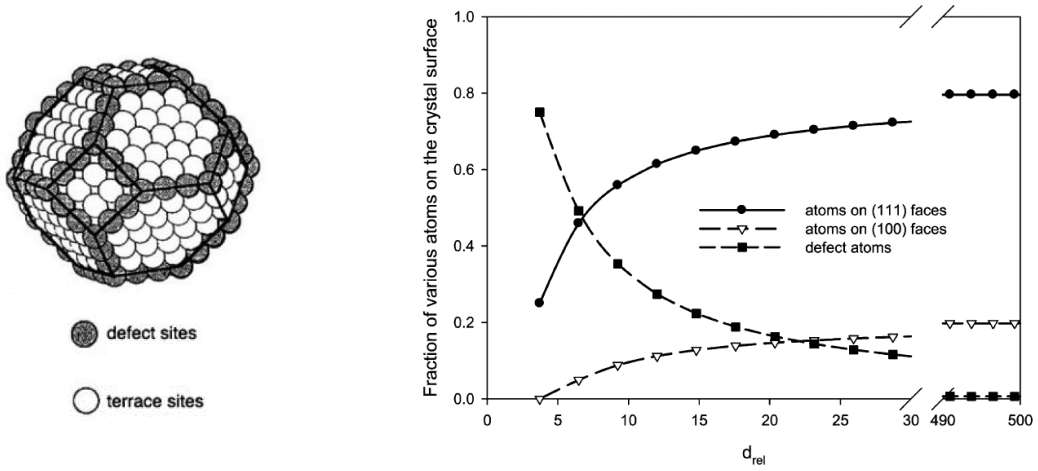

Figure 1.2 An f.c.c. cubooctahedral palladium and platinum atom and variation of various atoms fraction on the surface. Reprinted from [94] with permission from Taylor & Francis Group.

The difference in TOF change with particle size between Pd and Pt can also be attributed to the different reaction mechanisms over Pd and Pt catalysts. Many studies, however, have not demonstrated the reaction structure sensitivity that may be due to the chlorine-containing precursors [9], support effects, and, most importantly, the metal polydispersity which is the most significant problem in size-effect studies. Therefore, the fine-tuning of an active metal nanoparticle size (in other words, its surface structure) can lead to dramatic changes in its catalytic behavior. It should be noted that improved performance of bimetallic catalysts via support impregnation with two metal precursors has been mentioned in numerous studies, but in none of them was the size-controlled nanoparticle effect in the structure-property relationship investigated, except in the most recent studies of Cargnello's group in 2017 [60, 96].

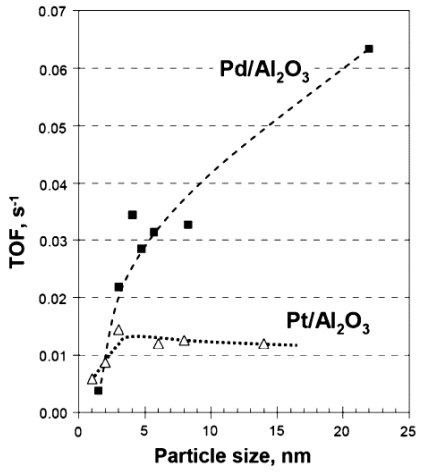

Figure 1.3 Dependence of TOF on metal particle size in methane oxidation over Pd/Al_2O_3 (at 320ºC) and Pt/Al_2O_3 (at 430ºC). Reprinted from [95] with permission from Springer Nature.

1.8 Mechanisms of the methane combustion reaction

The exothermic reaction of total oxidation of methane is shown in the following equation [97]:

$$CH_4 + 2O_2 \rightarrow CO_2 + 2H_2O \qquad \Delta H^0_{298} = -192\ kcal.mol^{-1} \tag{2}$$

Activation of the first C-H bonds in saturated hydrocarbons is the rate-limiting step of the oxidation reaction [98] and among hydrocarbons, methane possesses the highest value with the gas phase dissociation enthalpy of a CH_3-H bond equal to 104 kcal.mol^{-1} [97]. However, on certain surfaces of Pd this value turns down to -10.7 kcal.mol^{-1} [99]. Generally, it has been agreed that the rate of lean methane oxidation over oxidized Pd is near zero order with respect to oxygen, first order with respect to methane, and 0 to -1.0 order with respect to water (Figure 1.4) [25, 97]. The negative first-order dependence of the reaction rate on water implies the inhibition effect of water to block PdO-active sites by formation of $Pd(OH)_2$.

In spite of the large amount of experimental work done on the methane combustion reaction, theoretical interpretation of the microscopic characteristics of the reaction mechanism is still matter of debate and there is no unanimity in the literature. A rational design of a superior catalyst can be achieved by understanding the reaction mechanism and having knowledge of molecular control. Mechanisms such as the Langmuir-Hinshelwood (LH), Eley-Rideal (ER), and MVK have

been proposed for Pt and Pd catalysts. A simple LH mechanism with the power-law rate expression of first order with respect to methane and almost zero order with respect to oxygen has been suggested for the reaction on Pt/Al_2O_3 [100], as Pt catalysts have stable and simple structures and during the combustion reaction the bulk oxide of Pt does not exist [101]. But, on the PdO surface, the reaction has been observed to involve lattice oxygen in the activation of the C-H bond, suggesting a redox mechanism like MVK [25, 102, 103]. This mechanism has been decided as the best fitted, considering adsorption of water over PdO sites as of the low affinity of water for reduced Pd [104] and thermodynamically favored formation of $Pd(OH)_2$ from oxides [35].

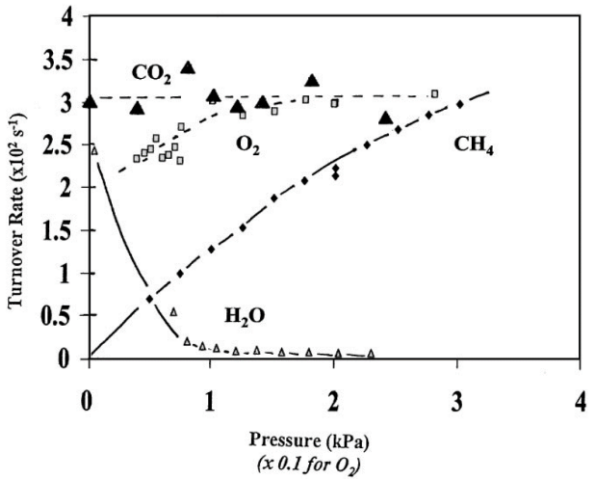

Figure 1.4 Effects of CH_4, O_2, H_2O, andCO_2 on methane oxidation rates at low temperatures (380ºC, 0.86 wt.% Pd/ZrO_2, dispersion 0.381). Reprinted from [25] with permission from Elsevier.

MVK mechanism suggested by Fujimoto et al. [25] in Figure 1.5 consists of elementary redox steps in which the asterisks stand for oxygen vacancies on PdO surfaces. The Rate-Determining Step (RDS) is a dissociative adsorption of methane (step 4) on a site pair consisting of adjacent Pd surface vacancies and surface Pd-O species. The positive effects of methane and oxygen concentration on the methane oxidation rate can be noted in step 4 as the RDS. The more CH_4^* and O^* species, the higher the rate of reaction. Moreover, the negative effect of hydroxyl formation decreasing the reaction rate occurs with an OH^* increase, which leads to formation of water and surface vacancies in step 5 and with accumulation of water vapor, the equilibrium goes back to the high concentration of OH^* and absence of surface vacancies, and eventually inhibits the methane oxidation reaction.

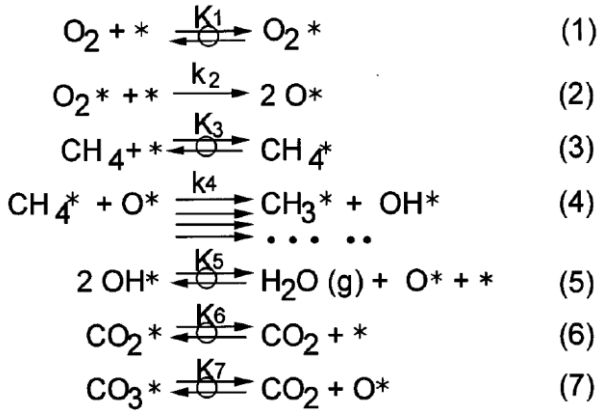

Figure 1.5 Proposed reaction pathways for the oxidation of methane on PdO_x crystallites. Reprinted from [25] with permission from Elsevier.

Fujimoto et al. [25] also suggested that small PdO clusters with stronger Pd-O bonds or incompletely oxidized PdO_x crystallites can lead to a lower surface density of vacancies and to a lower methane oxidation rate. That also explains why transformation of PdO to a Pd metal state or to oxygen-deficient Pd oxides results in lower methane conversion activity on the Pd catalyst.

Despite substantial studies on the kinetic mechanisms of monometallic Pd and Pt catalysts, the lack of study on the kinetic mechanisms of bimetallic Pd-Pt catalysts is still outstanding. The reaction rate of Pd-Pt catalysts has been modelled successfully using an empirical Langmuir-Hinshelwood Hougen-Watson (LHHW) type of equation that considers the inhibition effect of water [57]. Investigation on the mechanism of a 2 wt.% $PdPt/Al_2O_3$ catalyst with different ratios was done by Qi et al. [101]; they considered the MVK reaction mechanism on Pd-rich catalysts and the LH and ER models on Pt-rich catalysts. This corresponds with Figure 1.6, in which asterisks stand for oxygen vacancies.

In case of the Pd-rich catalyst, the mechanism is the same as Fujimoto et al. [25], which includes the dissociation of O_2 into two oxygen vacancies and the dissociation of CH_4 on matched pair sites as RDS. The pair sites consist of an unsaturated metal site and an adjacent O^*. Also, when OH^* species are the most abundant surface intermediate, the CH_4 dissociation steps are irreversible and the surface vacancies are regenerated by the quasi-equilibrated desorption of CO_2 and H_2O. Despite the irreversible dissociative adsorption of O_2 on Pd-rich catalysts (step 2a), the equilibrated adsorption-desorption of the gas-phase oxygen occurs on Pt-rich catalysts due to the existence of

metastable bulk Pt oxides. H_2O has a very subtle impact on Pt catalysts, therefore it can easily desorb from the surface vacancies even at high water concentrations.

Based on the DFT calculations, they concluded that an increase of the Pt content leads to the minimal existence of bulk PdO and/or two monolayers of PdO phases and thus an increase of activation energy for methane combustion. Qi et al. [101] also reported that for Pd-rich catalysts, H_2O strongly inhibits the reaction by occupying vacancies in an adsorption-desorption equilibrium step but CO_2 has no effect at concentrations below 3-5 kPa. And for Pt-rich catalysts neither H_2O nor CO_2 influence the reaction, even at high concentrations (< 8 kPa) [101].

Kinetic model (a and b)	Pd-like (MvK)	Rate and equilibrium constant	Pt-like (LH and E-R)	Rate and equilibrium constant
Step 1	$O_2+^*\rightleftharpoons O_2^*$	K_{1a}	$O_2+^*\rightleftharpoons O_2^*$	K_{1b}
Step 2	$O_2^*+^*\rightarrow 2O^*$	k_{2a}	$O_2^*+^*\rightleftharpoons 2O^*$	k_{2bf},k_{2br}
Step 3	$CH_4+^*\rightleftharpoons CH_4^*$	K_{3a}	$CH_4+2O^*\rightarrow CH_3O^*+OH^*$	k_{3b}
Step 4	$CH_4^*+O^*\rightarrow CH_3^*+OH^*$	$k_{4.1a}$		
	$CH_3^*+O^*\rightarrow CH_2^*+OH^*$		$CH_3O^*+O^*\rightarrow CH_2O^*+OH^*$	
	$CH_2^*+O^*\rightarrow CH^*+OH^*$		$CH_2O^*+O^*\rightarrow CHO^*+OH^*$	
	$CH^*+O^*\rightarrow C+OH^*$		$CHO^*+O^*\rightarrow CO^*+OH^*$	
	$C^*+O^*\rightleftharpoons CO^*+^*$	$K_{4.2a}$		
Step 5	$CO^*+O^*\rightleftharpoons CO_2^*+^*$	K_{5a}	$CO^*+O^*\rightleftharpoons CO_2^*+^*$	K_{5b}
Step 6.1	$CO_2^*\rightleftharpoons CO_2+^*$	$K_{6.1a}$	$CO_2^*\rightleftharpoons CO_2+^*$	$K_{6.1b}$
Step 6.2	$CO_2+O^*\rightleftharpoons CO_3^*$	$K_{6.2a}$	$CO_2+O^*\rightleftharpoons CO_3^*$	$K_{6.2b}$
Step 7	$OH^*+OH^*\rightleftharpoons H_2O^*+O^*$	K_{7a}	$OH^*+OH^*\rightleftharpoons H_2O^*+O^*$	K_{7b}
Step 8	$H_2O^*\rightleftharpoons H_2O+^*$	K_{8a}	$H_2O^*\rightleftharpoons H_2O+^*$	K_{8b}

Figure 1.6 Methane combustion reaction on supported Pd-like and Pt-like catalysts. Reprinted from [101] with permission from Royal Society of Chemistry.

1.9 Novelty and objectives

The novelty of the thesis lies in the rational size-controlled bimetallic catalyst design approach in development of combustion catalysts with high activity and stability in methane abatement in wet

conditions and energy production. This approach, as opposed to traditional methods of altering size via impregnation and calcination, is believed to deliver a new class of bimetallic catalysts for catalytic combustion along with deep insight into catalytic combustion over bimetallic catalysts, especially by studying the full range of the ratios of two metals. Contrary to the conventional approach in bimetallic catalysis that is used in industry, in which the catalysts are first synthesized by mixing precursors in different ratios and then analyzed in terms of their structure (which may not allow intrinsic bimetallicity), in this new approach the desired structures will be defined first and then synthesized, which is the application of rational catalyst design using recent advances in nanotechnology.

The two long-term objectives, which are defined by the challenges in methane catalytic combustion and bimetallic catalysis in general, are the first development of highly active, water-tolerant, low-temperature methane combustion catalysts meant to achieve a high degree of abatement of methane as a greenhouse gas. Second, demonstration of the feasibility of the approach, and then paving the way for the widespread use of bimetallic catalyst controlled syntheses in various environmental applications. These rather ambitious objectives are not so idealistic if the unprecedented opportunities for catalysis that have recently been opened by new methods of synthesizing nanoparticles of a desired structure and size are taken into consideration [91, 92, 105]. The short-term objectives, representing tasks that need to be accomplished in order to achieve the long-term objectives, involve first synthesizing a series of bimetallic Pd-Pt catalysts with different controlled nanoparticle structures and sizes, representing a new class of catalytic combustion. Second is a study of their catalytic performance in the low-temperature catalytic combustion of methane with water (up to 5%). Third involves finding correlations between the bimetallic nanoparticle structure and size and its catalytic activity and stability in order to propose an optimal catalytic system.

1.10 Approach

1. In Chapter 1, a brief introduction of the importance of methane emission control from the exhaust of NGVs and also the role of catalytic combustion in this regard is reported. The use of mono and bimetallic Pd-based catalysts on different supports and the inhibitory effect of

water in the methane combustion reaction is reviewed. At the end, the reaction mechanisms and requisite of synthesis of size-controlled nanoparticles are discussed.

2. In Chapter 2, the synthesis procedure of the size-controlled nanoparticles and the effect of the solvent/reductant (ethanol and ethylene glycol (EG)) and metal precursor (palladium chloride, palladium acetate, and hexachloroplatinic acid) on the structure, size, size distribution, and agglomeration of PVP-protected Pd and Pt nanoparticles are addressed.

3. Chapter 3 sheds light on the effect of Pt on the state of the active Pd surface under low-temperature, dry lean methane combustion conditions. In situ XANES and EXAFS spectroscopy measurements were conducted for monometallic Pd, Pt and Pd-Pt 2:1 catalysts to show that a monometallic Pd catalyst is fully oxidized in the full temperature range, whereas any Pt addition promotes Pd reduction even in a reactive oxidizing environment, just with a significantly lower activity in the reaction as compared to the oxidized Pd.

4. Chapter 4 provides an insight into the wet, lean methane combustion mechanism on the bimetallic Pd-Pt/Al_2O_3 catalyst via in situ X-ray absorption spectroscopy (XAS) studies at temperatures of 200-600ºC to show that the presence of water leads to the increased fraction of metallic Pd due to the lack of surface oxygen. Thus, this results in Pt atoms available for methane dissociation, which does not occur in the dry methane-lean feed in which oxygen poisons Pt. In other words, PdO activates methane in dry combustion, and Pt(0) does so in the wet feed.

5. Chapter 5 evaluates the effect of the Pd:Pt ratio (from 5:1, 4:1… to 1:4, 1:5) on the stability of the bimetallic Pd-Pt/Al_2O_3 catalysts during and after 40-hour in situ hydrothermal ageing at 400-550ºC with 5% water in low-temperature lean methane combustion. It is revealed that stability is governed significantly by the ratio of Pd/Pt rather than the catalyst preparation method. The most optimal combination of activity and stability is Pd:Pt 1:1 (atomic) ratio. It is also suggested that platinum vaporization is significant in the wet feed at low surface oxygen concentrations even at the temperature interval of 400-550ºC, and that significant structural changes occur in situ even at such low temperatures.

6. In Chapter 6, the role of SnO_2 support in comparison with Al_2O_3 support is discussed to show that the beneficial role of SnO_2 to enhance activity of PdO sites by providing more oxygen overrides the Pt-promoting role in a bimetallic Pd-Pt/Al_2O_3 catalyst. SnO_2, thus, can be considered as a potential replacement of Pt in NGV catalytic converters.

7. Chapter 7 contains the conclusions associated with this project, recommendations, and future work.

1.11 References

[1] BP Statistical Review of World Energy 2017, 2017. http://www.bp.com/en/global/corporate/energy-economics/statistical-review-of-world-energy.html. (Accessed 9/19/2017 2017).

[2] B.E. Knox, H.B. Palmer, Chem. Rev. 61 (1961) 247-255.

[3] J.N. Armor, Appl. Catal. A: Gen. 194-195 (2000) 3-11.

[4] F. Klingstedt, A.K. Neyestanaki, R. Byggningsbacka, L.E. Lindfors, M. Lundén, M. Petersson, P. Tengström, T. Ollonqvist, J. Väyrynen, Appl. Catal. A: Gen. 209 (2001) 301-316.

[5] M.M. Khalasane, J. Info. Knowl. Res. Mec. Eng. 4 (2016) 668-674.

[6] K.C. Taylor, Automobile Catalytic Converters, Springer-Verlag, Berlin, 1984.

[7] C.H. Bartholomew, R.J. Farrauto, Fundamentals of Industrial Catalytic Processes, John Wiely & Sons, Hoboken, New Jersey, 2011.

[8] M. Kumar, G. Rattan, R. Prasad, Canadian Chem. Trans. 3 (2015) 381-409.

[9] P. Gélin, M. Primet, Appl. Catal. B: Environ. 39 (2002) 1-37.

[10] Y.-H. Chin, M. Garcia-Dieguez, E. Iglesia, J. Phys. Chem. C 120 (2016) 1446-1460.

[11] C.F. Cullis, B.M. Willatt, J. Catal. 83 (1983) 267-285.

[12] Y.-H. Chin, D.E. Resasco, Catalysis 14 (1999) 1-39.

[13] Z. Li, G.B. Hoflund, J. Nat. Gas Chem. 12 (2003) 153-160.

[14] C.B. Alcock, G.W. Hooper, Proc. R. Soc. Lond. A 254 (1960) 551-561.

[15] H. Zhang, M. Jin, Y. Xia, Chem. Soc. Rev. 41 (2012) 8035-8049.

[16] R.F. Hicks, H. Qi, M.L. Young, R.G. Lee, J. Catal. 122 (1990) 280-294.

[17] K. Persson, A. Ersson, K. Jansson, J.L.G. Fierro, S.G. Järås, J. Catal. 243 (2006) 14-24.
[18] K. Persson, K. Jansson, S.G. Järås, J. Catal. 245 (2007) 401-414.
[19] A. Maione, F. André, P. Ruiz, Appl. Catal. B: Environ. 75 (2007) 59-70.
[20] A. Dianat, N. Seriani, M. Bobeth, W. Pompe, L.C. Ciacchi, J. Phys. Chem. C 112 (2008) 13623-13628.
[21] R.J. Farrauto, M.C. Hobson, T. Kennelly, E.M. Waterman, Appl. Catal. A: Gen. 81 (1992) 227-237.
[22] J.G. McCarty, Catal. Today 26 (1995) 283-293.
[23] R. Burch, F.J. Urbano, Appl. Catal. A: Gen. 124 (1995) 121-138.
[24] M. Lyubovsky, L. Pfefferle, Appl. Catal. A: Gen. 173 (1998) 107-119.
[25] K.I. Fujimoto, F.H. Ribeiro, M. Abalos-Borja, E. Iglesia, J. Catal. 179 (1998) 431-442.
[26] G. Groppi, C. Cristiani, L. Lietti, P. Forzatti, Stud. Surf. Sci. Catal. 130 (2000) 3801-3806.
[27] J.-D. Grunwaldt, M. Maciejewski, A. Baiker, Phys. Chem. Chem. Phys. 5 (2003) 1481-1488.
[28] O. Demoulin, M. Navez, E.M. Gaigneaux, P. Ruiz, A.-S. Mamede, P. Granger, E. Payen, Phys. Chem. Chem. Phys. 5 (2003) 4394-4401.
[29] P. Gelin, L. Urfels, M. Primet, E. Tena, Catal. Today 83 (2003) 45-57.
[30] V. Meeyoo, D.L. Trimm, N.W. Cant, Appl. Catal. B: Environ. 16 (1998) L101-L104.
[31] P. Hurtado, S. Ordonez, H. Sastre, F.V. Diez, Appl. Catal. B: Environ. 47 (2004) 85-93.
[32] J.A. Moulijn, A.E.v. Diepen, F. Kapteijn, Appl. Catal. A: Gen. 212 (2001) 3-16.
[33] M.S. Spencer, M.V. Twigg, Annu. Rev. Mater. Res. 35 (2005) 427-464.
[34] C.F. Cullis, T.G. Nevell, D.L. Trimm, J. Chem. Soc., Faraday Trans. 1 68 (1972) 1406-1412.
[35] R. Burch, F.J. Urbano, P.K. Loader, Appl. Catal. A: Gen. 123 (1995) 173-184.
[36] D. Ciuparu, N. Katsikis, L. Pfefferle, Appl. Catal. A: Gen. 216 (2001) 209-215.
[37] C.L. Pieck, C.R. Vera, E.M. Peirotti, J.C. Yori, Appl. Catal. A: Gen. 226 (2002) 281-291.
[38] D. Ciuparu, E. Perkins, L. Pfefferle, Appl. Catal. A: Gen. 263 (2004) 145-153.
[39] S. Eriksson, M. Boutonnet, M. Boutonnet, Appl. Catal. A: Gen. 312 (2006) 95-101.
[40] K. Persson, L.D. Pfefferle, W. Schwartz, A. Ersson, S.G. Järås, Appl. Catal. B: Environ. 74 (2007) 242-250.
[41] L.S. Escandón, D. Niño, E. Díaz, S. Ordóñez, F.V. Díez, Catal. Commun. 9 (2008) 2291-2296.
[42] W.R. Schwartz, D. Ciuparu, L.D. Pfefferle, J. Phys. Chem. C 116 (2012) 8587-8593.

[43] R. Gholami, M. Alyani, K.J. Smith, Catalysts 5 (2015) 561-594.
[44] D. Ciuparu, E. Perkins, L. Pfefferle, Appl. Catal. A: Gen. 263 (2004) 145-153.
[45] W.R. Schwartz, D. Ciuparu, L.D. Pfefferle, J. Phys. Chem. C 116 (2012) 8587-8593.
[46] T.V. Choudhary, S. Banerjee, V.R. Choudhary, Appl. Catal. A: Gen. 234 (2002) 1-23.
[47] G. Lapisardi, L. Urfels, P. Gélin, M. Primet, A. Kaddouri, E. Garbowski, S. Toppi, E. Tena, Catal. Today 117 (2006) 564-568.
[48] K. Persson, A. Ersson, K. Jansson, N. Iverlund, S. Järås, J. Catal. 231 (2005) 139-150.
[49] N.M. Kinnunen, J.T. Hirvi, M. Suvanto, T.A. Pakkanen, J. Mol. Catal. A: Chem. 356 (2012) 20-28.
[50] A. Ersson, H. Kušar, R. Carroni, T. Griffin, S. Järås, Catal. Today 83 (2003) 265-277.
[51] R. Strobel, J.-D. Grunwaldt, A. Camenzind, S.E. Pratsinis, A. Baiker, Catal. Lett. 104 (2005) 9-16.
[52] C. Micheaud, P. Marécot, M. Guérin, J. Barbier, Appl. Catal. A: Gen. 171 (1998) 229-239.
[53] B. Coq, F. Figueras, J. Mol. Catal. A: Chem. 173 (2001) 117-134.
[54] H. Yamamoto, H. Uchida, Catal. Today 45 (1998) 147-151.
[55] K. Narui, H. Yata, K. Furuta, A. Nishida, Y. Kohtoku, T. Matsuzaki, Appl. Catal. A: Gen. 179 (1999) 165-173.
[56] Y. Deng, T.G. Nevell, Catal. Today 47 (1999) 279-286.
[57] R. Abbasi, L. Wu, S.E. Wanke, R.E. Hayes, Chem. Eng. Res. Des. 90 (2012) 1930-1942.
[58] K. Persson, A. Ersson, S. Colussi, A. Trovarelli, S.G. Järås, Appl. Catal. B: Environ. 66 (2006) 175-185.
[59] Y. Ozawa, Y. Tochihara, A. Watanabe, M. Nagai, S. Omi, Appl. Catal. A: Gen. 259 (2004) 1-7.
[60] E.D. Goodman, S. Dai, A.-C. Yang, C.J. Wrasman, A. Gallo, S.R. Bare, A.S. Hoffman, T.F. Jaramillo, G.W. Graham, X. Pan, M. Cargnello, ACS Catal. 7 (2017) 4372-4380.
[61] A. Dianat, J. Zimmermann, N. Seriani, M. Bobeth, W. Pompe, L.C. Ciacchi, Suf. Sci. 602 (2008) 876-884.
[62] J.B. Miller, M. Malatpure, Appl. Catal. A: Gen. 495 (2015) 54-62.
[63] B. Yue, R. Zhou, Y. Wang, X. Zheng, Appl. Catal. A: Gen. 295 (2005) 31-39.
[64] B. Yue, R. Zhou, Y. Wang, X. Zheng, J. Mol. Catal. A: Chem. 238 (2005) 241-249.

[65] N. Ma, K. Suematsu, M. Yuasa, K. Shimanoe, ACS Appl. Mater. Interfaces 7 (2015) 15618-15625.
[66] H. Widjaja, K. Sekizawa, K. Eguchi, Bull. Chem. Soc. Jpn. 72 (1999) 313-320.
[67] D. Ciuparu, F. Bozon-Verduraz, L. Pfefferle, J. Phys. Chem. B 106 (2002) 3434-3442.
[68] W.R. Schwartz, L.D. Pfefferle, J. Phys. Chem. C 116 (2012) 8571-8578.
[69] H. Yoshida, T. Nakajima, Y. Yazawa, T. Hattori, Appl. Catal. B: Environ. 71 (2007) 70-79.
[70] W.C. Conner, J.L. Falconer, Chem. Rev. 95 (1995) 759-788.
[71] T. Schalow, M. Laurin, B. Brandt, S. Schauermann, S. Guimond, H. Kuhlenbeck, D.E. Starr, S.K. Shaikhutdinov, J. Libuda, H.J. Freund, Angew. Chem. Int. Ed. 44 (2005) 7601-7605.
[72] M. Ahmadi, H. Mistry, B.R. Cuenya, J. Phys. Chem. Lett. 7 (2016) 3519-3533.
[73] G.N. Vayssilov, Y. Lykhach, A. Migani, T. Staudt, G.P. Petrova, N. Tsud, T. Skála, A. Bruix, F. Illas, K.C. Prince, V. Matolín, K.M. Neyman, J. Libuda, Nature Mater. 10 (2011) 310-315.
[74] H. Widjaja, K. Sekizawa, K. Eguchi, H. Arai, Catal. Today 35 (1997) 197-202.
[75] T. Takeguchi, O. Takeoh, S. Aoyama, J. Ueda, R. Kikuchi, K. Eguchi, Appl. Catal. A: Gen. 252 (2003) 205-214.
[76] K. Eguchi, H. Arai, Appl. Catal. A: Gen. 222 (2001) 359-367.
[77] K. Sekizawa, H. Widjaja, S. Maeda, Y. Ozawa, K. Eguchi, Appl. Catal. A: Gen. 200 (2000) 211-217.
[78] R. Kikuchi, S. Maeda, K. Sasaki, S. Wennerström, K. Eguchi, Appl. Catal. A: Gen. 232 (2002) 23-28.
[79] D. Roth, P. Gelin, E. Tena, M. Primet, Top. Catal. 16/17 (2001) 77-82.
[80] R.G. Shahrestani, Kinetic and deactivation studies of methane oxidation over palladium catalysts in the presence of water, University of British Colombia, Vancouver, Canada, 2015.
[81] Z. Zhao, B. Wang, J. Ma, W. Zhan, L. Wang, Y. Guo, Y. Guo, G. Lu, Chinese J. Catal. 38 (2017) 1322-1329.
[82] G. Santarossa, K. Hahn, A. Baiker, Langmuir 29 (2013) 5487-5499.
[83] N. Murata, T. Suzuki, M. Kobayashi, F. Togoh, K. Asakura, Phys. Chem. Chem. Phys. 15 (2013) 17938-17946.
[84] S. Das, V. Jayaraman, Prog. Mater. Sci. 66 (2014) 112-255.
[85] S.H. Kim, K.T. Lee, S. Lee, J.H. Moon, B.-T. Lee, Jpn. J. Appl. Phys. 41 (2002) L 1002- L 1005.

[86] T. Okanishi, T. Toshiaki, T. Takeguchi, R. Kikuchi, K. Eguchi, Appl. Catal. A: Gen. 298 (2006) 181-187.
[87] N. Ma, K. Suematsu, M. Yuasa, T. Kida, K. Shimanoe, ACS Appl. Mater. Interfaces 7 (2015) 5863-5869.
[88] D. Koziej, M. Hübner, N. Barsan, U. Weimar, M. Sikora, J.-D. Grunwaldt, Phys. Chem. Chem. Phys. 11 (2009) 8620-8625.
[89] F. Zaera, Prog. Surf. Sci. 69 (2001) 1-98.
[90] N. Toshima, Metal Nanoparticles Used as Catalysts, in: C.I. Contescu, K. Putyera (Eds.), Dekker Encyclopedia of Nanoscience and Nanotechnology, Taylor & Francis Group, New York, 2008.
[91] N. Toshima, H. Yan, Y. Shiraishi, Recent progress in bimetallic nanoparticles: their preparation, structures and functions, Elsevier, The Netherlands, 2008.
[92] C. Burda, X. Chen, R. Narayanan, M.A. El-Sayed, Chem. Rev. 105 (2005) 1025-1102.
[93] A. Molnar, A. Sarkany, M. Varga, J. Mol. Catal. A: Chem. 173 (2001) 185-221.
[94] N. Semagina, L. Kiwi-Minsker, Catal. Rev. 51 (2009) 147-217.
[95] A.Y. Stakheev, A.M. Batkin, N.S. Teleguina, G.O. Bragina, V.I. Zaikovsky, I.P. Prosvirin, A.K. Khudorozhkov, V.I. Bukhtiyarov, Top. Catal. 56 (2013) 306-310.
[96] J.J. Willis, E.D. Goodman, L. Wu, A.R. Riscoe, P. Martins, C.J. Tassone, M. Cargnello, J. Am. Chem. Soc. 139 (2017) 11989-11997.
[97] D. Ciuparu, M.R. Lyubovsky, E. Altman, L.D. Pfefferle, A. Datye, Catal. Rev. 44 (2002) 593-649.
[98] M. Aryafar, F. Zaera, Catal. Lett. 48 (1997) 173-183.
[99] Y.-N. Wang, R.G. Herman, K. Klier, Surf. Sci. 279 (1992) 33-48.
[100] L. Ma, D.L. Trimm, C. Jiang, Appl. Catal. A: Gen. 138 (1996) 275-283.
[101] W. Qi, J. Ran, R. Wang, X. Du, J. Shi, J. Niu, P. Zhang, M. Ran, RSC Adv. 6 (2016) 109834-109845.
[102] J. Au-Yeung, K. Chen, A.T. Bell, E. Iglesia, J. Catal. 188 (1999) 132-139.
[103] P. Hurtado, S. Ordóñez, H. Sastre, F.V. Díez, Appl. Catal. B: Environ. 51 (2004) 229-238.
[104] D. Ciuparu, R. Altman, L. Pfefferle, J. Catal. 203 (2001) 64-74.
[105] O.M. Wilson, M.R. Knecht, J.C. Garcia-Martinez, R.M. Crooks, J. Am. Chem. Soc. 128 (2006) 4510-4511.

Chapter 2. Effect of the solvent and metal precursor on the structure of PVP-protected Pd and Pt nanoparticles[1]

2.1 Method details

In recent years, with the aim of colloidal chemistry methods, metal nanocatalysts have emerged as monodispersed nanoparticles with a controlled size and morphology. The fundamental approaches that have been taken to achieve a control over the nanoparticle size and shape in catalytic application show the great influence of these issues on catalytic reaction rates, activities, and selectivities [1]. Metal salts as precursors for particle formation, steric stabilizers to direct particle size and shape, and solvents to act as a reaction medium and/or reductant are the main components of a colloidal system in which the choice of each component depends on the target catalyst and morphology. In the area of catalysis, the goal of most catalyst syntheses is to study catalytic properties as a function of metal nanoparticle size and shape; thus, the influence of different synthesis parameters on final particles is crucial to obtain size- and shape-controlled nanoparticles with desirable activity and selectivity.

Numerous studies have reported on the synthesis of palladium and platinum nanoparticles with colloidal-solution techniques due to their widespread catalytic applications [2-6]. Teranishi et al. [7, 8] found that the mean diameter of monodispersed Pd and Pt nanoparticles with dihydrogen tetrachloropalladate (II) and hexachloroplatinic (IV) acid could be controlled in a one-step alcohol reduction by changing the amount of a stabilizer (poly (N-vinyl-2-pyrrolidone), PVP) and the kind and/or the concentration of alcohol. They used a low-boiling-point alcohol, such as methanol, ethanol, or 1-propanol, and showed that the higher boiling point alcohol with higher concentration and higher amount of PVP lead to the smaller nanoparticles as a result of a faster reduction rate and improved polymer protection. Shiraishi et al. [9] and Toshima et al. [10] showed the formation of superstructure Pt nanoclusters in colloidal dispersions of PVP-protected platinum nanoclusters by the ethanol reduction of hexachloroplatinic(IV) acid in the presence of PVP. The superstructure

[1] Chapter 2 of the thesis has been submitted to the MethodsX journal as "Effect of the solvent and metal precursor on the structure of PVP-protected Pd and Pt nanoparticles" H. Nassiri, N. Semagina MethodsX (2017). Nanoparticles syntheses and TEM characterizations and analyses, manuscript preparation, and writing were all conducted by the author under the supervision and final approval of Dr. Natalia Semagina.

sizes decrease with increasing molar ratio of PVP to platinum. However, even at a molar ratio of 40, the size of the superstructure is 28 nm. Esparza et al. [11] obtained dispersed Pt nanoparticles of uniform size with the same precursor but they used an aqueous solution of $NaBH_4$ as a strong reducing agent in addition to methanol. EG was used frequently as a reductant for the aforementioned nanoparticles with or without NaOH to adjust the pH of the solution and/or to produce unprotected nanoclusters [12-14]. Wang et al. [13] discussed very briefly the effect of metal concentration and water in an alkaline EG system. However, systematic studies of the effect of the main components of a colloidal system have rarely been reported; typically, final procedures are provided for nanoparticle applications [15] or obtaining specific shapes [16, 17]. In certain applications, a uniform dispersion of nanoparticles in addition to an effective control of particle size is required [1, 18]. Additionally, as individual nanoparticles have a tendency to form agglomerates during the preparation process, the control of particles interaction is critical to obtain a stable dispersion.

The aim of the present study is to evaluate the effect of solvent composition, precursor nature, and concentration on the size and structure of PVP-stabilized Pd and Pt nanoparticles. The practical significance is in the synthesis technique development for the monodispersed nanoparticles that could be suitable for catalytic or other applications in which control over size and shape are crucial. We investigated the effect of selected parameters on particle size, particle size distribution, and agglomeration. Chlorine-containing and Cl-free metal precursors are addressed as well, as Cl is a known poison for catalytic applications. The metal nanoparticle concentration effect is paramount for nanoparticle isolation before catalysis: the higher concentration allows a lower waste-to-product ratio. High-boiling and low-boiling systems, such as ethanol-water and EG-water, were used as two common solvating and reducing media. Different alcohol concentrations were investigated, as the syntheses are performed under reflux conditions and the temperature is known to influence the particle size by changing the nucleation rate of the reduced metallic atoms and stabilization of the complexes formed between Pt and Pd with PVP. To keep the number of variables as low as possible, the PVP to metal ratio was kept constant in all syntheses as 40. We believe that this study may provide detailed guidance to those practitioners requiring a variety of monodispersed Pd or Pt nanoparticles with required sizes with no or minimal variations in the synthesis system.

2.2 Synthesis details

Hexachloroplatinic (IV) acid (H_2PtCl_6, 8% w/v solution in water, Sigma-Aldrich), palladium chloride ($PdCl_2$, 5% w/v solution in dilute HCl, Acros Organics), palladium (II) acetate ($Pd(AcO)_2$, Sigma-Aldrich), 1,4-Dioxane (>99.9% Sigma-Aldrich) poly N-vinylpyrrolidone (PVP, average molecular weight 40,000, Sigma-Aldrich), ethanol (90.5 vol.%, Ricca Chemical Co.) and Ethylene glycol (>99.9%, Fischer Scientific) were used as received. Milli-Q water (18.2 MΩ.cm) was used throughout the work.

Pd and Pt monometallic nanoparticles were synthesized using the one-step alcohol reduction method on the basis of 0.1 mmol metal. To synthesize Pt nanoparticles with hexachloroplatinic (IV) acid and Pd nanoparticles with palladium chloride, the metal precursor with 0.444 g of PVP was added to a 500-ml flask and mixed with 100, 200, or 400 ml of solvent solution (i.e., alcohol-water solution) for a metal concentration of 1, 0.5, or 0.25 mM, respectively. The alcohol-to-water ratio depends on the desired volumetric concentration of alcohol in the system and varies from 20 vol.% to 80 vol.%. In the case of Pd nanoparticle synthesis with palladium acetate, first, the precursor was dissolved in 10 ml of dioxane and then was mixed with the same amount of PVP and solvent solution which had been used in other nanoparticle syntheses in this study. The resulting mixture was stirred and heated until it came to boil and then refluxed in air under vigorous stirring for 3 h to complete the synthesis of PVP-protected nanoparticles. A dark colloidal dispersion of nanoparticles was obtained at the end of synthesis without any precipitates.

Transmission electron microscopy (TEM) photographs were taken using a 200-kV JEOL-2100 electron microscope. Specimens were prepared by placing a drop of the colloidal dispersion on a copper grid covered with a perforated carbon film and then evaporating the solvent. The particle diameters were measured from the enlarged TEM photographs. The particle size distribution histograms were obtained on the basis of the linear diameter measurements for approximately 200 particles.

2.3 Obtained nanoparticles

2.3.1 System of ethanol-water

2.3.1.1 Pd nanoparticles from $PdCl_2$ precursor

As ethanol concentration in the system increased from 20 to 80 vol.%, average Pd nanoparticle size and size distribution increased, as seen in Table 2.1. TEM images and size distribution histograms for each of the samples can be found in Supporting Information (Figures 2.S1-S4). A representative TEM image is shown in Figure 2.1(a); the obtained well-dispersed particles were found typical for all solvent compositions and precursor concentrations. The solvent boiling temperature decreased with ethanol concentration increase; as the synthesis was performed under reflux, the temperature decrease may result in a lower nucleation rate, domination of particle growth and occurring coarsening, or Ostwald ripening, as previously suggested for different colloidal nanoparticles [19]. The increase in Pd concentration from 0.25 to 1.00 mM did not significantly affect the particle size, which was expected, as the PVP/metal molar ratio was kept the same at 40 for all systems.

2.3.1.2 Pt nanoparticles from H_2PtCl_6 precursor

Unfortunately, the successful technique for Pd nanoparticle preparation could not be implemented for Pt. As shown in Figure 2.1(b) and Table 2.1, the colloidal synthesis of PVP-protected platinum nanoparticles by the ethanol reduction of H_2PtCl_6 led to the formation of superstructures in all alcohol concentrations from 40% to 80%, whereas no nanoparticle formation was observed at a 20% alcohol concentration. All superstructures are composed of nanoparticles of ~2 nm size; the superstructure size diminishes from ~100 nm down to 4 nm. The high tendency to make superstructures has been also seen in other works [9, 10]. The similar trend of superstructure size decrease with ethanol fraction increase was observed earlier [20], although at a lower PVP/Pt ratio. This was ascribed to the increased amount of Pt(0) nuclei at higher ethanol concentrations, leading to enhanced probability for successive collisions during growth and agglomeration. Our attempts to break the superstructures with ultrasound were not successful, indicating their strong interactions. Such superstructures may have limited application in catalysis, as they will likely

sinter under high temperature reaction conditions, and/or the access to the active nanoparticle surface will be hindered by diffusion limitations within the superstructure.

Table 2.1 Size of Pd and Pt nanoparticles or superstructures (nm) synthesized in ethanol-water system at PVP/metal = 40 mol/mol

	Metal concentration, mM	EtOH concentration, vol. %			
		20	40	60	80
Reflux temperature, °C		87	84	83	81
Precursor: $PdCl_2$	0.25	1.6±0.5	1.6±0.4	2.1±0.5	1.8±0.4
	0.50	1.4±0.4	2.0±0.6	1.9±0.5	3.0±1.1
	1.00	1.5±0.3	2.0±0.3	1.6±0.3	2.0±0.4
Precursor: H_2PtCl_6	1.00	N-R[a]	98[b]±12	35[b]±12	4[b]±1

[a] not reduced; [b] superstructures composed of 2-nm near-spherical nanoparticles

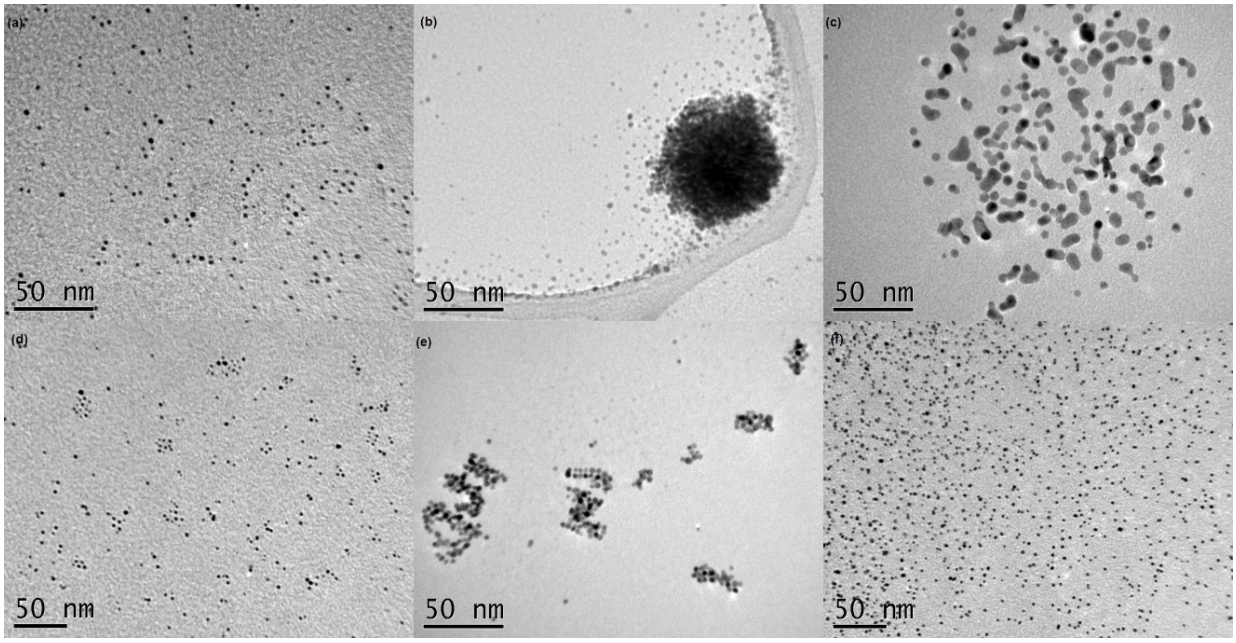

Figure 2.1 Representative TEM images: a) Pd nanoparticles (0.5 mM $PdCl_2$ in 40% EtOH-H_2O); b) Pt superstructure (1.0 mM H_2PtCl_6 in 60% EtOH-H_2O); c) Pd anisotropic particles (1.0 mM $PdCl_2$ in EG); d) Pd nanoparticles (0.5 mM $Pd(AcO)_2$ in 100% EG); e) Pt superstructures (1.0 mM H_2PtCl_6 in EG); f) Pt nanoparticles (1.0 mM H_2PtCl_6 in 80% EG-H_2O)

2.3.2 System of EG-water

2.3.2.1 Pd nanoparticles from $PdCl_2$ precursor

When $PdCl_2$ was used for nanoparticle synthesis in EG, anisotropic particles in the 6-18 nm range were obtained (Table 2.2, Figure 2.1(c)). EG is a poor coordinating cation solvator compared to ethanol. A donor number or donicity of Gutmann is considered an empirical semiquantitative measurement of the nucleophilic properties of electron-pair donor solvents [21], which are 32, 20, and 18 for ethanol, EG, and water, respectively. Whereas uniform size-controlled nanoparticles were obtained from $PdCl_2$ in ethanol and ethanol-water systems, the use of EG resulted in a wider distribution of Pd nanoparticles due to the reduced cation coordination with the solvent.

Table 2.2 Size of Pd and Pt nanoparticles or superstructures (nm) synthesized in an EG-water system at PVP/metal = 40 mol/mol

Precursors	Metal concentration, mM	EG concentration, vol.%				
		20	40	60	80	100
Reflux temperature, °C		102	105	111	126	198
Precursor: $PdCl_2$	1.00	-	-	-	-	6-18[a]
Precursor: $Pd(AcO)_2$	0.25	1.7±0.6	2.5±0.9	2.5±1.1	2.2±0.8	2.7±0.7
	0.50	2.5±1.4	2.4±1.3	2.3±1.1	2.0±1.0	2.0±0.6
	1.00	2.3±1.6	2.3±1.1	2.4±1.0	2.3±0.8	2.2±0.8
Precursor: H_2PtCl_6	0.25	2.2±0.8	1.7±0.6	1.7±0.5	2.0±0.4	2.1±0.6
	0.50	2.1±0.7	1.9±0.5	1.7±0.4	2.0±0.4	2-10[b]
	1.00	1.9±0.4	1.8±0.5	2.0±0.4	2.0±0.4	2-70[b]

[a] anisotropic particles; [b] superstructures composed of 2-nm near-spherical nanoparticles

2.3.2.2 Pd nanoparticles from $Pd(AcO)_2$.

$Pd(AcO)_2$ is soluble in organic solvents; its use for nanoparticle synthesis in EG and EG-water systems yielded nearly monodispersed particles (Table 2.2). TEM images and size distribution histograms for each of the samples can be found in Supporting Information (Figures 2.S5-S8). A representative TEM image for Pd nanoparticles synthesized from $Pd(AcO)_2$ in an EG-water system is shown in Figure 2.1(d). Similarly to $PdCl_2$ in an ethanol-water system (Table 2.1), the change of Pd^{2+} concentration from 0.25 to 1.00 mM did not affect particle size (Table 2.2). The reflux

temperature increase with the addition of EG to water resulted in narrower particle size distribution and lower maximum size. As discussed earlier, temperature increase is known to promote faster nucleation vs. growth resulting in smaller particles [19].

2.3.2.3 Pt nanoparticles from H_2PtCl_6

The use of EG or 80% EG with water led to near-spherical particles, but similarly to the Pt nanoparticles in ethanol-water system, they tended to form superstructures instead of being separated (Figure 2.1(e) and Figures 2.S9-S12 in Supporting Information). As soon as more water was added, individual nanoparticles with a narrow size distribution were obtained (Figure 1(f) and Table 2.2). As compared to the ethanol-water system, where superstructures of up to 100 nm were obtained, the use of a high-boiling-point EG-water system ensured the fast nucleation and suppression of growth and coagulation. The presence of water changes the ionic strength of the precursor solution. With an increase in pH, metal precursor and its hydrolyzed counterparts have varying dimensions when chloride ions are exchanged with hydroxyl [12]. Although the presence of water may cause increased particle size and broad size distribution by the formation of metal hydroxide in the first step of the synthesis process [14], the use of water may also result in glycolate and acetate formation from EG that may stabilize small nanoparticles [12-14, 22].

The precursor concentration did not affect size distribution, apart from the systems with excess EG. Superstructure formation and average size increased with increasing metal concentration, most likely due to lower local precursor and nanoparticle concentrations in the diluted systems.

2.4 Summary

A comparative study of Pd and Pt nanoparticle formation in the presence of stabilizer PVP (PVP-to-metal molar ratios of 40) was performed in EG-water or ethanol-water media using a variety of metal precursors and their concentrations (0.25-1.00 mM). EG is a better reductant for H_2PtCl_6 and $Pd(AcO)_2$ precursors, whereas ethanol works for $PdCl_2$ to achieve monodispersed nanoparticles. All nanoparticles ranged from 1.3 to 3.0 nm depending on the conditions; the use

of the ethanol-water system for Pt nanoparticle formation resulted in superstructures, which were also found in the case of excess EG at high precursor concentrations.

Acknowledgements. NSERC financial support (Strategic project grants STPGP 430108-12 and STPGP 478979-15) is kindly acknowledged.

2.5 References

[1] K.M. Koczkur, S. Mourdikoudis, L. Polavarapu, S.E. Skrabalak, Dalton Trans. 44 (2015) 17883-17905.

[2] S. Guoa, E. Wang, Nano Today 6 (2011) 240-264.

[3] A. Miyazaki, I. Balint, Y. Nakano, J. Nanopart. Res. 5 (2003) 69-80.

[4] H. Naohara, Y. Okamoto, N. Toshima, J. Power Sources 196 (2011) 7510-7513.

[5] Y. Wang, S. Xie, J. Liu, J. Park, C.Z. Huang, Y. Xia, Nano Lett. 13 (2013) 2276-2281.

[6] Q. Yuan, Z. Zhou, J. Zhuang, X. Wang, Chem. Commun. 46 (2010) 1491-1493.

[7] T. Teranishi, M. Miyake, Chem. Mater. 10 (1998) 594-600.

[8] T. Teranishi, M. Hosoe, J. Phys. Chem. B 103 (1999) 3818-3827.

[9] Y. Shiraishi, M. Nakayama, E. Takagi, T. Tominaga, N. Toshima, Inorganica Chimica Acta 300-302 (2000) 964-969.

[10] N. Toshima, T. Yonezawa, K. Kushihashi, J. Chem. Soc. Faraday Trans. 89 (1993) 2537-2543.

[11] R.I. Esparza, G. Rosas, E. Valenzuela, S.A. Gamboa, U. Pa, R. Pérez, Revista Matéria 13 (2008) 579-586.

[12] P. Mäki-Arvela, D.Y. Murzin, Appl. Catal. A: Gen. 451 (2013) 251-281.

[13] Y. Wang, J. Ren, K. Deng, L. Gui, Y. Tang, Chem. Mater. 12 (2000) 1622-1627.

[14] Y. Wang, X. Wang, Solvent and simple ion-stabilized metal nanoclusters: chemical synthesis and application, Elsevier, Amsterdam, 2007.

[15] J. Shen, N. Semagina, ACS Catal. 4 (2014) 268-279.

[16] J. Chen, B. Lim, E.P. Lee, Y. Xia, Nano Today 4 (2009) 81-95.

[17] Z. Peng, H. Yang, Nano Today 4 (2009) 143-164.

[18] F. Bonet, V. Delmas, S. Grugeon, R.H. Urbina, P.Y. Silvert, K. Tekaia-Elhsissen, Nanostructured Materials 11 (1999) 1277-1284.
[19] T. Tran, T. Nguyen, Colloids and Surfaces B: Biointerfaces 88 (2011) 1-22.
[20] S. Wang, W.J. Tseng, J. Nanopart. Res. 11 (2009) 947-953.
[21] M. Montalti, A. Credi, L. Prodi, M.T. Gandolfi, Handbook of photochemistry, 3rd ed., Taylor & Francis Group LLC, USA, 2006.
[22] X. Li, W.X. Chen, J. Zhao, W. Xing, Z.D. Xu, Carbon 43 (2005) 2168-2174.

2.6 Supporting Information

2.6.1 $PdCl_2$ in ethanol-water system

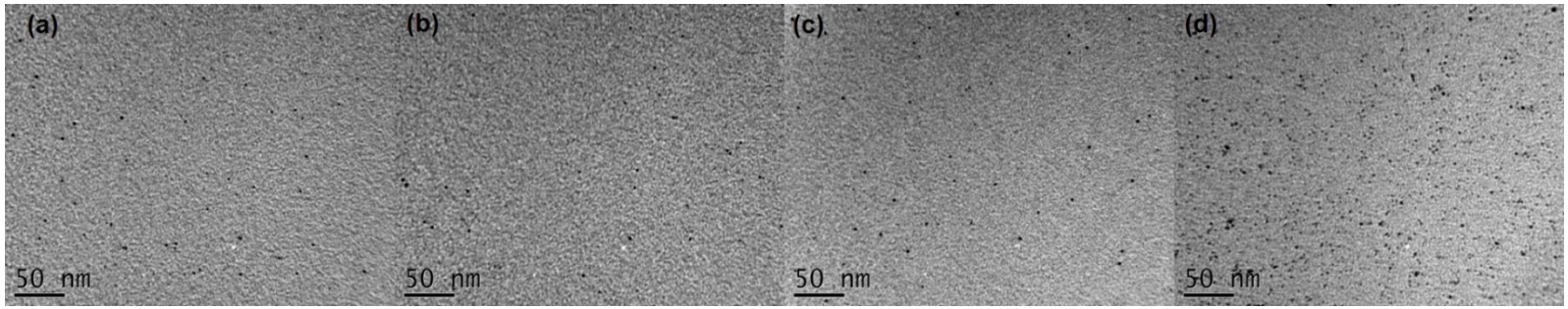

Figure 2.S1 TEM images of PVP protected Pd nanoparticles, 0.25 mM metal concentration with $PdCl_2$ precursor in ethanol-water system; (a) 20 vol.% EtOH, (b) 40 vol.% EtOH, (c) 60 vol.% EtOH, (d) 80 vol.% EtOH.

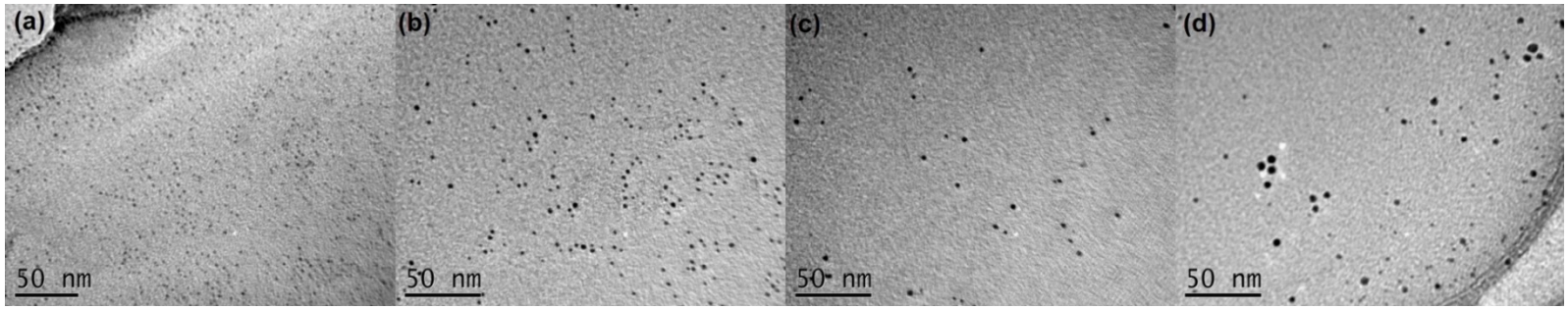

Figure 2.S2 TEM images of PVP protected Pd nanoparticles, 0.50 mM metal concentration with $PdCl_2$ precursor in ethanol-water system; (a) 20 vol.% EtOH, (b) 40 vol.% EtOH, (c) 60 vol.% EtOH, (d) 80 vol.% EtOH.

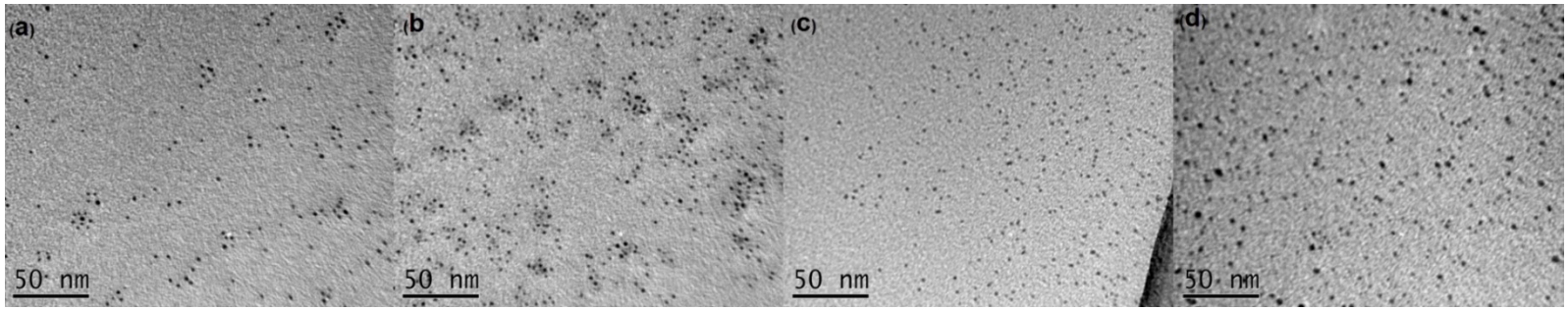

Figure 2.S3 TEM images of PVP protected Pd nanoparticles, 1.00 mM metal concentration with $PdCl_2$ precursor in ethanol-water system; (a) 20 vol.% EtOH, (b) 40 vol.% EtOH, (c) 60 vol.% EtOH, (d) 80 vol.% EtOH.

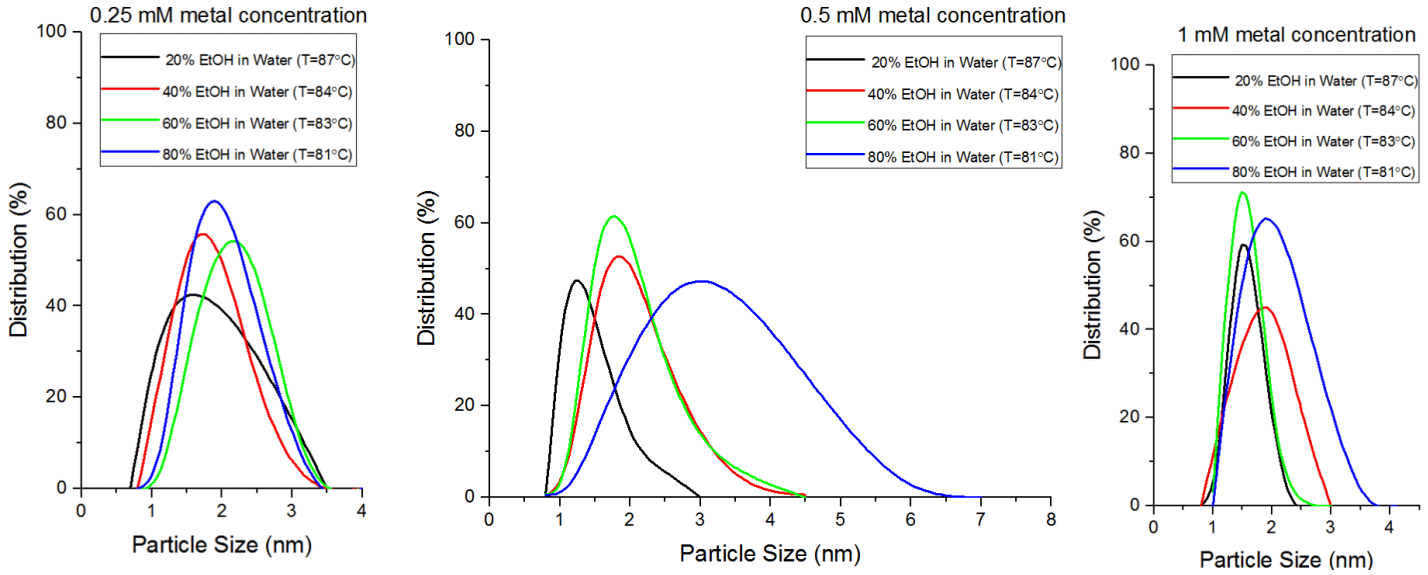

Figure 2.S4 Particle size distributions of PVP-protected Pd nanoparticles with $PdCl_2$ precursor in ethanol-water system with different metal concentrations.

2.6.2 $Pd(AcO)_2$ in EG-water

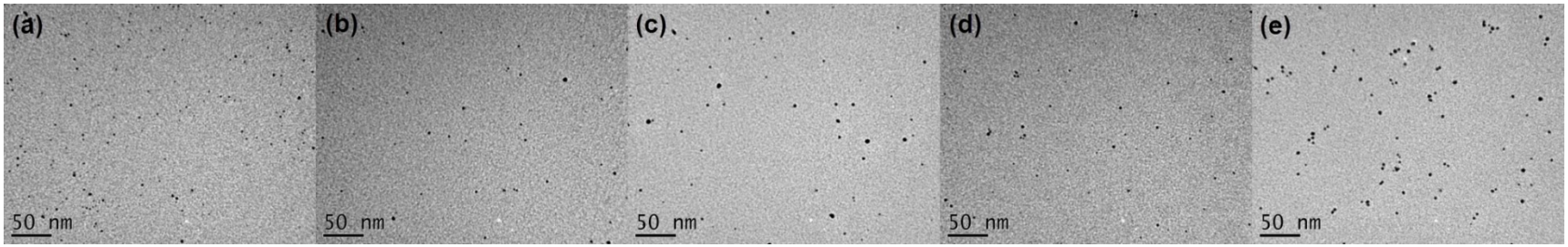

Figure 2.S5 TEM images of PVP protected Pd nanoparticles, 0.25 mM metal concentration with $Pd(AcO)_2$ precursor in ethylene glycol-water system; (a) 20 vol.% EG, (b) 40 vol.% EG, (c) 60 vol.% EG, (d) 80 vol.% EG, (e) 100 vol.% EG.

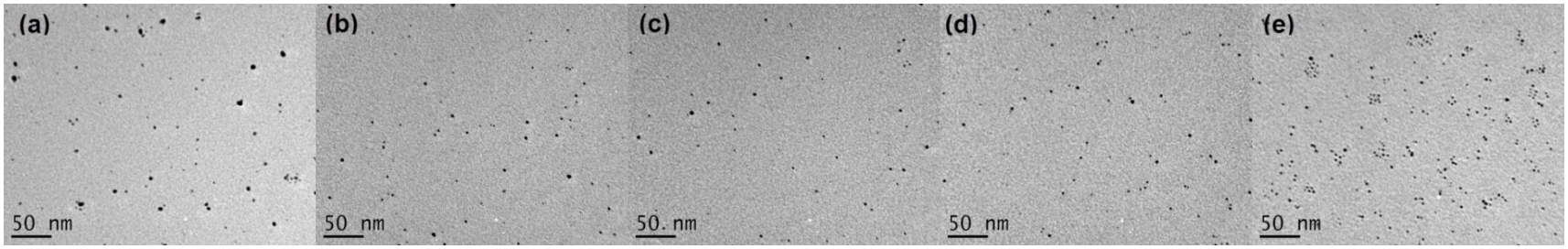

Figure 2.S6 TEM images of PVP protected Pd nanoparticles, 0.5 mM metal concentration with $Pd(AcO)_2$ precursor in ethylene glycol-water system; (a) 20 vol.% EG, (b) 40 vol.% EG, (c) 60 vol.% EG, (d) 80 vol.% EG, (e) 100 vol.% EG.

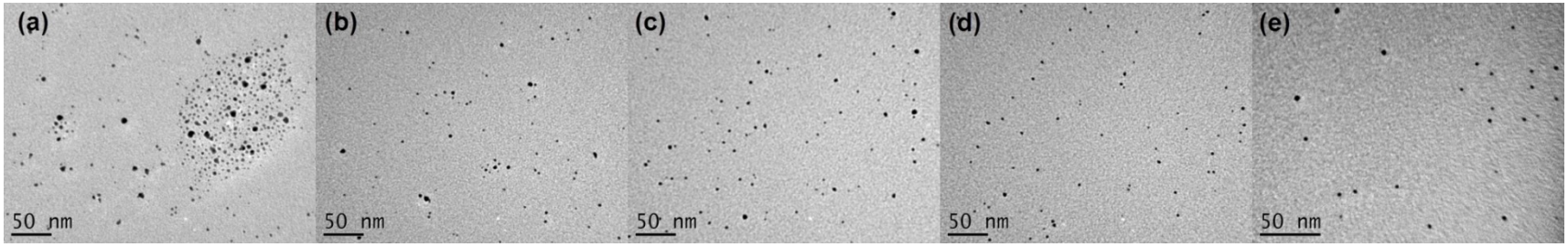

Figure 2.S7 TEM images of PVP protected Pd nanoparticles, 1.00 mM metal concentration with $Pd(AcO)_2$ precursor in ethylene glycol-water system; (a) 20 vol.% EG, (b) 40 vol.% EG, (c) 60 vol.% EG, (d) 80 vol.% EG, (e) 100 vol.% EG.

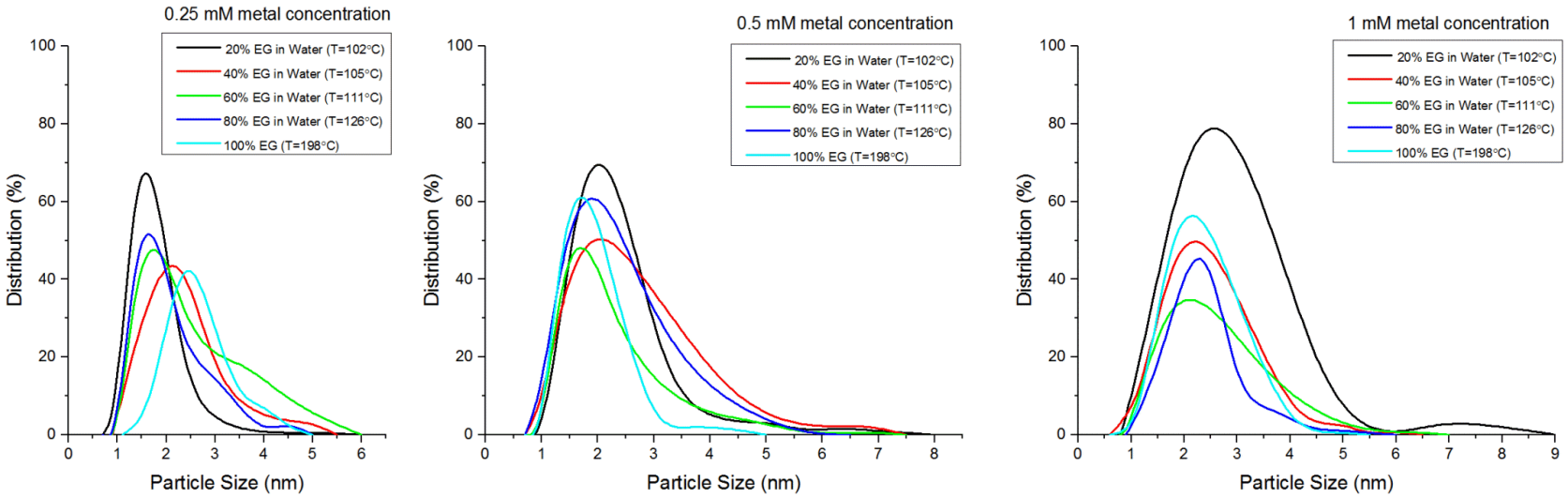

Figure 2.S8 Particle size distributions of PVP-protected Pd nanoparticles with $Pd(AcO)_2$ precursor in ethylene glycol-water system with different metal concentrations.

2.6.3 H_2PtCl_6 in ethylene glycol-water system

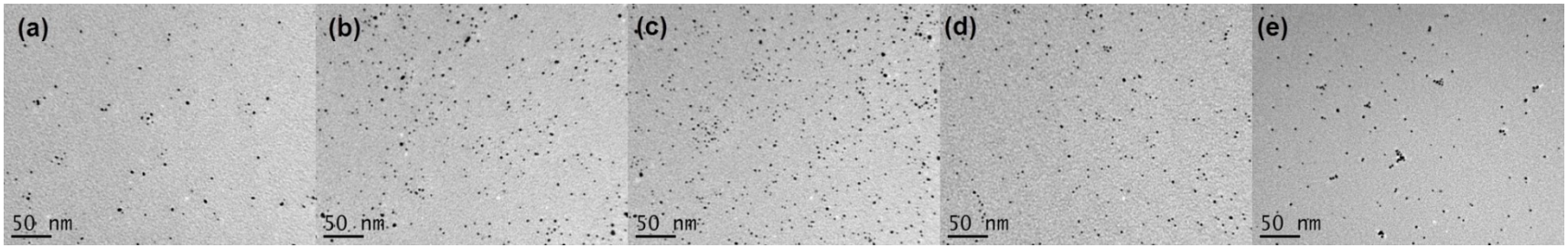

Figure 2.S9 TEM images of PVP protected Pt nanoparticles, 0.25 mM metal concentration with H_2PtCl_6 precursor in ethylene glycol-water system; (a) 20 vol.% EG, (b) 40 vol.% EG, (c) 60 vol.% EG, (d) 80 vol.% EG, (e) 100 vol.% EG.

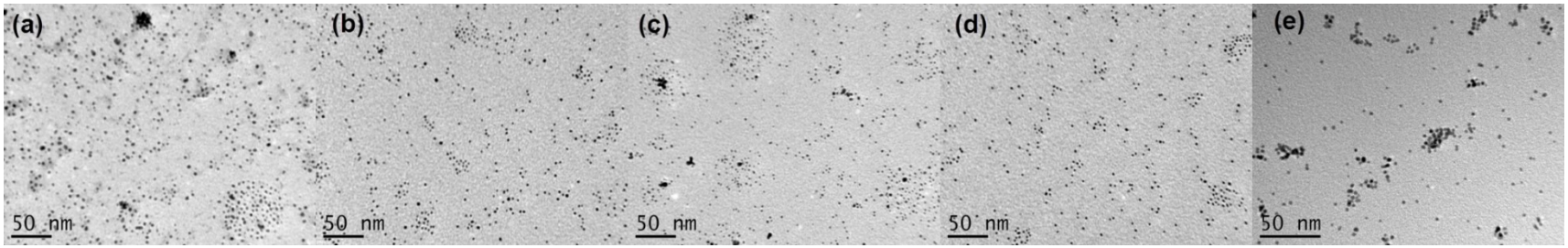

Figure 2.S10 TEM images of PVP protected Pt nanoparticles, 0.50 mM metal concentration with H_2PtCl_6 precursor in ethylene glycol-water system; (a) 20 vol.% EG, (b) 40 vol.% EG, (c) 60 vol.% EG, (d) 80 vol.% EG, (e) 100 vol.% EG.

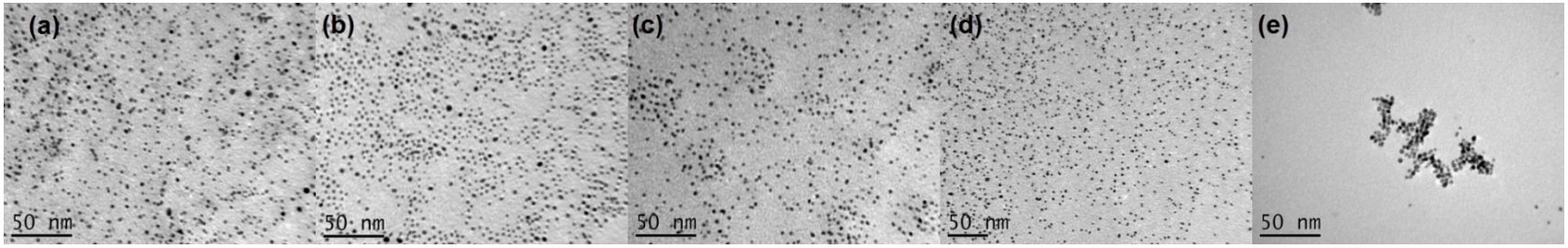

Figure 2.S11 TEM images of PVP protected Pt nanoparticles, 1.00 mM metal concentration with H_2PtCl_6 precursor in ethylene glycol-water system; (a) 20 vol.% EG, (b) 40 vol.% EG, (c) 60 vol.% EG, (d) 80 vol.% EG, (e) 100 vol.% EG.

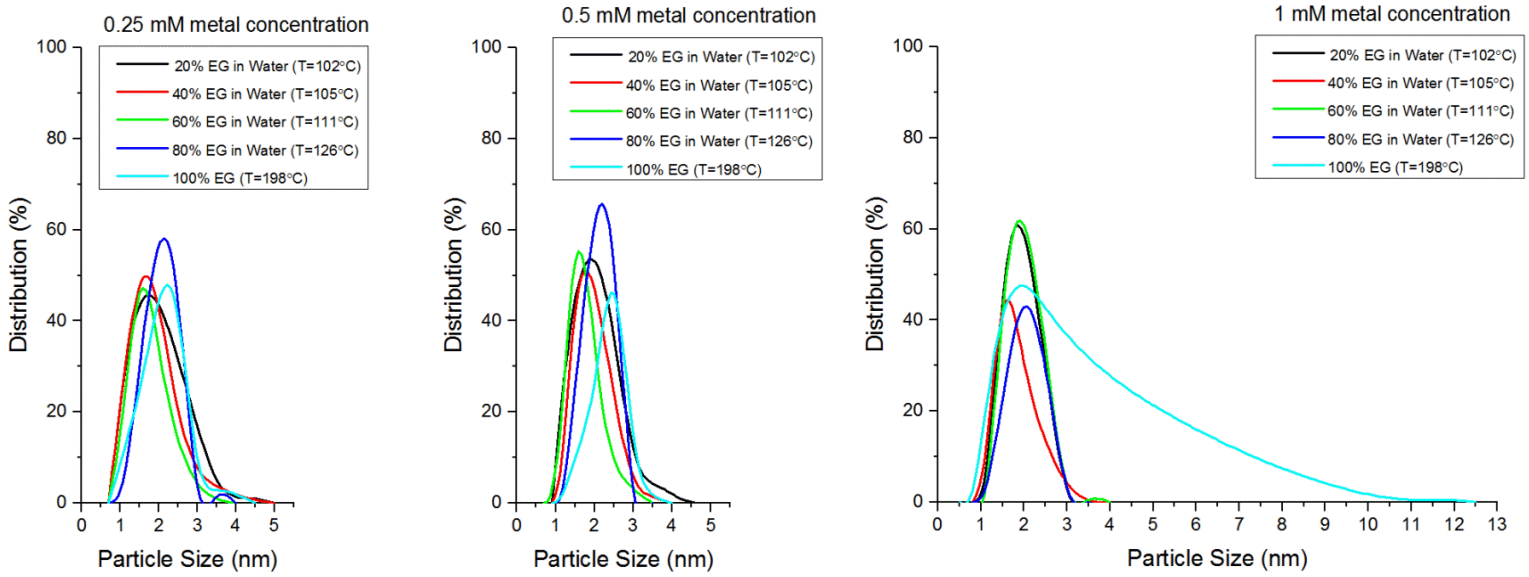

Figure 2.S12 Particle size distributions of PVP-protected Pt nanoparticles with H_2PtCl_6 precursor in ethylene glycol-water system with different metal concentrations.

Chapter 3. Platinum inhibits low-temperature dry lean methane combustion via palladium reduction in Pd-Pt/Al_2O_3: An in situ X-ray absorption study[2]

3.1 Introduction

Catalyst development for low-temperature natural-gas (NG) combustion has received significant attention because of the forecasted increase in NG-fuelled devices [1] and the need for efficient emission control of methane with a greenhouse gas potential exceeding that of CO_2 by 23 times [2]. There are many examples of methane emissions that encompass a wide range of conditions. For example, the increasing interest in NG-fuelled vehicles has increased demand for an effective catalyst that can oxidize methane in a lean wet environment. There are also numerous examples of fugitive CH_4 emission sources that are lean and dry. A large source of methane emissions is the vent gas from underground coal mines which are burned to produce heat [3]. The oil and gas industry also has many fugitive emission sources, including emissions from natural gas compressor stations and the vent gas from oil wells [2]. The volumetric efficiency and operating temperature range of current Pd-based catalysts require improvement for successful device commercialization, which promotes the search for suitable metal promoters and supports [2, 4].

The active chemical state of Pd in lean methane combustion has been a matter of debate. The turnover rates increased by an order of magnitude with a 3-fold increase of the Pd/PdO_x ratio as measured by NH_3-TPD, and the coexistence of metallic Pd with PdO was claimed as paramount [5]. However, a further ratio increase to 5 was found to be detrimental to catalytic activity [5]. Farrauto et al. showed the loss of activity when metallic Pd was formed under reducing reaction conditions [6]. The group of Iglesia reported [7] that the methane oxidation rate coefficients at

[2] Chapter 3 of the thesis has been published as "Platinum Inhibits Low-Temperature Dry Lean Methane Combustion via Palladium Reduction in Pd-Pt/Al_2O_3: An In Situ X-ray Absorption Study." H. Nassiri, K.-E. Lee, Y. Hu, R.E. Hayes, R.W.J. Scott, N. Semagina, ChemPhysChem. 18 (2017) 238-244. The paper is reprinted with the permission of co-authors. The reaction setup for methane oxidation was originally designed and built by Dr. Long Wu and Dr. Robert E. Hayes. The lab view program to communicate with the reaction setup was written by Les Dean. The NAA analysis was performed by Dr. John Duke at the University of Alberta. The in situ EXAFS was performed by Dr. Kee-Eun Lee under the supervision of Dr. Yongfeng Hu at Canadian Light Source and Dr. Robert W.J. Scott at the University of Saskatchewan. Part of the ex situ EXAFS was performed by the author under the technical support of Dr. Ning Chen at Canadian Light Source and Dr. Robert W.J. Scott. EXAFS data modeling was done by Dr. Kee-Eun Lee and Dr. Robert W.J. Scott. The author performed all the syntheses, catalytic reactions, analyses and other characterizations. Manuscript preparation and writing were conducted by the author under the supervision and final approval of Dr. Natalia Semagina, Dr. Robert E. Hayes, and Dr. Robert W.J. Scott.

various oxygen pressure at 700ºC are a single function of total oxygen content in Pd/Al_2O_3 catalysts with nanoparticle sizes from 1.8 to 8.8 nm. The conclusion was drawn from oxygen uptake and evolution measurements, methane combustion kinetic measurements and thermodynamic calculations. Using in situ extended X-ray absorption fine structure (EXAFS), Grunwaldt et al. detected the presence of metallic Pd on a Pd/ZrO_2 catalyst at 500-550ºC and suggested its beneficial effect, considering that the activity of pre-reduced catalyst was higher than that of the oxidized catalyst [8]. An operando Raman study of the Pd/Al_2O_3 catalyst in the 25-500ºC range detected only Pd oxide forming under reaction conditions [9], which is consistent with thermodynamic expectations and the kinetic investigation of Pd/ZrO_2 catalysts by Fujimoto et al. [10].The latter study explained the frequently reported requirement of the coexistence of Pd-PdO_x by a Mars-van Krevelen mechanism when CH_4 is activated on site pairs consisting of O atoms and O vacancies on the PdO_x surface. These vacancies can also be easily poisoned by water, which is known for its strong inhibitory effect on Pd-catalyzed methane combustion. Thus, the knowledge of the required chemical state of Pd under reaction conditions and the ability to control it, if necessary, is paramount to designing an efficient and stable NG combustion catalyst.

In the quest for a suitable promoter to enhance the performance of Pd in methane combustion, platinum has been extensively used [11-15]. Monometallic Pt is a poor methane combustion catalyst under lean conditions [16]. In an oxidative atmosphere, Pt on γ-alumina support is more susceptible to sintering than Pd; thus, in Pd-Pt formulations, Pd stabilizes Pt as a result of a strong interaction between PdO and the support [17, 18]. In bimetallic catalysts, the chemical states of Pd and Pt can be affected by their ratios, preparation methods, and catalyst support to enhance or suppress methane conversion [13, 15, 19-25]. The reactivities of Pd and Pt towards oxygen depend on the temperature and partial pressure of oxygen [7, 17, 26-29], metal support [27, 30] and nanoparticle size [7, 31]. In addition to metallic Pd and Pt, oxide species such as PdO, PdO_2, PtO, PtO_2 and Pt_3O_4 may be present [32-35]. In bimetallic catalysts, the formation of the mixed-oxide phases of $Pd_xPt_{1-x}O_y$ was shown via DFT calculations by Dianat et al. [35] The addition of Pt to Pd was suggested to stabilize the higher oxidation state of Pd. Oxygen-binding energy in the Pd-Pt catalysts was found to be higher on Pd-rich surfaces [36] because of the charge transfer from Pd to Pt atoms. The extent of Pd segregation to the surface after oxidative aging at 750ºC was found to be insignificant in one study [37] but was claimed to be important in another [38].

An improvement in the dissociation of methane and oxygen adsorption was suggested by Persson et al. [32] as the reason for the higher activity of bimetallic Pd-Pt catalysts as compared to monometallic Pd. Kinnunen et al. [11] believed that the proportions of metal and metal-oxide surface sites determine the catalytic activity when a small amount of Pt was necessary to enhance the low-temperature conversion, but a higher Pt content was detrimental due to the suppressed reoxidation of Pd. A thermogravimetric analysis of Pd, Pt and Pd-Pt catalysts in air showed that Pt stabilized Pd in its reduced form and shifted the onset of deactivation by PdO→Pd transformation to lower temperatures in the range of 850-950ºC, leading to lower intrinsic activity in lean-methane combustion [14]. At the same time, Pt improved the sintering resistance of Pd, which resulted in an overall beneficial effect on methane combustion at low Pt loadings (Pt mass fraction <10%) [14]. In line with these observations, an ex situ X-ray absorption study of Pd-Pt catalysts oxidized at 750 °C revealed that Pt helps Pd to maintain in its reduced form when only 20-30% of Pd was present in its oxide form [37].

The reported observations of the effect of Pt on Pd [14, 37] covered temperatures above 600ºC, which is beyond the range of interest for low-temperature methane combustion, and did not investigate the metal chemical states under the reaction conditions. The current work sheds light on the effect of Pt on Pd/PdO_x distribution in $Pd\text{-}Pt/Al_2O_3$ methane combustion catalysts in a low-temperature range of interest (200-550ºC) using an in situ X-ray absorption study and the effect of the reduced Pd in dry lean methane combustion.

3.2 Experimental section

3.2.1 Materials

Hexachloroplatinic (IV) acid (H_2PtCl_6, 8% w/v solution, Sigma-Aldrich), Pd (II) acetate ($Pd(AcO)_2$, Sigma-Aldrich), 1,4-dioxane (>99.9% Sigma-Aldrich), poly N-vinylpyrrolidone (PVP, average molecular weight of 40,000, Sigma-Aldrich), ethylene glycol (>99.9%, Fischer Scientific), gamma alumina (γ-Al_2O_3, average pore size 58 Å, specific surface area 155 m^2/g, 100 µm particle diameter, Sigma-Aldrich), and Pd oxide (PdO, 99.97% trace metal basis, Sigma-Aldrich) for the in situ EXAFS analysis were used as received. Milli-Q water (18.2 MΩ.cm) was used.

3.2.2 Catalyst preparation

Pd and Pt monometallic nanoparticles were synthesized by the one-step alcohol reduction method on the basis of 0.2 mmol metal. To synthesize Pt nanoparticles, H_2PtCl_6 and PVP with a molar ratio of 40 PVP to metal were added to a 500-ml flask and mixed with 80 vol.% ethylene glycol in a water solution. In the case of Pd nanoparticle synthesis, $Pd(AcO)_2$ was first dissolved in 10 ml of dioxane and then mixed with the aforementioned amount of PVP and solvent solution. The resulting mixture was stirred and heated until it boiled and then refluxed in air under vigorous stirring for 3 h to complete the synthesis of PVP-protected nanoparticles. Bimetallic Pd-Pt nanoparticles were synthesized with the co-reduction of metal precursors with the required molar ratios of Pd:Pt. The rest of the process was exactly the same as that of the monometallic nanoparticles. A dark colloidal was obtained at the end of synthesis without any precipitates. Nanoparticles were supported on γ-Al_2O_3 by acetone precipitation to obtain 0.3 wt.% metal loading. All samples were dried and calcined in air at 550ºC for 16 h. Hereafter, the catalyst after calcination that is ready for the reaction is referred to as the calcined (or oxidized) catalyst.

3.2.3 Catalyst characterizations

The metal loading on catalysts was determined by NAA. Samples were irradiated for 110 s in the Cd-shielded, epithermal site of the reactor core. They were counted for 30 min each on an Aptec CS11-A31C gamma detector approximately 12 h after irradiation. TEM photographs were taken with a JEOL-2100 TEM device operating at 200 kV. CO pulse chemisorption analysis was performed with an AutoChem 2920 instrument (Micromeritics, USA). Prior to this analysis, approximately 100 mg of the samples was reduced in 25 ml/min of 10% H_2 in Ar from room temperature to 550ºC at the rate of 20ºC/min. Then, pulse chemisorption was performed by dosing 3% CO in He at room temperature. The volumetric flow rates of CO in He loop gas and He carrier gas were adjusted to 25 ml/min. CO uptake per gram of pure support (γ-Al_2O_3) was also evaluated using 2 g of alumina, which was subtracted from the values for the supported catalysts. The deviation of CO chemisorption results for selected catalysts was 0.07 $mol_{CO}/mol_{surface\ metals}$.

In situ X-ray absorption (XAS) measurements were conducted at Canadian Light Source. Full in situ methane oxidation XAS measurements were performed for the Pd K-edge and Pt L_3-edge on

the Hard X-ray MicroAnalysis (HXMA) beamline. The energy range used for the Pd K-edge was from 24,050 eV to 25,400 eV. Pd K-edge experiments were conducted using a Si (220) monochromator crystal, Pt mirrors and ion chambers filled with an N_2/Ar gas mixture, while Pt L_3-edge spectra were collected using a Si (111) crystal and Rh mirrors. The samples were loaded into a six-shooter sample cell (Figure 3.1) as pressed pellets of alumina supports containing ca. 2 wt.% metal elements and data was collected in transmission mode. The entire setup for the in situ XAS measurements is depicted in Figure 3.2.

Figure 3.1 Six-shooter sample holder for in situ XAS data collection. The total diameter of the six shooter is 18 mm, and the diameter of each hole for the sample is 4 mm. The small hole at the top connects to the thermocouple, and the larger central hole is used for beam alignment

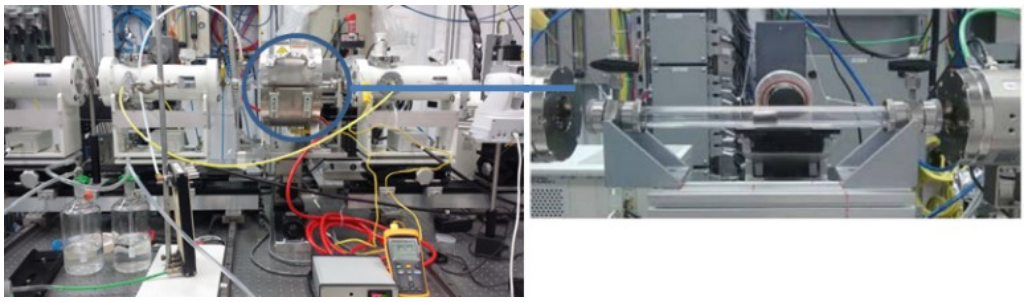

Figure 3.2 In situ methane oxidation setup at the HXMA beam line (left) and the sample holder in the quartz tube (right). The blue circled part is a small furnace for the in situ XAS measurements, and the sample holder within the quartz tube resides in the furnace

Initially, calcined monometallic and bimetallic samples (Pd and Pd-Pt 2:1) were measured, and then, in situ methane oxidation measurements were conducted. For reference compounds, Pd and Pt foils and PdO were analyzed. Two-dimensional mapping of the sample holder was conducted before the measurement to find the exact location of each sample. The range of mapping was ±15 mm from the zero point using the motorized set-up at the beam line. For methane oxidation

under dry conditions, 0.1% CH_4 in N_2 and compressed air (ultra-zero level, <2 ppm H_2O) were combined. The samples were incrementally heated from 200 to 500ºC under the flow of methane and air in dry conditions. The flow rates of CH_4/N_2 and compressed air used were 154 ml/min and 103 ml/min, respectively.

Linear combination fitting of normalized XANES μ(E) spectra was performed using the IFEFFIT software package [39]. The XANES spectra of PdO and the reduced Pd sample were used as reference materials representing the Pd(II) and Pd(0) species, respectively. Fits were performed on data at each temperature over the range of -25 to 65 eV around the absorption edges.

3.2.4 Catalytic performance in the methane combustion reaction

The methane combustion reaction was studied in a conventional tubular reactor over the monometallic Pd and Pt and bimetallic Pd-Pt nanocatalysts. The reduction of monometallic Pd catalysts was conducted at 350ºC for 2 hours under a hydrogen gas stream. The details of the reaction setup can be found in our group's previous studies [15, 40]. The reactor of 0.925 cm internal diameter was packed with catalysts corresponding to 1.2 mg of active Pd. In the case of the monometallic Pt catalyst, 1.2 mg of Pt were used. Then, a gas mixture of 10 vol.% CH_4 in nitrogen along with dry air was fed to the reactor at a flow rate of 8.5 ml/min and 205 ml/min, respectively, for a CH_4 concentration of ca. 4,000 ppm in the reactor. The composition of the product gas was analyzed by an online Agilent 7890A gas chromatograph equipped with TCD and FID detectors. In an ignition test, the temperature was increased stepwise from 200 to 500ºC at the rate of 3ºC/min and kept at each temperature for 30 min to investigate the catalytic performance in a heating ramp. Selected catalysts were repeated and methane combustion results reproduced within 2% error. Negligible conversion was obtained for the neat Al_2O_3 support up to 500ºC.

The methane conversion and kinetic parameters at 350ºC, as reported in Table 3.1 and Figure 3.5, were confirmed to represent intrinsic reaction conditions under isothermal reactor operation. In the most susceptible case of transport limitations for the most active Pd catalyst, Mears criterion for external mass transfer limitations (MTL) was found as 10^{-4} (no external MTL exist if the value is below 0.15) [41]. The Weisz-Prater criterion for internal MTL was found as 0.32 with the Knudsen diffusion-limited pore diffusion, which corresponds to the internal effectiveness factor of 0.97 for

a first-order reaction and, thus, negligible internal MTL [42]. The absence of external temperature gradient was confirmed by Mears correlation (value of 10^{-8} which is below the maximum limit of 0.15 for the negligible gradient) [41]. The maximum internal temperature rise was calculated using parameter β as 10^{-4} K assuming activation energy of 92 kJ/mol [43] and constant heat of combustion of -890 kJ/mol.

3.3 Results and discussion

Table 3.1 summarizes the range of synthesized Pd-Pt and monometallic catalysts supported on commercial γ-Al_2O_3 and their dispersions as determined from CO chemisorption. The catalyst notation is based on the molar ratio of the two metals and reflects the metal loadings as determined by neutron activation analysis (NAA). The samples were calcined in air at 550ºC for 16 h, which is a recommended commercial procedure preceding automotive catalytic converter testing for lean burn applications. For the dispersion determination, 1:1 stoichiometry of the adsorbed CO per surface mole of Pd and/or Pt was assumed.

Table 3.1 Characteristics of the synthesized catalysts supported on γ-Al_2O_3

Catalyst	Pd/Pt molar ratio	Pd loading,[a] wt.%	Pt loading,[a] wt.%	Dispersion,[b] %	CH_4 conversion at 350ºC, [c] %
Pd	-	0.2550	-	43	52
Pd-Pt 4:1	4	0.1780	0.0772	53	65
Pd-Pt 2:1	2	0.1520	0.1240	31	28
Pd-Pt 1:1	1	0.0875	0.1700	23	15
Pd-Pt 1:2	0.5	0.0659	0.1910	20	14
Pd-Pt 1:4	0.25	0.0328	0.2150	16	4
Pt	0	-	0.295	13	1

[a] as per NAA; [b] from CO chemisorption assuming 1:1 CO/metal stoichiometry; [c] Pd amounts in all tests were kept as 1.2 mg; 1.2 mg of monometallic Pt was used. Intrinsic kinetic regime in an isothermal operation at 350ºC was confirmed.

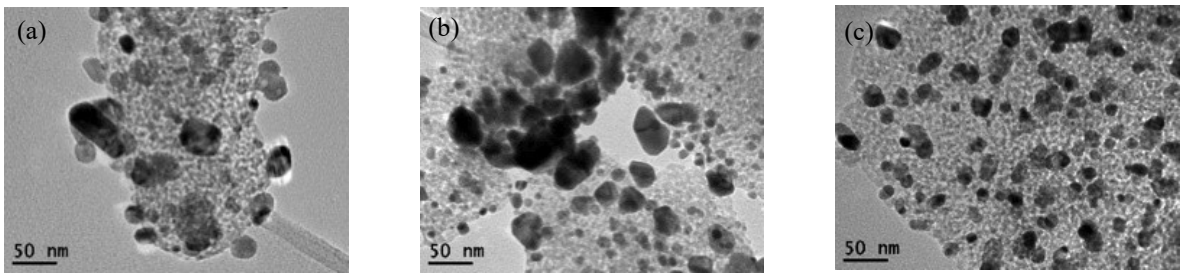

Figure 3.3 TEM images of the calcined supported catalysts: (a) Pd, (b) Pt, and (c) Pd-Pt 2:1

As expected [44], the addition of Pd to Pt prevented its excessive sintering, which also can be seen in the transmission electron microscopy (TEM) images of the calcined catalysts (Figure 3.3). The richer the catalysts in Pd content are, the lower the degree of sintering is.

The catalysts were tested in dry lean methane combustion, and the corresponding methane conversions in the temperature-programmed reactions are shown in Figure 3.4. Only the first ignition curve is reported for each catalyst, the duration of which is short enough as compared to the 16-h-long pre-calcination at 550ºC so that the effect of in situ restructurization may be considered negligible. The curve for monometallic pre-reduced Pd is not shown as it is identical to that of oxidized Pd within a 3% error. Monometallic Pt shows extremely low activity as compared to Pd; Pt is indeed known for efficient methane combustion only under fuel-rich conditions [16]. Because Pt showed very low activity, all tests with monometallic Pd and bimetallic Pd-Pt catalysts were performed at the same Pd loading in the reactor (1.2 mg). The methane conversions at 350ºC are also summarized in Table 3.1.

Obviously (Table 3.1 and Figure 3.4), the higher the Pd-Pt ratio is, the more efficient the combustion at lower temperatures is. As metal dispersions also increase with the ratio, a hypothesis on the negative effect of Pt due to larger particle size was verified by calculating catalyst activity per mole of surface Pd atoms because of its significantly higher activity than that of Pt. Assuming for now the structure-insensitive reaction, surface-normalized activities (turnover frequency, TOF) should stay constant per active component irrespective of nanoparticle size. For the calculation, first order to methane and zero order to oxygen were assumed [10], and the found rate constants were used to calculate the initial reaction rates at 350ºC (Figure 3.5).

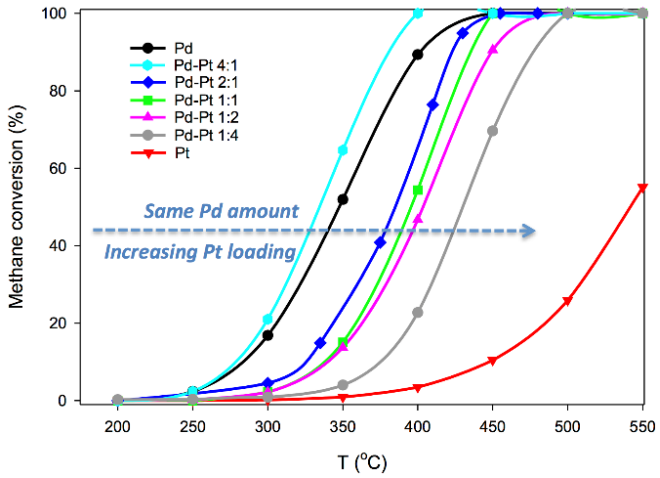

Figure 3.4 Ignition curves recorded in the dry lean methane combustion. Pd amounts in all tests were kept as 1.2 mg, except for monometallic Pt (also 1.2 mg). The curve for monometallic pre-reduced Pd is not shown as it is identical to that one of oxidized Pd, within 3% error. Ignition curves were obtained in a PBR (not XAS cell).

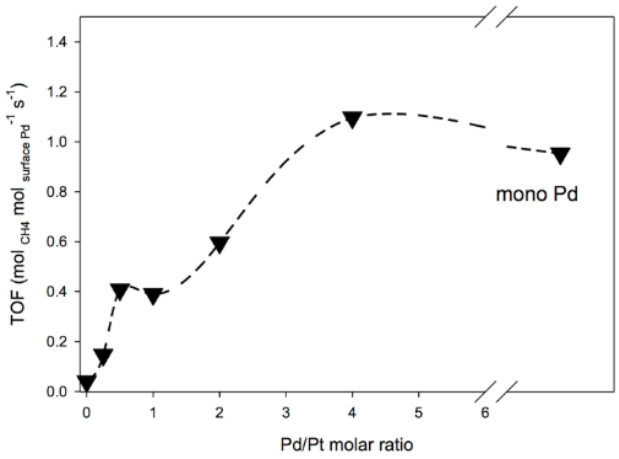

Figure 3.5 Initial turnover frequencies normalized per surface Pd atoms (or Pt for monometallic Pt) at 350ºC as a function of Pd/Pt ratio assuming the same surface and bulk composition

As seen in Figure 3.5, the surface-normalized activities drop by an order of magnitude with the increase in Pt content in the bimetallic catalysts, indicating that Pt does not simply dilute the active Pd surface. Pd-surface-normalized activities were calculated based on the assumption of the same surface Pd-Pt ratio as in the bulk. The extent of Pd segregation to the surface after oxidative aging

at 750ºC was found to be insignificant in one study [37] but was claimed to be important in the another [38]. If it happened, the decrease in Pd-surface-normalized activity with Pt addition would be even more dramatic.

Pd-catalyzed methane combustion is known as a structure-sensitive reaction, with a 65-fold increase in TOF with Pd dispersion decrease from 50% to 10% [27]. In this work, TOF for the monometallic Pd catalyst is the largest value, even though the dispersion in some Pd-Pt catalysts decreases to 16% upon Pt addition (Table 3.1). Thus, the effect of Pt addition cannot be explained by the reaction structure sensitivity either, which should bring about an increase rather than a decrease in TOF.

To shed light on the mechanism of the effect of Pt, an in situ X-ray absorption near edge structure (XANES) and EXAFS spectroscopy measurements were conducted for the monometallic Pd, Pt and Pd-Pt 2:1 catalysts, which represent the central point of the negative effect of Pt (Figures 3.4 and 3.5) with the dispersion (31%), which is rather similar to Pd (43%). The measurements were performed in a dry lean methane-air mixture (O_2/CH_4 molar ratio of 134, < 1 ppm H_2O) over a temperature range of 200 to 500ºC and compared to the standard materials (Pd and Pt foils and PdO). Figure 3.6 shows the Pd K-edge and Pt L_3-edge XANES spectra of the calcined Pd, Pt and Pd-Pt samples before the reaction. The Pd K-edge XANES probes the electronic transition from the 1s to 5p orbitals and is sensitive to both oxidation state and coordination environment of the Pd atoms [45]. The calcined Pd-Pt 2:1 sample compared well to that of the Pd foil, indicating that the majority of Pd is in the zero valent state. On the contrary, the spectrum of the calcined monometallic Pd sample resembled that of PdO, implying that Pd is mostly oxidized to Pd(II) in this sample. Thus, the presence of Pt in bimetallic Pd-Pt particles leads to the stabilization of Pd(0) in the particles towards oxidation, in agreement with what is already known for the calcined Pd-Pt systems [14, 37]. The Pt L_3-edge XANES spectra showed the same features between the Pt and Pd-Pt 2:1 samples, indicating that there is no difference in the oxidation state of Pt upon Pd addition.

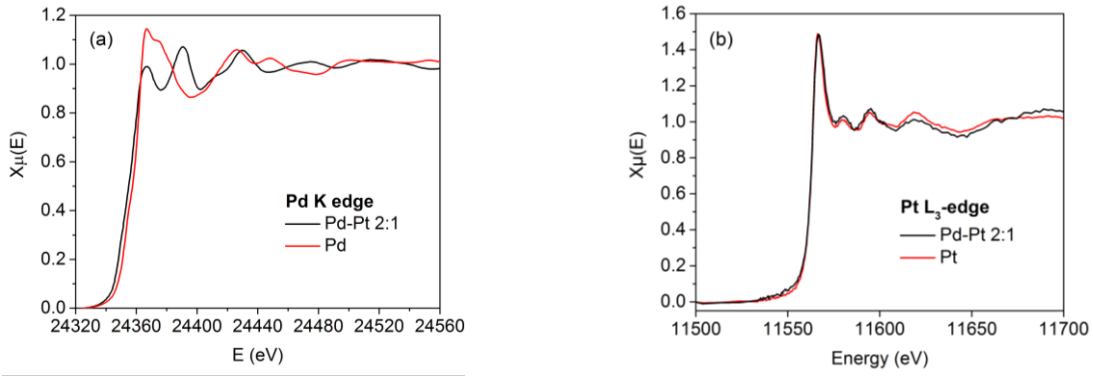

Figure 3.6 XANES spectra of calcined Pd, Pd-Pt 2:1, and Pt samples before methane combustion reaction: (a) Pd K-edge and (b) Pt L_3-edge

The in situ measurement under a CH_4/dry air mixture shows a substantial change in the speciation of Pd upon increases in temperature. The calcined Pd sample consisted only of PdO; thus, to compare it with the bimetallic catalyst containing mostly Pd(0), reduction of the monometallic Pd catalyst was conducted at 350ºC for 2 h under an H_2 gas stream. Figure 3.7 shows the Pd K-edge in E space for the supported Pd and Pd-Pt 2:1 under in situ CH_4/dry air conditions. The spectra were collected at incrementally increasing temperatures in methane/air flows. Upon increases in temperature, the Pd-Pt 2:1 sample slowly became more oxidized, whereas rapid oxidation was seen in the monometallic Pd sample. To understand the change in speciation of Pd in the Pd-Pt 2:1 and Pd samples, linear combination fitting using Pd(0) and PdO standards was performed at each temperature; the results are shown in Table 3.2 and Figure 3.8.

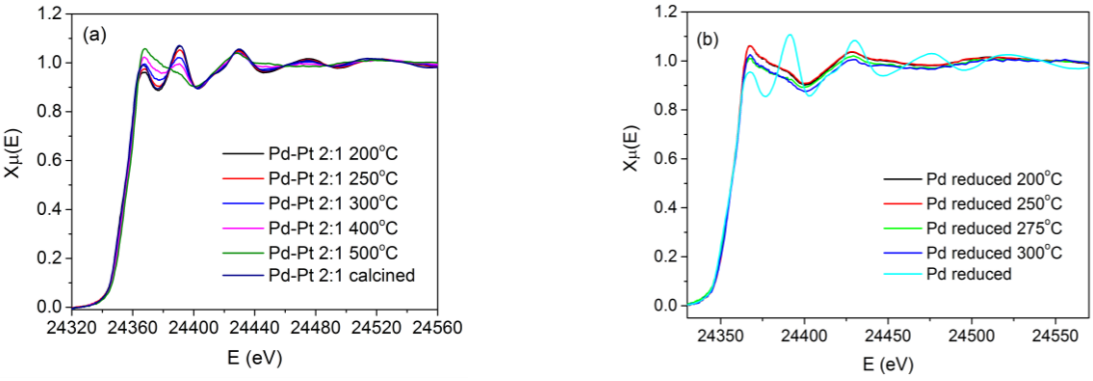

Figure 3.7 XANES spectra under CH_4/dry air conditions for: (a) calcined Pd-Pt 2:1 sample and (b) reduced Pd sample

Table 3.2 Linear combination fitting for Pd-Pt 2:1 sample in CH_4/dry air environment

Reaction temperature, °C	Pd(II) from PdO, wt.%	Pd(0), wt.%
Before reaction, calcined	< 2	> 98
200°C	4	96
250°C	16	84
300°C	37	63
400°C	62	38
500°C	90	10

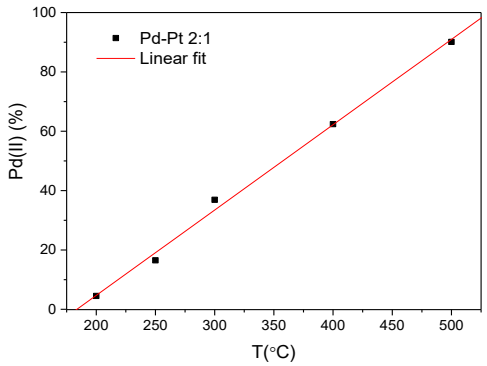

Figure 3.8 Linear combination fitting results of the Pd K-edge XANES spectra showing the percentage of PdO formed as a function of temperature in CH_4/dry air environment

The linear combination fitting shows that the Pd-Pt 2:1 sample was slightly oxidized at 200ºC under CH_4/dry air conditions, and the level of oxidation increased linearly up to 90% at 500ºC. Even at 500ºC, significant amounts of Pd(0) are still present in these particles. The Pd-Pt 2:1 sample still showed the metallic Pd feature with a slightly declined intensity and an edge shift, which was not observed in the Pd/Al_2O_3 sample. The EXAFS results below also verify that small amounts of Pd(0) are still present in the bimetallic sample. In the case of the reduced monometallic Pd sample, nearly complete Pd oxidation to PdO is seen at 200ºC, which was completed by 250ºC, and there were no further spectral changes beyond that temperature. It is known [46] that surface Pd oxidation is complete at room temperature and the bulk oxidation is diffusion limited and takes place at 200-700ºC. The ignition curve measured for the prereduced Pd catalyst was identical to

the oxidized catalyst as shown in Fig. 2 (within a 3% conversion variation as a typical measurement error), in agreement with the in situ X-ray absorption results.

Figure 3.9 shows the Fourier-transformed Pd K-edge EXAFS plot in R-space as a function of temperature for the Pd-Pt and reduced Pd samples under in situ CH_4/dry air condition. The peaks in the 1.9 Å to 2.5 Å range correspond to first-shell Pd-Pd and Pd-Pt contributions, whereas the peak at 1.5 Å corresponds to Pd-O first-shell contributions. For the Pd-Pt 2:1 sample, the amplitude of the Pd-Pd and Pd-Pt contributions decreases while a new Pd-O contribution emerges beyond 300ºC, which agrees well with the above linear-combination fitting data. Pt EXAFS data showed no changes over the entire temperature range examined (not shown). For the Pd K-edge data shown in Figure 3.9 (a), the intensity of the Pd-M peaks is reduced in amplitude and broadened at higher temperatures due to increased thermal disorder in the sample. As a consequence of this thermal broadening, it was not possible to fit EXAFS data accurately at various temperatures to extract quantitative coordination numbers for each of the Pd-O, Pd-Pd and Pd-Pt contributions. The Pd-Pt 2:1 sample at 500ºC shows a significant Pd-O contribution but still retains weak Pd-M contributions. In addition, a weak second-shell Pd-Pd contribution from PdO is seen at ca. 3 Å for the 500ºC bimetallic sample. Figure 3.9 (b) shows the Pd K-edge EXAFS plot in the R-space of the reduced monometallic Pd sample at various temperatures under CH_4/dry air conditions; beyond 200ºC, the EXAFS mainly shows the Pd-O first-shell contribution at 1.5 Å and a second-shell Pd-Pd contribution at 3.0 Å (due to PdO). This agrees with the above XANES data, which showed that the pure Pd sample is nearly completely oxidized by 200ºC.

Thus, the in situ X-ray absorption studies revealed that i) irrespective of Pd's initial reduced or oxidized state, only PdO exists at 200-500ºC under oxidative reaction conditions; ii) the state of Pt is not affected by the presence of Pd and does not change under reaction conditions; and iii) the Pd/PdO weight ratio in bimetallic Pd-Pt 2:1 catalysts decreases from 98/2 to 10/90 in the 200-500ºC range during the combustion.

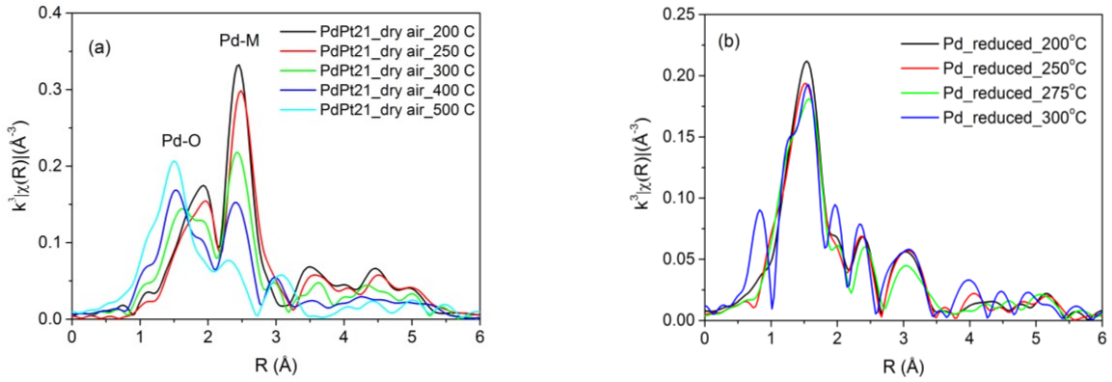

Figure 3.9 Pd K-edge EXAFS spectra in R-space for (a) Pd-Pt 2:1 and (b) reduced Pd in CH_4/dry air environment

Coupling these observations with the kinetic data indicating the negative effect of the addition of Pt to the performance of the Pd catalyst, which is not connected to surface dilution, size effect or structure sensitivity (Figures 3.4 and 3.5, Table 3.1), it follows that Pt promotes the formation of a reduced Pd phase, which is significantly less active than in the methane combustion reaction as opposed to the oxidized Pd. A similar negative effect of metallic Pd was reported earlier by Farrauto et al. [6], and the active oxidized Pd working state was also claimed in an operando Raman study [9]. Metallic Pd is characterized by higher activation barrier for C-H bond activation in methane as compared to PdO clusters [47]. The current study provides in situ evidence of the importance of oxidized Pd and its dependence on the co-presence of Pt for dry lean methane combustion in the 200-500ºC temperature range.

3.4 Conclusions

Pd-Pt/γ-Al_2O_3 catalysts with Pd/Pt molar ratios of 0.25 to 4 were studied in a dry lean methane combustion in the temperature range of 200-500ºC, along with monometallic Pt and oxidized and reduced monometallic Pd catalysts. The samples were pre-calcined at 550ºC for 16 h and assessed in the first ignition temperature-programmed reaction. The higher the Pt proportion, the lower the catalyst activity per gram of metal(s) and their surface proportion, as determined by CO chemisorption. The activity drop was too dramatic and could not be explained by the dispersion decrease or reaction structure sensitivity. In situ XANES and EXAFS spectroscopy measurements were conducted for monometallic Pd, Pt and Pd-Pt 2:1 catalysts. Monometallic Pd is fully oxidized

in the investigated temperature range, whereas the addition of Pt promotes Pd reduction even under the reactive oxidizing environment. The Pd/PdO weight ratio in bimetallic Pd-Pt 2:1 catalysts decreases from 98/2 to 10/90 in the 200-500ºC temperature range under reaction conditions. Thus, Pt promotes the formation of a reduced Pd phase, which is significantly less active in the methane combustion reaction as compared to the oxidized Pd. The study sheds light on the effect of Pt on the state of an active Pd surface under low-temperature dry lean methane combustion conditions, which is of importance for methane-emission control devices. Care should be exercised not to extrapolate these findings on the negative effect of Pt on Pd catalyst performance in methane-rich combustion, at different temperature ranges, in the presence of water in the feed (as in automotive converters) and long-term catalyst stability.

Acknowledgements

Financial support from NSERC (Strategic grant STPGP 430108-12), CFI (Leaders' Opportunity Fund, grant 24766) is appreciated. The X-ray absorption work was performed at the Canadian Light Source, which is supported by the Canadian Foundation for Innovation, Natural Sciences and Engineering Research Council of Canada, the University of Saskatchewan, the Government of Saskatchewan, Western Economic Diversification Canada, the National Research Council Canada, and the Canadian Institutes of Health Research. We thank Dr. John Duke (University of Alberta) for NAA, and Dr. Ning Chen for assistance with XAS measurements on the HXMA beamline.

3.5 References

[1] International Energy Outlook 2016, US energy information administration (EIA), 2016, pp. 1-276.

[2] R.E. Hayes, Chem. Eng. Sci. 59 (2004) 4073-4080.

[3] S. Su, J. Agnew, Fuel 85 (2006) 1201-1210.

[4] M. Cargnello, J.J.D. Jaén, J.C.H. Garrido, K. Bakhmutsky, T. Montini, J.J.C. Gámez, R.J. Gorte, P. Fornasiero, Science 337 (2012) 713-717.

[5] N.M. Kinnunen, J.T. Hirvi, T. Venäläinen, M. Suvanto, T.A. Pakkanen, Appl. Catal. A: Gen. 397 (2011) 54-61.
[6] R.J. Farrauto, M.C. Hobson, T. Kennelly, E.M. Waterman, Appl. Catal. A: Gen. 81 (1992) 227-237.
[7] Y.-H. Chin, M. Garcia-Dieguez, E. Iglesia, J. Phys. Chem. C 120 (2016) 1446-1460.
[8] J.-D. Grunwaldt, M. Maciejewski, A. Baiker, Phys. Chem. Chem. Phys. 5 (2003) 1481-1488.
[9] O. Demoulin, M. Navez, E.M. Gaigneaux, P. Ruiz, A.-S. Mamede, P. Granger, E. Payen, Phys. Chem. Chem. Phys. 5 (2003) 4394-4401.
[10] K.I. Fujimoto, F.H. Ribeiro, M. Abalos-Borja, E. Iglesia, J. Catal. 179 (1998) 431-442.
[11] N.M. Kinnunen, J.T. Hirvi, M. Suvanto, T.A. Pakkanen, J. Mol. Catal. A: Chem. 356 (2012) 20-28.
[12] A. Ersson, H. Kušar, R. Carroni, T. Griffin, S. Järås, Catal. Today 83 (2003) 265-277.
[13] G. Lapisardi, L. Urfels, P. Gélin, M. Primet, A. Kaddouri, E. Garbowski, S. Toppi, E. Tena, Catal. Today 117 (2006) 564-568.
[14] R. Strobel, J.-D. Grunwaldt, A. Camenzind, S.E. Pratsinis, A. Baiker, Catal. Lett. 104 (2005) 9-16.
[15] R. Abbasi, L. Wu, S.E. Wanke, R.E. Hayes, Chem. Eng. Res. Des. 90 (2012) 1930-1942.
[16] E. Becker, P.-A. Carlsson, H. Grönbeck, M. Skoglundh, J. Catal. 252 (2007) 11-17.
[17] C.F. Cullis, B.M. Willatt, J. Catal. 83 (1983) 267-285.
[18] C.H. Bartholomew, Studies in Surface Science and Catalysis, in: B. Delmon, G.F. Froment (Eds.), Catalyst Deactivation 1994, Esevier 1994, p. 1.
[19] C. Micheaud, P. Marécot, M. Guérin, J. Barbier, Appl. Catal. A: Gen. 171 (1998) 229-239.
[20] H. Yamamoto, H. Uchida, Catal. Today 45 (1998) 147-151.
[21] K. Persson, A. Ersson, K. Jansson, N. Iverlund, S. Järås, J. Catal. 231 (2005) 139-150.
[22] K. Narui, H. Yata, K. Furuta, A. Nishida, Y. Kohtoku, T. Matsuzaki, Appl. Catal. A: Gen. 179 (1999) 165-173.
[23] Y. Deng, T.G. Nevell, Catal. Today 47 (1999) 279-286.
[24] K. Persson, A. Ersson, S. Colussi, A. Trovarelli, S.G. Järås, Appl. Catal. B: Environ. 66 (2006) 175-185.
[25] Y. Ozawa, Y. Tochihara, A. Watanabe, M. Nagai, S. Omi, Appl. Catal. A: Gen. 259 (2004) 1-7.

[26] P. Gélin, M. Primet, Appl. Catal. B: Environ. 39 (2002) 1-37.
[27] Y.-H. Chin, D.E. Resasco, Catalysis 14 (1999) 1-39.
[28] Z. Li, G.B. Hoflund, J. Nat. Gas Chem. 12 (2003) 153-160.
[29] C.B. Alcock, G.W. Hooper, Proc. R. Soc. Lond. A 254 (1960) 551-561.
[30] H. Zhang, M. Jin, Y. Xia, Chem. Soc. Rev. 41 (2012) 8035-8049.
[31] R.F. Hicks, H. Qi, M.L. Young, R.G. Lee, J. Catal. 122 (1990) 280-294.
[32] K. Persson, A. Ersson, K. Jansson, J.L.G. Fierro, S.G. Järås, J. Catal. 243 (2006) 14-24.
[33] K. Persson, K. Jansson, S.G. Järås, J. Catal. 245 (2007) 401-414.
[34] A. Maione, F. André, P. Ruiz, Appl. Catal. B: Environ. 75 (2007) 59-70.
[35] A. Dianat, N. Seriani, M. Bobeth, W. Pompe, L.C. Ciacchi, J. Phys. Chem. C 112 (2008) 13623-13628.
[36] A. Dianat, J. Zimmermann, N. Seriani, M. Bobeth, W. Pompe, L.C. Ciacchi, Suf. Sci. 602 (2008) 876-884.
[37] T.R. Johns, J.R. Gaudet, E.J. Peterson, J.T. Miller, E.A. Stach, C.H. Kim, M.P. Balogh, A.K. Datye, ChemCatChem 5 (2013) 2636-2645.
[38] A. Morlang, U. Neuhausen, K.V. Klementiev, F.-W. Schütze, G. Miehe, H. Fuess, E.S. Lox, Appl. Catal. B: Environ. 60 (2005) 191-199.
[39] B. Ravel, M. Newville, J. Synchrotron Radiat. 12 (2005) 537-541.
[40] J. Shen, R.E. Hayes, X. Wu, N. Semagina, ACS Catal. 5 (2015) 2916-2920.
[41] H.S. Fogler, Elements of chemical reaction engineering, 4th ed., Pearson Education Inc.2006.
[42] M.A. Vannice, Kinetics of catalytic reactions, Springer, New York, 2005.
[43] F.H. Ribeiro, M. Chow, R.A. Dalla, J. Catal. 146 (1994) 537-544.
[44] C. Carrillo, T.R. Johns, H. Xiong, A. DeLaRiva, S.R. Challa, R.S. Goeke, K. Artyushkova, W. Li, C.H. Kim, A.K. Datye, J. Phys. Chem. Lett. 5 (2014) 2089-2093.
[45] J.L. DuBois, P. Mukherjee, T.D.P. Stack, B. Hedman, E.I. Solomon, K.O. Hodgson, J. Am. Chem. Soc. 122 (2000) 5775-5787.
[46] T.E. Hoost, K. Otto, Appl. Catal. A: Gen. 92 (1992) 39-58.
[47] C.B. Y.-H. Chin, M. Neurock, E. Iglesia, J. Am. Chem. Soc. 135 (2013) 15425-15442.

Chapter 4. Water shifts PdO-catalyzed lean methane combustion to Pt-catalyzed rich combustion in Pd-Pt catalysts: In situ X-ray absorption spectroscopy[3]

4.1 Introduction

Nature's way to extinguish fires with rain, blocking oxygen access to combustible material, manifests itself similarly in flameless catalytic combustion. The current work deals with Pd-containing catalysts used for lean methane combustion in a wet atmosphere at temperatures of 300-500ºC, which occur in catalytic converters aimed at reducing methane emissions from natural-gas fuelled vehicles (NGV). When water is present in the feed, the activity of supported Pd catalysts decreases at temperatures below 450ºC [1-8], which has been assigned either to the formation of inactive $Pd(OH)_2$ [4, 9-15] or hydroxyl/water accumulation on the support that hinders oxygen mobility and exchange and impedes combustion [16, 17].

One of the ways to diminish the negative effect of water is to introduce a platinum promoter [2, 3, 18], which is also used commercially in automotive three-ways catalysts to oxidize CO and hydrocarbons in the exhaust. Compared to the monometallic Pd catalyst, the activity loss of Pd-Pt bimetallic catalysts is less severe in the presence of water [2, 19-21]. Ex situ catalyst characterization techniques have mostly been reported, with no mechanistic studies of the water effect on the Pd-Pt catalysts at temperatures of practical interest (300-500ºC). In situ infrared spectroscopy has indicated that lower hydroxyl concentrations are present on the supported Pd-Pt catalysts compared to Pd, but the analyses were performed at 200ºC [20]. It was suggested that the

[3] Chapter 4 of the thesis has been published as "Water shifts PdO-catalyzed lean methane combustion to Pt-catalyzed rich combustion in Pd-Pt catalysts: In situ X-ray absorption spectroscopy." H. Nassiri, K.-E. Lee, Y. Hu, R.E. Hayes, R.W.J. Scott, N. Semagina, J. Catal. 352 (2017) 649-656. The paper is reprinted with the permission of co-authors. The reaction setup for methane oxidation was originally designed and built by Dr. Long Wu and Dr. Robert E. Hayes. The lab view program to communicate with the reaction setup was written by Les Dean. The NAA analysis was performed by Dr. John Duke at the University of Alberta. The in situ EXAFS was performed by Dr. Kee-Eun Lee under the supervision of Dr. Yongfeng Hu at Canadian Light Source and Dr. Robert W.J. Scott at the University of Saskatchewan. Part of the ex situ EXAFS was performed by the author under the technical support of Dr. Ning Chen at the Canadian Light Source and Dr. Robert W.J. Scott. EXAFS data modeling was done by Dr. Kee-Eun Lee and Dr. Robert W.J. Scott. The author performed all the syntheses, catalytic reactions, analyses and other characterizations. The literature review and preparation of the first draft of the manuscript were conducted by the author. Dr. Natalia Semagina performed the final manuscript writing. The work is conducted under the supervision and final approval of Dr. Natalia Semagina, Dr. Robert E. Hayes, and Dr. Robert W.J. Scott.

Pd-Pt catalyst is less affected by hydroxyl formation because it has other ways of methane activation, rather than on PdO [20]. In a study of alternated CH_4 lean combustion/CH_4-reducing wet pulses over Pd-Pt catalysts, the difference between Pd and bimetallic catalysts was attributed to the likely ability of metallic Pt to activate methane under net reducing conditions, which was suppressed under net oxidizing conditions [18]. The effect of water presence, however, was not evaluated.

The current study investigates the effect of water in the feed on Pd and Pt species in a bimetallic Pd-Pt/Al_2O_3 catalyst during lean methane combustion by means of in situ X-ray absorption spectroscopy (XAS). It suggests the mechanism by which the bimetallic catalyst shows an improved performance in the wet feed compared to the monometallic Pd under practically relevant temperatures (300-500ºC).

4.2 Experimental methods

A detailed description of the materials and catalyst syntheses can be found in our earlier work [22]. Pd nanoparticles were synthesized from palladium acetate in a colloidal dispersion in the presence of poly N-vinylpyrrolidone using an alcohol-reduction method. Pt nanoparticles were prepared similarly from hexachloroplatinic (IV) acid. Bimetallic Pd-Pt nanoparticles were synthesized by co-reduction of the metal precursors with molar ratio of Pd:Pt 2:1. The nanoparticles were deposited on γ-Al_2O_3, followed by calcination in air at 550ºC for 16 h. Final metal loadings were determined by neutron activation analysis (NAA). CO chemisorption was performed on the catalysts after reduction as described earlier [22]. For the calculation of dispersion and active particle diameter (hemisphere), stoichiometric factors for CO adsorption were assumed to be 1:1 for CO:Pd and CO:Pt. The deviation of CO chemisorption results for selected catalysts was 0.07 $mol_{CO}/mol_{surface\ metals}$.

In situ XAS measurements were conducted at the Canadian Light Source for the Pd K-edge and Pt L_3 edge on the HXMA (Hard X-ray Micro Analysis) beamline. X-ray absorption near edge structure (XANES) and extended X-ray absorption fine structure (EXAFS) analyses were performed. The detailed description and photographs of the catalyst sample holder and the set-up for the in situ analysis can be found in our earlier publication [22]. For reference compounds, Pd

and Pt foils, $Pd(OH)_2$ (palladium hydroxide on carbon, 20 wt.% loading, Sigma-Aldrich) and PdO (99.97% trace metal basis, Sigma-Aldrich) were analyzed. To evaluate the change in the Pd/PdO speciation, the calcined Pd-containing catalysts were reduced at 350ºC for 2 h in H_2 before the in situ XANES temperature-programmed analysis, unless stated otherwise. For methane oxidation under dry conditions, 0.1% CH_4 in N_2 and compressed air (ultra-zero level, <2 ppm H_2O) were combined. In the case of wet conditions, bubblers were connected to the compressed air to produce saturated water vapor at 101 kPa atmospheric pressure, which corresponds to 2.3 vol.% water in the feed. For dry and wet air conditions, the samples were incrementally heated from 200 to 600ºC under the flow of methane and air. The sample was held at each temperature for 30 minutes while measurements were taken at that temperature. The flow rates of CH_4/N_2 and compressed air used were 154 and 103 mL/min, respectively. Linear combination fitting of normalized XANES μ(E) spectra was performed with the Athena program, using Pd foil, PdO, and $Pd(OH)_2$ standards. The software package IFEFFIT was used for data processing [23]. The EXAFS fitting was performed in k-space between 2-14 $Å^{-1}$ and in R-space between 1.2-3.0 Å for the Pd-edge using theoretical phase-shifts and amplitudes generated by FEFF. Face-centered cubic (fcc) bulk lattice parameters (i.e., first shell coordination numbers of 12) were used to determine the amplitude reduction factor, S_o^2, for Pd (0.93) by analyzing Pd reference foil. A homogeneous Pd-Pt alloy model for FEFF fitting was constructed based on bulk Pd-Pt lattice parameters.

Catalytic performance in methane combustion reaction was evaluated in a tubular reactor at atmospheric pressure with online GC analysis, as described previously [22, 24, 25]. Pd and Pd-Pt catalyst amounts in the lean combustion corresponded to 1.2 mg Pd loading in the reactor, and 1.2 mg Pt loading for the monometallic Pt catalyst. The methane-lean feed consisted of a gas mixture of 10 vol.% CH_4 in N_2 (8.5 ml/min standard temperature and pressure (STP)) and dry or wet (5 vol.% water) air (205 ml/min STP), for a CH_4 concentration of approximately 4000 ppm in the feed. Water was pumped through the reactor by a Series II Legacy HPLC pump. The reactor temperature was increased stepwise from 200 to 550ºC at the rate of 3ºC/min and kept at each temperature for 30 min to investigate the catalytic performance in a heating ramp (ignition test). These conditions correspond to the data points measured during the in situ XAS. When indicated, the catalysts were reduced in situ prior to the reactions at 350ºC for 2 h in hydrogen. Selected

catalysts were repeated and methane combustion results reproduced within 2% error. Negligible conversion was obtained for the neat Al_2O_3 support up to 550ºC.

The ignition tests in the dry methane-rich feed were conducted at the methane-to-oxygen stoichiometric ratio of 1:1, which is below the stoichiometric 1:2 ratio. Pd and Pd-Pt catalyst amounts corresponded to 0.6 mg Pd loading in the reactor, and 0.6 mg Pt loading for the monometallic Pt catalyst. The methane-rich feed consisted of a gas mixture of 10 vol.% CH_4 in N_2 (8.5 ml/min STP) and 2 vol.% O_2 in N_2 (42.5 ml/min STP). All the gas mixtures (Praxair) were certified.

4.3 Results

4.3.1 Catalytic performance in the lean feed

Figure 4.1 shows the ignition curves obtained with Pd, Pt and Pd-Pt catalysts in the feed with and without added 5 vol.% water. Catalysts amounts corresponded to 1.2 mg of Pd in the Pd and Pd-Pt catalysts and 1.2 mg of Pt in the Pt-only catalyst. In the dry feed, reduced monometallic Pd and Pd-Pt catalysts (350ºC for 2 h in H_2) were found to show the behavior identical to the calcined-only samples with 3% deviation in methane conversion. Palladium is known for its higher activity in lean methane combustion compared to platinum [26-28]. In the dry feed, the Pd-Pt bimetallic catalyst exhibited lower activity than monometallic Pd, which was assigned to the increased fraction of inactive Pd(0) vs. active PdO in the presence of Pt [22]. However, Pt-containing catalysts were not significantly affected by the water addition to the stream, whereas Pd was poisoned (Figure 4.1), which is line with earlier findings by other groups on the beneficial effect of the addition of Pt to Pd for wet combustion [2, 3, 19-21]. Reduced Pd catalyst, when exposed to the wet feed, exhibited even lower conversion than its calcined form.

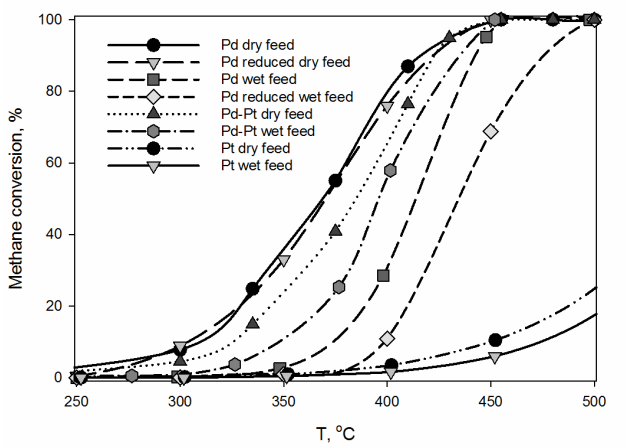

Figure 4.1 Ignition curves in the dry and wet lean methane combustion. Catalyst amounts correspond to 1.2 mg Pd in Pd-containing catalysts and 1.2 mg in the Pt only catalyst. The catalysts were calcined prior to the reactions, unless otherwise stated. Ignition curves were obtained in a PBR (not XAS cell).

CO chemisorption performed on the catalysts before and after the catalytic tests showed that the Pd catalyst maintained its 1.7-nm Pd particle size, whereas Pt sintered from 5.7 to 9.1 nm particles; and the bimetallic catalyst showed a relatively insignificant particle increase from 2.5 to 2.7 nm (Table 4.1). Platinum is known for its low thermal stability, which can be improved by the addition of palladium [29, 30]. Thus, the observed drop in activity for Pd catalyst cannot be explained by a potential loss in active surface area.

Table 4.1 Characteristics of the alumina-supported catalysts.

Samples	Pd loading, wt.%	Pt loading, wt.%	CO uptake, μmol/$g_{catalyst}$		Metal(s) dispersion, %	Active particle diameter, nm	
			Calcined catalyst	Used catalyst	Calcined catalyst	Calcined catalyst	Used catalyst
Pd	0.2550	-	9	10	57	1.9	1.8
Pt	-	0.2950	3	2	20	5.7	9.1
Pd-Pt	0.1520	0.1240	7	6	45	2.5	2.7

Turnover frequencies (TOFs) were calculated for the reactions under wet conditions at 340ºC for a differential reactor performance (for methane conversions below 8%). Verification of the kinetic regime is provided in the Supporting Information [24, 31-38]. TOFs for Pd and Pd-Pt catalysts

were found as 1.5 and 6.4 mmol/($mol_{surface\ atoms}$·s), while monometallic Pt showed a negligible activity. As will be shown in Section 4.3.3, the in situ EXAFS confirmed that the original Pd-Pt calcined sample had an alloy structure, and no segregation of Pd and Pt was seen up to 300ºC upon heating in the wet feed (the EXAFS modeling above 300ºC was not performed due to significant broadening of the EXAFS oscillations at high k values). Similarly, Pd segregation to the surface of Pd-Pt catalysts after oxidative ageing at 750ºC was found to be insignificant [39].

Thus, the addition of Pt to the Pd catalyst significantly increases the catalyst's surface activity under wet conditions. This trend is opposite to what we found earlier for dry methane combustion [22] when platinum decreased the surface activity of Pd by promoting the formation of less active metallic palladium compared to the active PdO. The improved activity of the bimetallic samples in the wet feed could not be assigned to Pd segregation to the surface. The presence of water likely affected the distribution of active sites or their functions, as explored below using in situ X-ray absorption spectroscopy.

4.3.2 In situ XAS in dry and wet lean feed: monometallic catalysts

Pd K-edge XANES spectra for Pd/Al_2O_3 recorded in situ during dry and wet methane combustion at different reaction temperatures are shown in Figures 4.2 (a) and 4.2 (b), respectively. Palladium species in XANES of calcined fresh Pd/Al_2O_3 catalyst were identified as PdO (as seen in our previous work [22]) that remained the only phase in the studied temperature range in the dry feed. The linear combination fitting was attempted using PdO, $Pd(OH)_2$ and Pd standards. Due to the similarity of the XANES spectra of PdO and $Pd(OH)_2$ (see Supporting Information for the spectra), it was impossible to specify the state of the oxidized Pd in the wet conditions based on the XANES data. To evaluate the change in the Pd/PdO speciation, the calcined Pd/Al_2O_3 catalyst was reduced at 350ºC for 2 h in H_2 before the in situ XANES temperature-programmed analysis. In the dry feed, the reduced Pd was almost completely oxidized by 200ºC, whereas in the wet feed, metallic Pd(0) progressively changed to an oxidized state with the increase in reaction temperature (Table 4.2, Figures 4.2 (b) and 4.3). Figures 4.4 (a) and 4.4 (b) show the Fourier-transformed Pd K-edge EXAFS oscillation in R-space under the CH_4/ air environments, which confirmed the immediate appearance of only Pd-O contributions at around 1.5 Å at 200ºC in the dry feed, while the wet feed gradually showed a decreased Pd-Pd contribution and increased Pd-O contribution with the

temperature increase. The Pt/Al_2O_3 catalyst in dry and wet conditions remained in its metallic form at all studied temperatures, as shown in Figure 4.5.

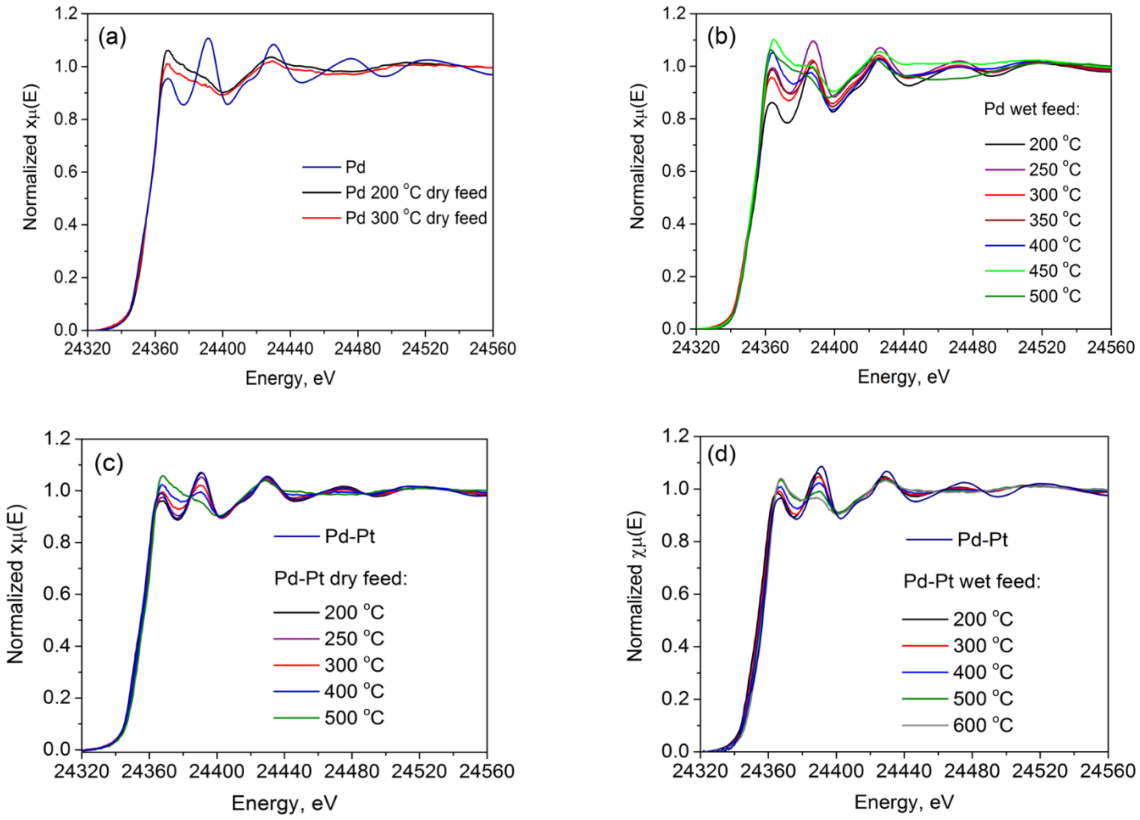

Figure 4.2 In situ XANES spectra demonstrating Pd K-edge for reduced Pd catalyst in dry (a) and wet (b) feed and Pd-Pt catalyst in dry (c) and wet (d) feed. Figures 4.2 (a) and 4.2 (c) are reprinted by permission of John Wiley & Sons, Inc. from [22].

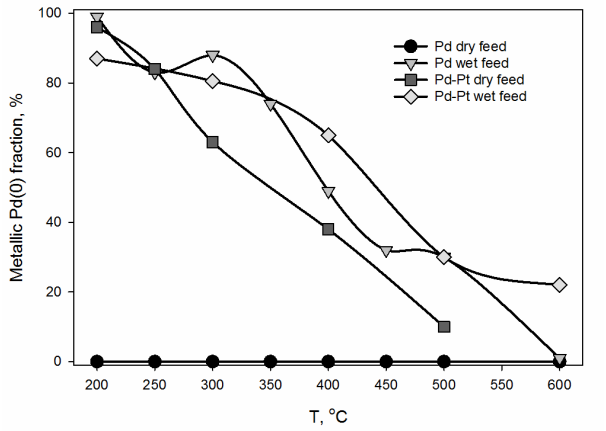

Figure 4.3 Linear combination fitting for the fraction of metallic Pd in the dry and wet feed. One standard deviation is <2%.

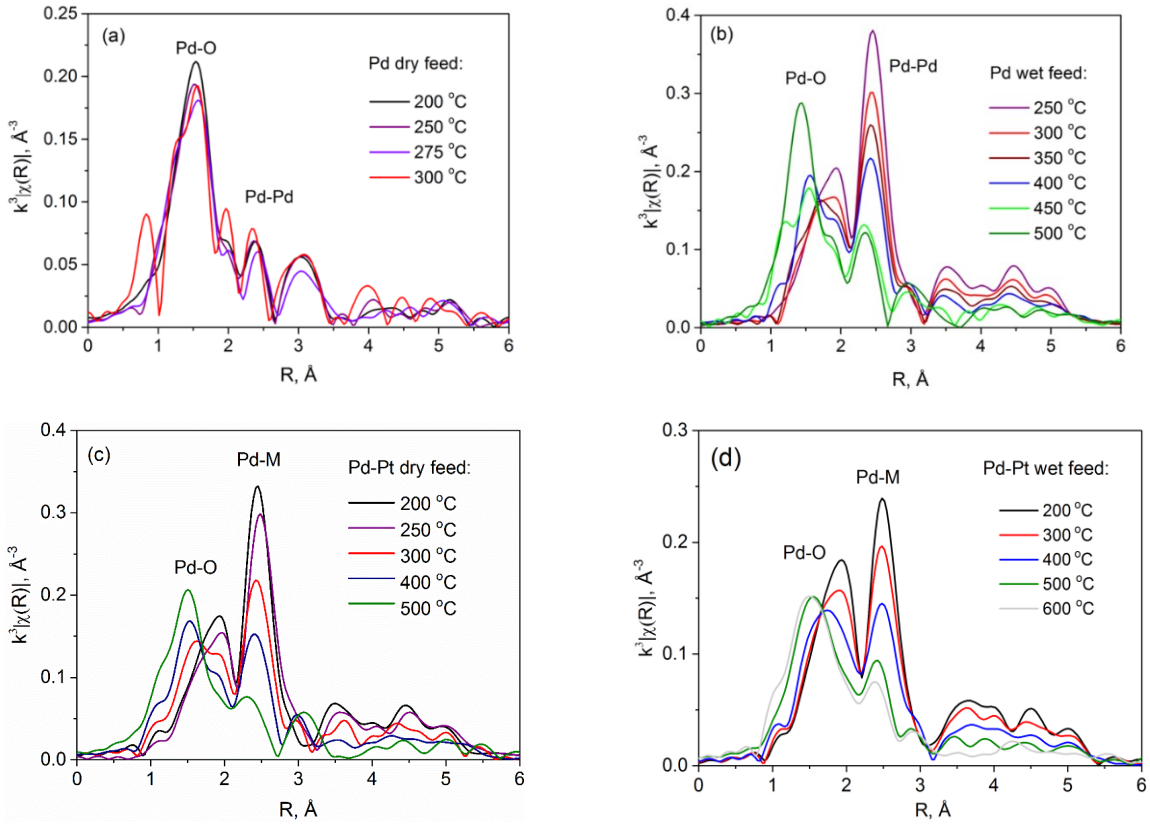

Figure 4.4 Pd K-edge EXAFS spectra in R-space for reduced Pd catalyst in dry (a) and wet (b) feed and Pd-Pt catalyst in dry (c) and wet (d) feed. Figures 4.4 (a) and 4.4 (c) are reprinted by permission of John Wiley & Sons, Inc. from [22].

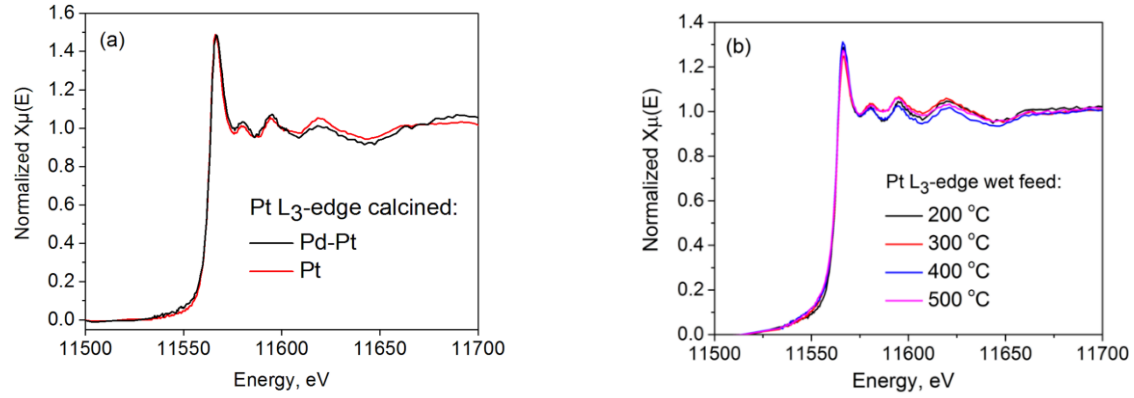

Figure 4.5 XANES Pt L_3-edge in calcined catalysts (a) and in wet feed (b) for monometallic Pt and bimetallic Pd-Pt catalysts. Figure 4.5 (a) is reprinted by permission of John Wiley & Sons, Inc. from [22].

Table 4.2 Linear combination fitting for Pd/Al_2O_3 in the wet feed*. Standard deviations are 1-2%.

Temperature	Standard materials for fitting	
	PdO**, Pd wt.%	Pd(0), Pd wt.%
200 °C	<2	>98
250 °C	17	83
300 °C	12	88
350 °C	26	74
400 °C	51	49
450 °C	68	32
500 °C	70	30
600 °C	100	<1

* in the dry feed, Pd was completely oxidized starting at 200ºC; ** due to the similar Pd edge in PdO and $Pd(OH)_2$ standards, it was impossible to specify the state of the oxidized Pd.

4.3.3 In situ XAS in dry and wet lean feed: bimetallic Pd-Pt catalyst

Pd K-edge XANES spectra for bimetallic Pd-Pt catalyst recorded in situ during dry and wet methane combustion at different reaction temperatures are shown in Figures 4.2 (c) and 4.2 (d). The linear combination fitting was performed using Pd, PdO and $Pd(OH)_2$ standards, which gave better fits than Pd and PdO alone. The fitting results obtained with the two sets of standards are shown in Table 4.3. Although it was impossible to decouple accurately the contribution of PdO and $Pd(OH)_2$, for both fitting methods, the metallic Pd(0) contents were similar in the wet feed with the largest discrepancy at 400ºC as 59% - 71%, which is within 6% deviation from the 65% average. The fitting results in terms of metallic Pd content are visualized in Figure 4.3 (the data for bimetallic catalyst in the wet feed were averaged between the two sets of fittings). The presence of water increases the fraction of metallic Pd both for monometallic and bimetallic catalysts. Figures 4.4 (c) and 4.4 (d) show the Fourier-transformed Pd K-edge EXAFS oscillation in the R-space under CH_4/ air environments. Both in the dry and wet conditions, a Pd-O contribution emerges around 1.5 Å at higher temperatures, whereas the Pd-M (where metal M is either Pt or

Pd) contributions at 1.9-2.5 Å decrease in amplitude and become broader upon temperature increases, which agrees with XANES data and confirms the presence of metallic Pd at high temperatures for all conditions and samples, apart from the monoPd catalyst in dry conditions in its oxidized state. EXAFS modelling confirmed that the as-synthesized Pd-Pt bimetallic catalysts had random alloy structures, with significant Pd-Pd and Pd-Pt contributions (Table 4.S2 in the Supporting Information) [40]. Upon heating in the wet feed, no segregation of Pd and Pt was seen up to 300ºC. At temperatures beyond 300ºC, we were unable to model the EXAFS data, as high levels of thermal disorder at higher temperatures led to significant broadening of the EXAFS oscillations at high k values.

The platinum component in the bimetallic catalyst remained in its metallic form at all temperatures in dry and wet conditions, similarly to monometallic Pt/Al_2O_3 (Figure 4.5).

Table 4.3 Linear combination fittings for the $Pd\text{-}Pt/Al_2O_3$ catalyst in the wet and dry feed using two sets of standard materials for the wet-feed data analysis. Standard deviations are 1-2%.

Temperature	Wet feed, fitting with $Pd(OH)_2$, PdO and Pd*			Wet feed, fitting with PdO and Pd		Dry feed, fitting with PdO and Pd	
	PdO, Pd wt.%	$Pd(OH)_2$, Pd wt.%	Pd(0), Pd wt.%	PdO, Pd wt.%	Pd(0), Pd wt.%	PdO, Pd wt.%	Pd(0), Pd wt.%
fresh	0	0	100	<2	>98	<2	>98
200 °C	0	13	87	13	87	4	96
300 °C	0	17	83	21	78	37	63
400 °C	0	29	71	41	59	62	38
500 °C	70	0	30	70	30	90	10
600 °C	78	0	22	78	22	-	-

* due to the similar Pd edge in PdO and $Pd(OH)_2$ standards, it is impossible to decouple the contribution of the oxide and hydroxide accurately. XANES data below 500ºC were fitted with $Pd(OH)_2$, which is assumed to decompose above 450ºC [10].

4.4 Discussion

4.4.1 Monometallic Pd and Pt catalysts

In the dry feed, the monometallic Pd catalyst was completely oxidized to PdO in 200-600ºC range, irrespective of initial Pd state (calcined or reduced), according to the reaction R1:

R1) $Pd + ½\ O_2 \rightleftharpoons PdO$ $\Delta H^o_{298} = -119$ kJ/mol

At any given temperature, there is a unique value of oxygen partial pressure, above which the Pd oxidation occurs given by the equation (1) [41]:

$$p_{O_2}^{0.5}(1\ atm)^{-0.5} = exp\left(-\frac{11273}{T\ (K)} - 2.89log_{10}(T) + 18.57\right) \quad (1)$$

The plot of the equilibrium oxygen pressure for Pd→PdO phase transformation as a function of temperature is shown in Figure 4.6. In the studied temperature range at the bulk fluid O_2 partial pressure of 21 kPa, PdO is expected and is in line with XAS for dry methane combustion on monometallic Pd catalyst (Figure 4.3).

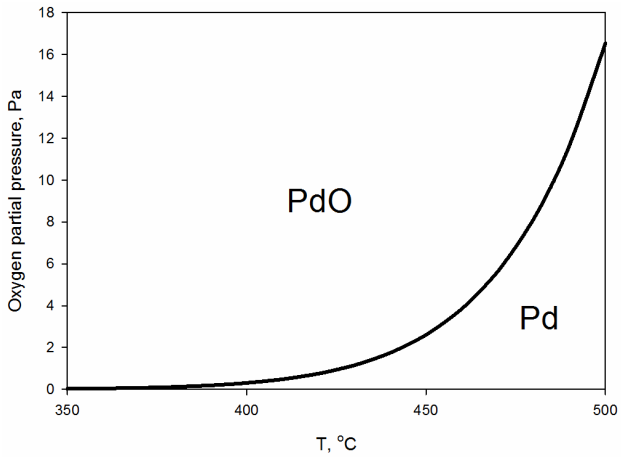

Figure 4.6 Equilibrium oxygen pressure for Pd ⇌ PdO phase transformation.

The water presence in the feed significantly suppressed PdO formation from pre-reduced Pd and increased the fraction of metallic Pd (Figure 4.3), for example, by half at 400ºC. Metallic Pd is known to be significantly less active than PdO in methane combustion [11, 42], thus, the activity drop for the monoPd catalyst in the wet feed compared to the dry feed can be correlated with the increased metallic Pd contribution.

Another reason for the loss of Pd activity in the wet feed, as suggested in several works [9-15], is the formation of inactive Pd hydroxide, with the negative first order to water in the methane conversion rate on monometallic Pd catalysts [14]. Standard enthalpies of formation of $Pd(OH)_2$ and PdO and H_2O at 298 K are -385 kJ/mol [9], -119 kJ/mol [43] and -242 kJ/mol [44]. The $Pd(OH)_2$ formation from PdO and reduced Pd can be described by reactions R2 and R3:

R2) $PdO + H_2O \rightleftharpoons Pd(OH)_2$ $\Delta H^o_{298} = -24$ kJ/mol

R3) $Pd + H_2O + ½\ O_2 \rightleftharpoons Pd(OH)_2$ $\Delta H^o_{298} = -143$ kJ/mol

The reaction R1-R3 are exothermic and their equilibrium constants decrease with temperature increase. As XAS revealed for the wet feed (Figure 4.3), Pd(0) was predominant species at lower temperature, which progressively transformed into oxidized Pd(II) upon heating. From the thermodynamic point of view, the higher fraction of reduced Pd(0) at lower temperatures can be produced by shifting equilibria to the left only if there is oxygen deficit. Since the bulk fluid O_2 partial pressure was the same for the dry and wet feed (21 kPa) in the verified absence of the diffusion limitations, the oxygen deficit relates to activated oxygen which is affected by the presence of water.

Pfefferle and colleagues' [16, 17] performed in situ infrared spectroscopy and isotopic studies of lean methane combustion for Pd catalysts on a variety of supports, including alumina, and showed that lattice oxygen from the support contributed heavily to the reaction products. Palladium active sites are reoxidized with oxygen from the support, following a redox Mars and van Krevelen mechanism. The presence of water causes hydroxyl accumulation on the support, which hinders the oxygen exchange process between the support and metallic active sites [16, 17]. At the low temperature region for Pd catalyst, the rate limiting step has been identified as water desorption from the catalyst surface [45], not methane activation as typically known for temperatures above 450ºC [14]. Our study thus provides in situ XAS evidence of the lack of oxygen on palladium active sites in the wet feed at low temperatures, which follows from the low fraction of oxidized Pd in the presence of water (Figure 4.3). Water, thus, "shifts" oxygen-rich combustion to the oxygen-deficient combustion, where activated oxygen concentration inversely depends on the water/hydroxyl concentration. As temperature increases, the rate of water desorption and oxygen

uptake increases [46], which provides higher activated oxygen concentrations and promotes PdO formation either by oxidation of Pd(0) (R1) and/or by decomposition of $Pd(OH)_2$.

Platinum is known for its low activity in lean methane combustion. By comparing oxygen surface uptake and methane conversion, Burch and colleagues reported that the maximum conversion was achieved at 50% of the oxygen surface monolayer and decreased at further oxygen uptake, when the surface becomes poisoned by oxygen [11]. The oxygen sticking coefficient on Pt is 15 times higher than that for methane [27]. As shown previously, oxygen sterically blocks Pt atoms for methane dissociation or inhibits the dissociation electronically [46].

4.4.2 Bimetallic Pd-Pt catalyst

As shown by the catalytic tests (Figure 4.1), the presence of Pt in combination with Pd rendered the catalyst relatively insensitive to the presence of water in the feed compared to the monometallic Pd. Given the similarity of the Pd edge for PdO and $Pd(OH)_2$, it was impossible to decouple accurately the contributions of metal oxide and hydroxide. The in situ spectroscopy results did not allow validation of a hypothesis if Pt addition inhibited the formation of combustion-inactive $Pd(OH)_2$ in favor of active PdO. The heats of formation of $Pd(OH)_2$ (-385 kJ/mol [9]) and PdO (-119 kJ/mol [43]) suggest that $Pd(OH)_2$ is thermodynamically favourable at lower temperatures, while higher temperatures, accompanied by water deficit, promote $Pd(OH)_2$ decomposition to PdO (reverse reaction R3).

Although the hydroxide/oxide contributions could not be decoupled by XAS, the importance of the current study is to report another observation, which likely can be an additional (or even a single reason) for the water effect on Pd and Pd-Pt catalysts. Figure 4.3 summarizes the metallic Pd fraction for all studied catalysts and conditions and shows that in the temperature window of interest (300-500ºC), the addition of water led to significant oxygen deficiency, which is revealed in the high fraction of metallic Pd.

Similarly to the monometallic Pd catalyst, for the bimetallic catalyst, the addition of water also led to the increased metallic Pd contribution, although not to the same extent as for the Pd-only catalyst because even in the dry feed, the presence of Pt inhibited PdO formation [22] (Figure 4.3). The trend in the metallic Pd contribution at 400ºC was found to be 0% (dry Pd) << 38% (dry Pd-Pt) <

49% (wet reduced Pd) < 65% (wet Pd-Pt), whereas the trend in conversions (Figure 4.1) was 90% (dry Pd) > 70% (dry Pd-Pt) > 58% (wet Pd-Pt) >> 11% (wet reduced Pd). Note how the presence of Pt increased the methane conversion from 11 to 58% in the wet feed, although the metallic Pd fraction was 49% for the reduced monoPd and 60% for the Pd-Pt catalysts. Thus, in the case of the bimetallic Pd-Pt catalyst, the water effect cannot be directly correlated with the Pd(0) fraction only.

The Pd-Pt catalyst always shows the presence of reduced Pt in the studied temperature window. Pt is known for much lower activity than PdO catalysts in lean methane combustion due to poisoning with oxygen [11, 26-28, 47]. However, under oxygen-deficient conditions, the metallic forms of either Pd or Pt perform significantly better than their oxides, as recently shown by an in situ infrared reflection absorption spectroscopy of monometallic Pd and Pt catalysts under stoichiometric and oxygen-poor dry methane combustion [48]. It was found that the higher the oxygen deficit was, the more metallic Pt outperformed metallic Pd. Although bimetallic catalysts were not studied, the authors hypothesized that in Pd-Pt catalysts, PdO could play a key role in oxygen-rich conditions, whereas metallic Pt could be catalytically active under oxygen-deficient conditions. In a study of alternated CH_4 lean combustion/CH_4-reducing wet pulses over Pd-Pt catalysts, the difference between Pd and bimetallic catalysts was attributed to the likely ability of metallic Pt to activate methane under net reducing conditions, which was suppressed under net oxidizing conditions [18].

To verify the increasing Pt contribution to the bimetallic catalyst performance upon the lack of oxygen, the ignition tests were performed in the dry methane-rich feed at the CH_4-to-O_2 molar ratio of 1:1, which is below the stoichiometric 1:2 ratio. The light-off activity of monometallic Pt in the rich feed (Figure 4.7 (a)) is in agreement with the previously reported behavior [26]. Figure 4.7 (b) compares the deviation of the Pd-Pt activity vs. Pt activity in the rich and lean, dry feeds. The deviations at each temperature were calculated as the difference in methane conversion over Pd-Pt and Pt catalyst divided by the conversion over Pt catalyst for the same feed (either rich or lean). As seen, the lack of oxygen increased the contribution of Pt to methane conversion over the bimetallic catalyst, which was more pronounced at lower temperatures.

Our study, thus, provides the evidence that water-promoted oxygen deficit shifts the methane oxidation mechanism from lean methane combustion on PdO in dry conditions to rich methane combustion on Pt in wet conditions for the bimetallic Pd-Pt catalyst. Because similar Pd metallic

fractions were found in Pd and Pd-Pt catalysts under wet conditions but the monometallic Pd catalyst showed lower reaction rates, it is apparent that in the presence of water metallic Pd is relatively inactive compared to the metallic Pt. Indeed, even under stoichiometric conditions, Pt is known for its higher activity than Pd [11]. Because the monometallic Pt was inactive in the studied temperature region, irrespective of water presence in the feed, the presence of oxidized Pd species contributes to the optimal catalyst performance, most likely by providing dissociated oxygen for combustion. Thus, in the presence of water and lack of oxygen, Pt supplies oxygen-free sites for methane activation.

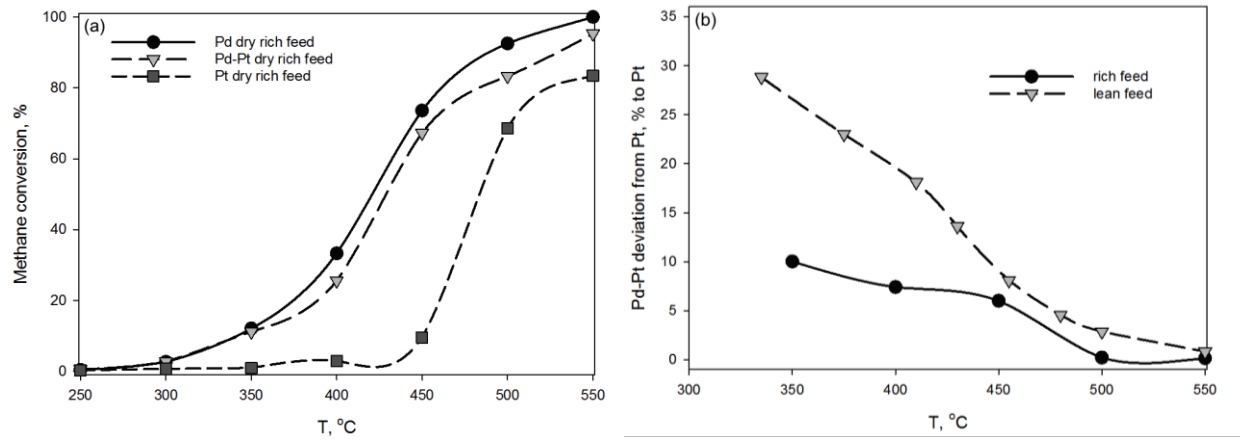

Figure 4.7 Dry methane combustion at 1:1 CH_4/O_2 molar ratio: (a) ignition tests and (b) deviations in methane conversion.

Although the rate laws were not obtained in this study, the suggested mechanism is in line with the reported rate laws for Pd, Pt, and Pd-Pt catalysts in the wet methane-lean feed (M stands for methane, W for water):

$$-r_{M,Pd} = \frac{k_{Pd}C_M}{C_W} \quad [14]; \quad -r_{M,Pt} = k_{Pt}C_M \quad [25]\ ; \quad -r_{M,Pd-Pt} = \frac{k_{Pd-Pt}C_M}{1+K_wC_W} \quad [25]$$

The hydroxylated sites are the most abundant surface intermediates in methane combustion over Pd, with a negligible fraction of free active sites [14]. With the addition of water-resistant Pt, the free active sites in the denominator of the Langmuir-Hinshelwood mechanism model [24] can be related to the fraction of Pt atoms that are not poisoned by either water or oxygen.

As stated above, platinum-induced inhibition of the additional influence of the platinum-inhibited $Pd(OH)_2$ formation from PdO cannot be excluded.

4.5 Conclusions

Monometallic Pd, Pt and bimetallic Pd-Pt (molar ratio 2:1) catalysts supported on γ-Al_2O_3 were studied in lean methane combustion in the absence and presence of water in the feed. Monometallic Pd was significantly deactivated in the wet feed, whereas the presence of Pt rendered the bimetallic catalyst relatively insensitive to water and increased its activity. Reduced Pd catalyst showed the same activity as calcined in the dry feed, but it was significantly less active in the wet feed as compared to the calcined Pd.

In situ XAS analyses showed that reduced Pd was in oxidized state at 200-600ºC in the dry feed, but only progressively changed from Pd(0) to oxidized Pd with the temperature increase in the wet feed. The fractions of metallic Pd were similar for the monometallic and bimetallic catalysts in the wet feed. It was impossible to decouple the contribution of PdO and $Pd(OH)_2$ accurately due to the similarity of their XANES edge.

Thermodynamic analysis shows that in the wet feed the Pd(0) fraction decreases with temperature increase because water renders the surface oxygen deficient at lower temperatures. The study provides an in situ XAS evidence of an oxygen deficit on Pd or Pd-Pt catalysts in the presence of water and supports Pfefferle and colleagues' hypothesis on the effect of water in catalytic methane combustion [16, 17].

The improved activity of Pd-Pt catalysts compared to Pd in the wet feed is explained by the lack of oxygen on the surface, which allows for Pt-catalyzed methane activation. In an excess of air, Pt is poisoned by oxygen and is not active in the combustion. The suggested mechanism is in line with the rate laws reported in literature for wet methane-lean combustion on Pd [14], Pt [24] and Pd-Pt [24] catalysts.

The study does not only provide a mechanistic insight into Pd-Pt catalyst functions but also suggests that this combination is of high practical interest for exhaust treatment for natural gas vehicles with a mixed mode of engine operation (lean or stoichiometric combustion).

Acknowledgments

Financial support from NSERC (Strategic grant STPGP 430108-12 and STPGP 478979-15), CFI (Leaders' Opportunity Fund, grant 24766) is appreciated. The X-ray absorption work was

performed at the Canadian Light Source, which is supported by the Canadian Foundation for Innovation, Natural Sciences and Engineering Research Council of Canada, the University of Saskatchewan, the Government of Saskatchewan, Western Economic Diversification Canada, the National Research Council Canada, and the Canadian Institutes of Health Research. We thank Dr. John Duke (University of Alberta) for NAA, and Dr. Ning Chen for assistance with XAS measurements on the HXMA beamline.

4.6 References

[1] D. Ciuparu, M.R. Lyubovsky, E. Altman, L.D. Pfefferle, A. Datye, Catal. Rev. 44 (2002) 593-649.

[2] T.V. Choudhary, S. Banerjee, V.R. Choudhary, Appl. Catal. A: Gen. 234 (2002) 1-23.

[3] R. Gholami, M. Alyani, K.J. Smith, Catalysts 5 (2015) 561-594.

[4] Z. Wu, J. Deng, Y. Liu, S. Xie, Y. Jiang, X. Zhao, J. Yang, A. Arandiyan, G. Guo, H. Dai, J. Catal. 332 (2015) 13-24.

[5] R.J. Farrauto, Science 337 (2012) 659-660.

[6] G. Li, W. Hu, F. Huang, J. Chen, M. Gong, S. Yuan, Y. Chen, L. Zhong, Can. J. Chem. Eng. 95 (2017) 1117-1123.

[7] M. Monai, T. Montini, C. Chen, E. Fonda, R.J. Gorte, P. Fornasiero, ChemCatChem 7 (2015) 2038-2046.

[8] D. Pi, W.Z. Li, Q.Z. Lin, Q.F. Huang, H.Q. Hu, C.Y. Shao, Energy Technol. 4 (2016) 943-949.

[9] C.F. Cullis, T.G. Nevell, D.L. Trimm, J. Chem. Soc., Faraday Trans. 1 68 (1972) 1406-1412.

[10] R. Burch, F.J. Urbano, P.K. Loader, Appl. Catal. A: Gen. 123 (1995) 173-184.

[11] R. Burch, P.K. Loader, F.J. Urbano, Catal. Today 27 (1996) 243-248.

[12] D. Roth, P. Gelin, M. Primet, E. Tena, Appl. Catal. A: Gen. 203 (2000) 37-45.

[13] F.H. Ribeiro, M. Chow, R.A. Dalla, J. Catal. 146 (1994) 537-544.

[14] K.I. Fujimoto, F.H. Ribeiro, M. Abalos-Borja, E. Iglesia, J. Catal. 179 (1998) 431-442.

[15] R. Burch, M.J. Hayes, J. Mol. Catal. A: Chem. 100 (1995) 13-33.

[16] W.R. Schwartz, L.D. Pfefferle, J. Phys. Chem. C 116 (2012) 8571-8578.

[17] W.R. Schwartz, D. Ciuparu, L.D. Pfefferle, J. Phys. Chem. C 116 (2012) 8587-8593.

[18] G.G. P. Castellazzi, P. Forzatti, Appl. Catal. B: Environ. 95 (2010) 303-311.

[19] G. Lapisardi, L. Urfels, P. Gélin, M. Primet, A. Kaddouri, E. Garbowski, S. Toppi, E. Tena, Catal. Today 117 (2006) 564-568.
[20] K. Persson, L.D. Pfefferle, W. Schwartz, A. Ersson, S.G. Järås, Appl. Catal. B: Environ. 74 (2007) 242-250.
[21] K. Nomura, K. Noro, Y. Nakamura, Y. Yazawa, H. Yoshida, A. Satsuma, T. Hattori, Catal. Lett. 53 (1998) 167-169.
[22] H. Nassiri, K.-E. Lee, Y. Hu, R.E. Hayes, R.W.J. Scott, N. Semagina, ChemPhysChem 18 (2017) 238-244.
[23] B. Ravel, M. Newville, J. Synchrotron Radiat. 12 (2005) 537-541.
[24] R. Abbasi, L. Wu, S.E. Wanke, R.E. Hayes, Chem. Eng. Res. Des. 90 (2012) 1930-1942.
[25] J. Shen, R.E. Hayes, X. Wu, N. Semagina, ACS Catal. 5 (2015) 2916-2920.
[26] R. Burch, P.K. Loader, Appl. Catal. B: Environ. 5 (1994) 149-164.
[27] E. Becker, P.-A. Carlsson, H. Grönbeck, M. Skoglundh, J. Catal. 252 (2007) 11-17.
[28] S.H. Oh, P.J. Mitchell, R.M. Siewert, J. Catal. 132 (1991) 287-301.
[29] M. Honkanen, T.W. Hansen, H. Jiang, M. Kärkkäinen, M. Huuhtanen, O. Heikkinen, K. Kallinen, J. Lahtinen, R.L. Keiski, J.B. Wagner, M. Vippola, J. Catal. 349 (2017) 19-29.
[30] T.R. Johns, R.S. Goeke, V. Ashbacher, P.C.Thune, J.W. Niemantsverdriet, B. Kiefer, C.H. Kim, M.P. Balogh, A.K. Datye, J. Catal. 328 (2015) 151-164.
[31] E.N. Fuller, P.D. Schettler, J.C. Giddings, Ind. Eng. Chem. 58 (1966) 18-27.
[32] R.E. Hayes, J.P. Mmbaga, Introduction to chemical reactor analysis, 2nd ed., CRC Press 2013.
[33] H.S. Fogler, Elements of chemical reaction engineering, 4th ed., Pearson Education Inc. 2006.
[34] G.P. W. Lyons, M. Lorenz, Standard handbook of petroleum and natural gas engineering, 3rd ed., Elsevier 2016.
[35] A.L. K. Stephan, J. Phys. Chem. Ref. Data 14 (1985) 227-234.
[36] K. Murtezaoglu, E. Oray, T. Dogu, G. Dogu, N. Saracoglum, C. Cabbar, J. Chem. Eng. Data 40 (1995) 720-725.
[37] J.F.L. Page, Applied heterogeneous catalysis: design, manufacture, use of solid catalysts, Technip, Paris, France, 1987.
[38] J. Perez-Ramirez, R.J. Berger, G. Mul, F. Kapteijn, J.A. Moulijn, Catal. Today 60 (2000) 93-109.

[39] T.R. Johns, J.R. Gaudet, E.J. Peterson, J.T. Miller, E.A. Stach, C.H. Kim, M.P. Balogh, A.K. Datye, ChemCatChem 5 (2013) 2636-2645.

[40] T. Otto, J.M. Ramallo-Lopez, L.J. Ciovanetti, F.G. Requejo, S.I. Zones, E. Iglesia, J. Catal. 342 (2016) 125-137.

[41] R.E. Hayes, S.T. Kolaczkowski, Intoduction to Catalytic Combustion, 1st ed., Gordon and Breach Science Publisher, Amsterdam, 1997.

[42] R.J. Farrauto, M.C. Hobson, T. Kennelly, E.M. Waterman, Appl. Catal. A: Gen. 81 (1992) 227-237.

[43] J.S. Warner, J. Electrochem. Soc. 114 (1967) 68-71.

[44] D.D. Wagman, W.H. Evans, V.B. Parker, R.H. Schumm, I.Halow, S.M.Bailey, K.L. Churney, R.L. Nutall, J. Phys. Chem. Ref. Data 11(suppl. 2) (1982) 1-392.

[45] D. Ciuparu, L. Pfefferle, Appli. Catal. A: Gen. 209 (2001) 415-428.

[46] D. Ciuparu, R. Altman, L. Pfefferle, J. Catal. 203 (2001) 64-74.

[47] M. Valden, N. Xiang, J. Pere, M. Pessa, Appl. Surf. Sci. 99 (1996) 83-89.

[48] H.R. X. Weng, M. Chen, H. Wan, ACS Catal. 4 (2014) 2598-2604.

4.7 Supporting Information

4.7.1 Verification of the kinetic regime

The kinetic regime was verified at 340ºC in the wet feed for the most active catalyst, which was bimetallic $PdPt/Al_2O_3$. Table 4.S1 contains calculations of the criteria for external and internal mass transfer limitations (MTL), external and internal heat transfer limitations (HTL), axial dispersion, and wall effects.

Table 4S.1 Verification of the kinetic regime for $PdPt/Al_2O_3$ catalyst at 340ºC in the wet feed.

Parameter	Equation	Value (calculated or experimental)
Reaction rate $-r_M$, [mol/(s·kg_{cat})]	$-r_M = \frac{F_{Mo}X}{W}$	5.9×10^{-5}, for initial methane molar flow rate $F_{Mo} = 6.32\times10^{-7}$ mol/s, catalyst amount W = 0.789 g, conversion X=0.075
Methane bulk diffusivity in air at 613 K D_{AB} [m^2/s]	$D_{AB} = \frac{1.013\cdot10^{-2}T^{1.75}\left[\frac{1}{M_A}+\frac{1}{M_B}\right]^{0.5}}{P\left[\left(\sum v_i\right)_A^{1/3}+\left(\sum v_i\right)_B^{1/3}\right]^2}$ (Fuller formula [S1, S2])	7.5×10^{-5}, for P =101325 Pa, molecular masses and diffusion volumes for methane and air as 16 g/mol, 29 g/mol, 24.42 and 20.1 [S1, S2]
Particle Reynolds number Re_p	$Re = \frac{U\rho_g d_p}{\mu}$ [S3]	0.35, for dynamic viscosity $\mu=3.2\times10^{-5}$ Pa·s [S4] and density ρ= 0.576 kg/m^3 (ideal gas) of air at 613 K, $d_p = 10^{-4}$ m, free-stream velocity 0.197 m/s (for 3/8" reactor i.d., 476 mL/min feed rate at 613 K and assuming bed porosity of 0.4)
Schmidt number	$Sc = \frac{\mu}{D_{AB}\rho_g}$ [S3]	0.74
Sherwood number Sh	$Sh = 2 + 0.6Re^{1/2}Sc^{1/3}$ Frössling correlation [S3]	2.3
Mass transfer coefficient k_c [m/s]	$k_c = \frac{D_{AB}Sh}{d_p}$ [S3]	1.7
Mears criterion for external diffusion	$\frac{-r_M\rho_b Rn}{k_c C_M} < 0.15$ If the condition is satisfied, then no external MTL are present [S3]	5×10^{-5}, for ρ_b bed density 2334 kg/m^3 (catalyst density ρ_c 3890 kg/m^3, bed porosity 0.4), particle radius R= 0.5×10^{-4} m, order n= 1, $C_M = C_{Mo}(1-X)$ with initial methane concentration of 0.0793 mol/m^3

Thus, the Mears criterion shows the absence of external mass transfer limitations			
Knudsen diffusivity [m^2/s]	$D_K = \frac{d_{pore}}{3}\sqrt{\frac{8RT}{\pi M}}$	[S2]	1.74×10^{-6}, for methane (molecular mass M 0.016 kg/mol) and catalyst pore diameter d_{pore} = 0.59 nm, specified by Sigma-Aldrich
Diffusivity in a pore [m^2/s]	$D_{pore} = \left(\frac{1}{D_{AB}} + \frac{1}{D_K}\right)^{-1}$	[S2]	1.7×10^{-6}
Particle porosity	$\phi_p = \frac{S\rho_c\, d_{Pore}}{4}$	[S2]	0.87, for catalyst surface area 155 m^2/g (Sigma-Aldrich) and catalyst density 3890 kg/m^3
Effective diffusivity [m^2/s]	$D_{eff} = \frac{\phi_P D_{pore}}{\tau}$	[S2]	3.8×10^{-7}, for tortuosity 3.9
Weisz-Prater criterion for internal MTL	$C_{WP} = \frac{-r_M \rho_c R^2}{D_{eff} C_M}$ If $C_{WP} < 0.3$ for a first-order reaction, then no internal MTL are present	[S3]	0.02, for C_M as the bulk concentration of 0.073 mol/m^3 since the absence of external MTL was proved
Thus, the Weisz-Prater criterion shows the absence of internal mass transfer limitations			
Nusselt number Nu	$Nu = 2 + 0.6Re^{1/2}Pr^{1/3}$	[S3]	2.3, for Prandtl number Pr = 0.68 for air at 613 K
Heat transfer coefficient h [$kJ/(m^2\cdot s\cdot K)$]	$h = \frac{k_t Nu}{d_p}$	[S3]	1.1, for thermal conductivity of air at 613 K as 0.047 W/(m·K) [S5]
External temperature gradient criterion	$\left\lvert\frac{-r_M(-\Delta H_{rx})\rho_b RE}{hT^2 R_{gas}}\right\rvert < 0.15$ If the condition is satisfied, then no external HTL are present [S3]		6×10^{-7}, for heat of reaction -890 kJ/mol and activation energy E 78.2 kJ/mol [S6]
Thus, external temperature gradient criterion shows the absence of external HTL			
Prater number β	$\beta = \frac{-H_{rxn} D_{eff} C_M}{k_{eff} T}$	[S2]	4×10^{-4}, for effective thermal conductivity of Al_2O_3 as 0.043 W/(m·K) [S7]
Maximum internal temperature rise [K]	$\Delta T_{max} = \beta T$	[S2]	0.28, so the maximum internal T can be 613.28 K instead of 613.00 K surface. The catalyst particle is thus isothermal

Thus, Prater number shows the absence of internal HTL

Plug-flow operation (absence of axial dispersion and wall effects)	$L_{bed}/d_p > 50$ (to neglect axial dispersion) [S8]	Bed length per particle diameter L_{bed}/d_p = 50.3
	$D_{reactor}/ d_p > 10$ (to neglect wall effects) [S9]	$D_{reactor}/ d_p$ = 93

Thus, the plug-flow operation ca be assumed

All the criteria above confirm that the reaction at 340ºC occurs in the kinetic regime and that ideal PBR mole balance is applicable

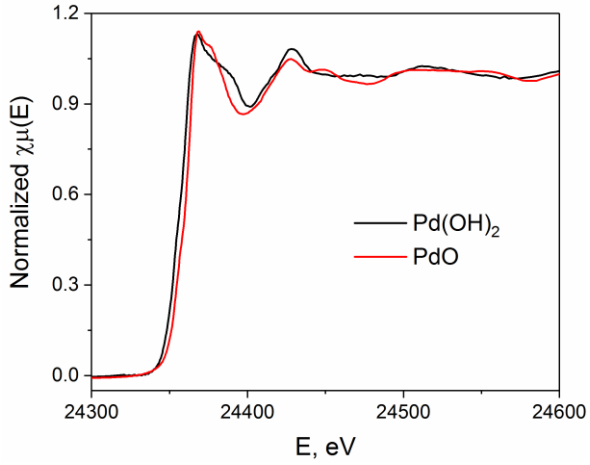

Figure 4S.1 In situ XANES spectra for Pd edge of PdO and $Pd(OH)_2$ standards.

Table 4S.2 Fitting results for 2:1 Pd-Pt catalysts under wet conditions.

Sample	**Path**	**CN**	**R/Å**	**σ^2/Å^2 ***	**E_0 shift/eV**
Fresh, room temperature	Pd-Pd	6.6(7)	2.731(6)	0.0055(6)	-9.7(6)
	Pd-Pt	4.6(1.0)	2.72(1)	0.006(1)	-9.7(6)
200 °C	Pd-Pd	6.5(8)	2.724(9)	0.009(1)	-9.5(6)
	Pt-Pt	5.5(1.3)	2.72(1)	0.010(3)	-9.5(6)
300 °C	Pd-Pd	6.4(9)	2.72(1)	0.011(1)*	-10.0(8)
	Pd-Pt	5.5(9)	2.71(2)	0.011(1)*	-10.0(8)
	Pd-O	0.8(4)	2.00(4)	0.011(1)*	-10.0(8)

*At higher temperatures, thermal disorder begins to significantly broaden EXAFS oscillations, and thus as an approximation, σ^2 terms were assumed to be similar for all contributions.

4.7.2 Supporting information references

[S1] E.N. Fuller, P.D. Schettler, J.C. Giddings, Ind. Eng. Chem. 58 (1966) 18-27.

[S2] R.E. Hayes, J.P. Mmbaga, Introduction to chemical reactor analysis, 2nd Ed., CRC Press, 2013.

[S3] H.S. Fogler, Elements of chemical reaction engineering, 4th Ed., Prentice Hall, 2005.

[S4] Standard handbook of petroleum and natural gas engineering, Eds.: W. Lyons, G. Plisga, M. Lorenz, 3rd Ed., Elsevier, 2016.

[S5] K. Stephan, A. Laesecke, J. Phys. Chem. Ref. Data, 14 (1985) 227-234.

[S6] R. Abbasi, L. Wu, S.E. Wanke, R.E. Hayes, Chem. Eng. Res. Des. 90 (2012) 1930-1942.

[S7] K. Murtezaoglu, E. Oray, T. Dogu, G. Dogu, N. Saracoglum C. Cabbar, J. Chem. Eng. Data 40 (1995) 720-725.

[S8] J.F. Le Page, Applied heterogeneous catalysis, TechniP, 1987.

[S9] J. Perez-Ramirez, R.J. Berger, G. Mul, F. Kapteijn, J.A. Moulijn, Catal. Today 60 (2000) 93-109.

Chapter 5. Stability of Pd-Pt catalysts in low-temperature wet methane combustion: metal ratio and particle reconstruction[4]

5.1 Introduction

Metallic nanoalloys have attracted considerable attention in catalysis because they not only show properties of individual elements, but also synergism due to the electronic and geometric effects of combination of two metals [1]. Palladium-platinum combinations benefit from strain and electronic effects [2-6], which make them catalysts of choice in a variety of oxidation and reduction reactions. Some examples of efficient performance of bimetallic Pd-Pt catalysts include hydrogenation of aromatic hydrocarbons or hydrodearomatisation [1], hydrogen oxidation and oxygen reduction reactions [2-6], formic acid [4-7] and methanol oxidation [8-13]. Emission control of methane in the exhaust of natural-gas vehicles (NGVs), which is a crucial issue because of a high greenhouse gas potential of methane [14], is another application of Pd-Pt catalysts. Pt addition to Pd increases the low temperature activity and improves thermal durability [15-18], which was shown not only in the combustion of methane but also of higher hydrocarbons like propane and propene [19]. Enhancement of catalytic activity and sintering stability by addition of Pt to Pd catalyst has been shown repeatedly [17, 19-26], but the studies contradict each other in terms of activity enhancement or suppression [27-29]. Such discrepancies is a common problem in bimetallic catalysis, where different catalyst formulations may result in various structure modes, chemical state and distribution of Pd and Pt and therefore, different catalytic behavior [19].

A study by Persson et al. [20] of the effect of different co-metals on Pd catalysts with 5 wt.% metal loadings and 1:1 molar ratio of metals showed that Pt is the most promising promoter to achieve stable high activity in methane combustion. Pt formed alloy with Pd as opposed to other metals

[4] Chapter 5 of the thesis has been submitted to the Chemical Engineering Science journal as "Stability of Pd-Pt catalysts in low-temperature wet methane combustion: metal ratio and particle reconstruction" H. Nassiri, R.E. Hayes, N. Semagina, Chem. Eng. Sci. (2017). The reaction setup for methane oxidation was originally designed and built by Dr. Long Wu and Dr. Robert E. Hayes. The lab view program to communicate with the reaction setup was written by Les Dean. The NAA analysis was performed by Dr. John Duke at the University of Alberta. HRTEM and TEM-EDX mapping were performed by Dr. Peng Li and Dr. Jing Shen at the University of Alberta Nanofabrication and Characterization Facility (nanoFAB). The author performed all the syntheses, catalytic reactions, analyses and other characterizations. Manuscript preparation and writing were conducted by the author under the supervision and final approval of Dr. Natalia Semagina and Dr. Robert E. Hayes.

that created spinel structures with alumina support (Co and Ni) or separate oxide particles like Rh, Ir, Cu, and Ag. An alloy formation along with higher PdO content and lower formation of inactive hydroxyl groups from water production were suggested as the reasons of the Pt effect on Pd as compared to other co-metals [20]. Studies performed for different ratios of Pd-Pt bimetallic catalysts showed that Pd-Pt 2:1 and 1:1 ratios are the best compositions from the viewpoint of activity and stability among Pd-Pt 4:1, 2:1, 1:1, and 1:2 combinations because of the close proximity of Pd and PdO active sites in the alloys [30]. The stability tests were performed in a dry feed for 8 hours [30]. The water effect was further investigated by in situ DRIFTS study [31] on Pd-Pt 2:1 and 1:1 catalysts, which revealed that lower concentration of hydroxyl groups on these two bimetallic catalysts (including on the support) is the reason of their high stability in the reaction. Lapisardi et al. [17] also studied the effect of metal ratios in Pd-Pt catalysts, namely, 13:1, 2:1, 1:1, and 1:15, and found that the ratios above 2 results in a higher activity because of the intimate interaction between two metals, but the stability tests were not performed. Yamamoto et al. [21] showed that the optimum Pd-Pt metal ratio is 3:1 that leads to lower degree of sintering of Pd and PdO crystallites and causes highest activity and stability. PdO presence on the surface of Pd-Pt particles and/or isolated PdO on the support is a well-described consequence of Pd-Pt catalyst ageing in air [32-34]. Goodman et al. [29] investigated the effect of different molar ratios of Pd-Pt (1:4, 2:3, 3:2, 4:1) in methane combustion through controlled particle size synthesis route. Among these combinations, only Pd-rich 4:1 catalyst demonstrated no deactivation after hydrothermal ageing HTA (4.2% water in the feed). It was suggested that HTA induces PdO segregation in a close contact with a Pd/Pt alloy, forming active and stable methane combustion sites. The ageing was performed for 8 hours in the temperature interval of 460-870ºC [29]. Honkanen et al. [25] used in situ environmental TEM to investigate the effect of temperature on sintering and reconstruction of Pd-Pt 2:1 catalyst in air and low-oxygen conditions at temperatures above 500ºC and concluded that the found critical temperatures for the structural changes are above the normal range of NGV exhaust temperature. The sintering can be also accelerated by the water vapor [35].

To the best of our knowledge, there is no systematic study reporting the effect of Pd-Pt ratio on the wet methane combustion from the viewpoint of stability at the practically-relevant conditions as it refers to NGV. Due to the lean combustion in NGV, the exhaust temperature is relatively low

(below 550ºC), while the negative water effect is only significant below 450ºC [36-43], which has been assigned to the formation of inactive $Pd(OH)_2$ [39, 44-50] and/or hydroxyl/water accumulation on the support that hinders oxygen availability combustion [51, 52]. Recently, for this low-temperature region (between 250 and 550ºC), we suggested that metallic Pt in the 2:1 Pd-Pt formulation catalyzes methane activation at lack of oxygen caused by water presence, as opposed to PdO-catalyzed activation in the dry feed [53].

In the current study, we aim to evaluate the effect of the metal ratios (nine bimetallic samples from 5:1 to 1:5 ratios) on the stability of Pd-Pt/Al_2O_3 catalysts' performance in wet lean methane combustion at the NGV's exhaust temperatures. HTA was performed at 400-550ºC cycles for the duration of 40 hours. By using a controlled nanoparticle synthesis, we also demonstrate the structural evolution of initial core-shell structures, as well as the formation of bimetallic alloys from individual Pd and Pt monoparticles even at such low temperatures. It appears that the effect of the metal ratio on the activity and long-term catalyst performance is more significant than the Pd-Pt catalyst preparation method.

5.2 Experimental

5.2.1 Catalyst preparation and characterization

Pd, Pt and Pd-Pt nanoparticles were synthesized in a colloidal dispersion via alcohol reduction in the presence of a stabilizer (poly N-vinylpyrrolidone, PVP). The synthesis details can be found in our earlier publication [54]. Apart from such bimetallic catalysts (termed here as "alloy") prepared via simultaneous reduction of metal precursors, bimetallic Pd core - Pt shell Pd(c)Pt(s) nanoparticles (1:1) were synthesized by a hydrogen-sacrificial method. First, Pd nanoparticles were synthesized as above. After the reflux, the Pd colloidal solution was allowed to cool down to room temperature followed by purging with hydrogen for 1 h. This procedure creates Pd hydride that further serves to reduce Pt precursor to form a shell around the preformed Pd nanoparticles. To create a Pt shell, the solution of 0.1 mM Pt precursor in 50 ml of water was added dropwise within one hour by a syringe pump. A dark colloidal dispersion of nanoparticles was obtained at the end of all syntheses without any precipitates. The synthesized nanoparticles were supported on γ-Al_2O_3 by acetone precipitation to obtain 0.3 wt.% target metal loading. All samples were dried

and calcined in air at 550ºC for 16 h. The catalyst after calcination is referred to as a "calcined catalyst". In addition to the bimetallic samples, two "mixed supported catalysts" (MS) were prepared as the physical mixture of calcined monometallic Pd and Pd catalysts at molar ratios Pd-to-Pt as 1:1 and 2:1. Another physical mixture was prepared by mixing the final colloidal solutions of monometallic Pd and Pt particles at molar ratio Pd-to-Pt as 1:1 at the time of precipitation on γ-Al_2O_3 which is named as "mixed colloids catalyst" (MC).

The actual metal loading in the calcined catalysts was determined by neutron activation analysis (NAA) and can be found in the Supporting Information. CO chemisorption was performed after reduction as described in the previous work [54]. TEM photographs were taken using a JEOL-2100 for 50-nm resolution images and JEOL JEM-ARM200CF for STEM and EDX mapping at 200 kV. The JEOL JEM-ARM200CF was an atomic resolution S/TEM with a probe Cs corrected Cold Field Emission Gun (cFEG), equipped with a large collection angle SDD EDX detector that enabled fast elemental mapping.

5.2.2 Catalytic performance in methane combustion reaction

Wet methane combustion reaction was studied in a tubular reactor with on-line GC analysis as described earlier [24, 55]. The evaluation of the kinetic regime and ideal PBR performance can be found in our previous publication [53]. The reactor was packed calcined catalysts corresponding to 1.2 mg of active Pd. In case of monometallic Pt catalyst, the amount of the supported catalyst corresponded 1.2 mg of Pt. A certified (Praxair) gas mixture of 10 vol.% CH_4/N_2 along with dry air were fed to the reactor at a flow rate of 8.5 ml/min and 205 ml/min, respectively, to achieve 4000 ppm CH_4 concentration. 5 mol.% water vapor was added to the feed stream by a Series II Legacy HPLC pump to evaluate the effect of water vapor on the catalytic activity.

The sequence of the tests was as follows: two ignition-extinction tests (one with dry feed, another with the wet feed) were performed by heating from 250ºC to 550ºC and cooling vice versa with the rate of 60ºC/min, with 50º-intervals, at which the temperatures were held for 45 min. This procedure was followed by a hydrothermal ageing test (HTA). In 22 h, the catalyst was cycled between 550ºC and 400ºC and kept at each temperature for 1 h. After 22 h, the temperature was held constant at 400ºC for about 18 h. Then the activity recovery at 400ºC was also checked by cutting off the water vapor from the feed stream during 6 h after the HTA test. Finally, the catalytic

test was terminated by another ignition-extinction test in the presence of water to check the catalytic activity after 40-hour HTA test (referred to as a "post-HTA" ignition-extinction). The catalyst sample after all these steps of the reaction is referred to as "used catalyst". Selected catalysts were repeated and methane combustion results reproduced within 2% error. Negligible conversion was obtained for the neat Al_2O_3 support up to 550ºC.

5.3 Results and discussion

5.3.1 Effect of Pd-Pt ratio on the hydrothermal ageing (HTA) performance

Figure 5.1 shows the stability experiments performed for Pd, Pt and Pd-Pt catalysts for the same Pd loading in the reactor. Pt catalyst is the least active, which for the lean methane combustion can be assigned to oxygen blocking Pt sites and preventing methane activation [56]. Monometallic Pd catalyst is relatively active at the start of the stability tests, but quickly deactivates and shows < 10% conversion only after 25 hours on stream. The activity and the fate of the bimetallic compositions depend on the Pd-to-Pt ratio. Pd-rich catalysts show significantly higher activity than Pd (at the same Pd amount in the reactor) but, similarly to monoPd, deactivate. As seen from Figures 5.1 (a) and 5.1 (c), the higher the Pd concentration, the faster the catalyst deactivation. Pt-rich compositions (Figures 5.1 (b) and 5.1 (c)), show lower initial activities but they either maintain them during the HTA tests or even improve the activity over time.

Nanoparticle sintering and decrease in the number of surface atoms could be a potential explanation of such behavior. However, CO chemisorption performed on the fresh calcined and used catalysts, revealed that Pd-rich catalysts did not change their particle size (while the activity decreased by 1.5-10 times, Figure 5.1 (c)), while the Pt-rich catalysts sintered but did not lose their activity. Under oxidative atmosphere, Pt on γ-alumina support is known to be more susceptible to sintering than corresponding Pd catalyst; Pd stabilizes Pt in this environment as a result of a strong interaction of PdO with the support [57-59]. Similarly, the extent of Pd-Pt coarsening due to ageing was found to decrease with increasing Pd content, with 1:1 Pd-Pt ratio being the most sintering resistant among Pt-rich catalysts [60]. The sintering behavior is also in line with a DFT study by Ha et al. [61] who investigated the stability of Pd-Pt 1:1, 1:3 and 3:1 clusters on oxide supports. They suggested that subtle entropic and electrostatic effects make 1:1 configuration the most stable one against sintering, and the electrostatic stabilization was showed for Pd-Pt 3:1 ratio. The

observed mismatch between the sintering (Figure 5.1 (c)) and deactivation behavior (Figures 5.1(a) and (b)) implies that sintering cannot be considered as a significant reason for deactivation of Pd and Pd-Pt catalysts.

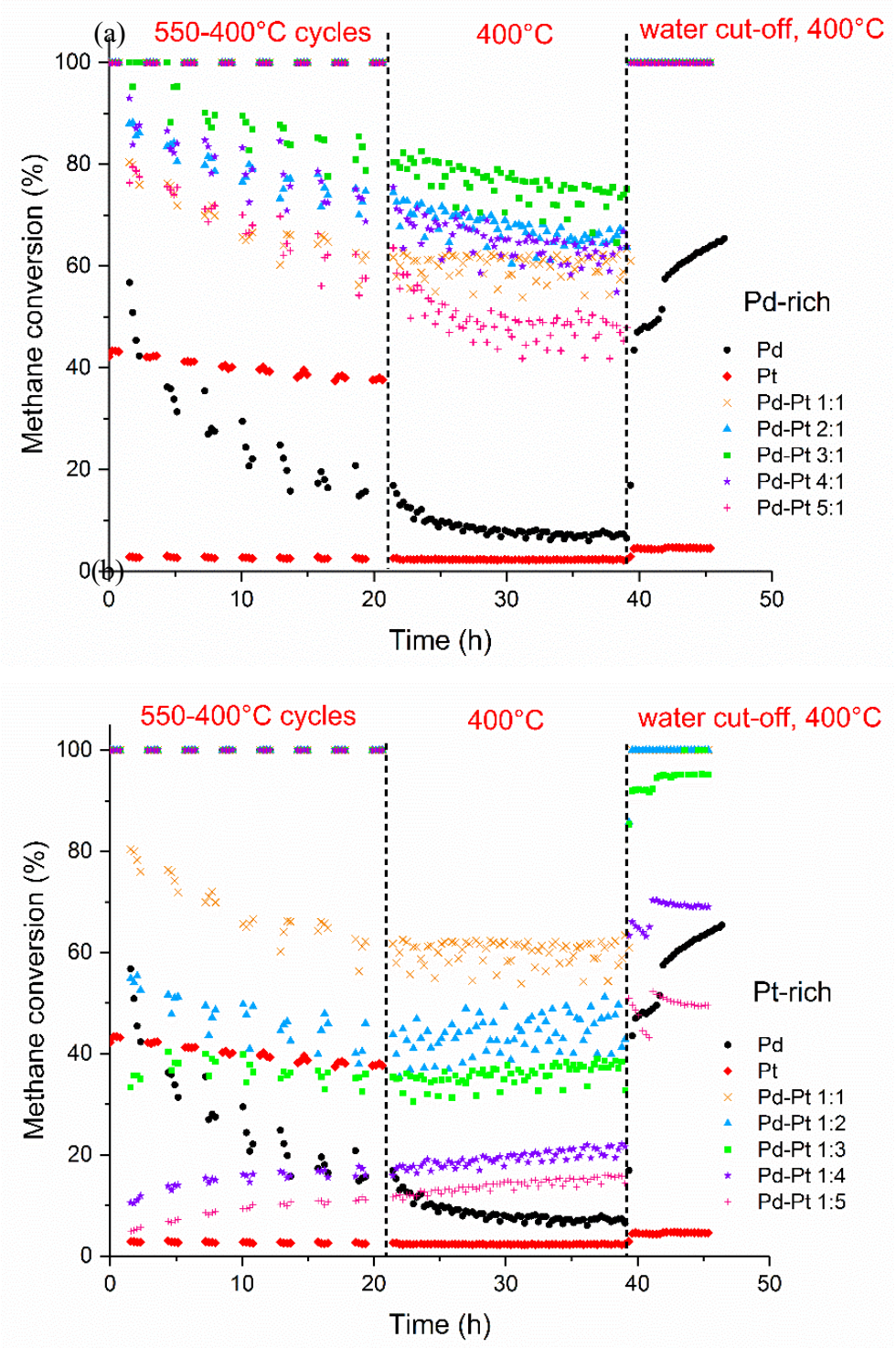

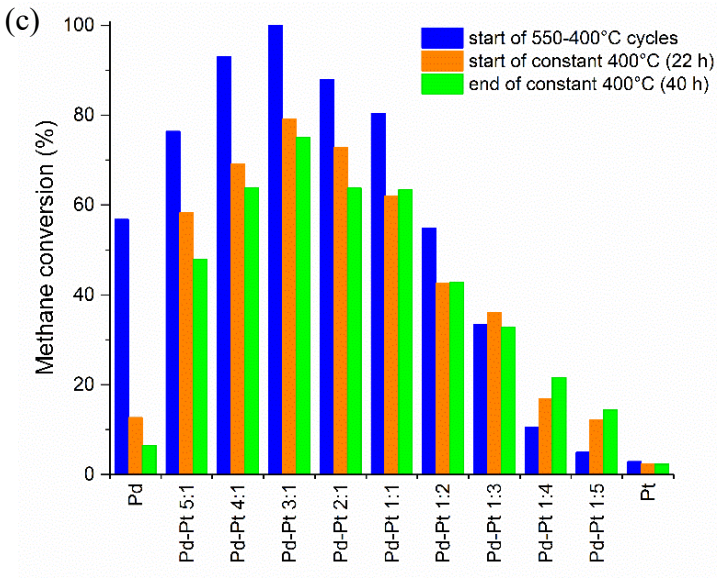

Figure 5.1 Hydrothermal ageing tests. Pd and Pd-Pt catalyst amounts correspond to the same Pd loading in the reactor (1.2 mg). Pt catalyst loading corresponds to 1.2 mg of Pt.

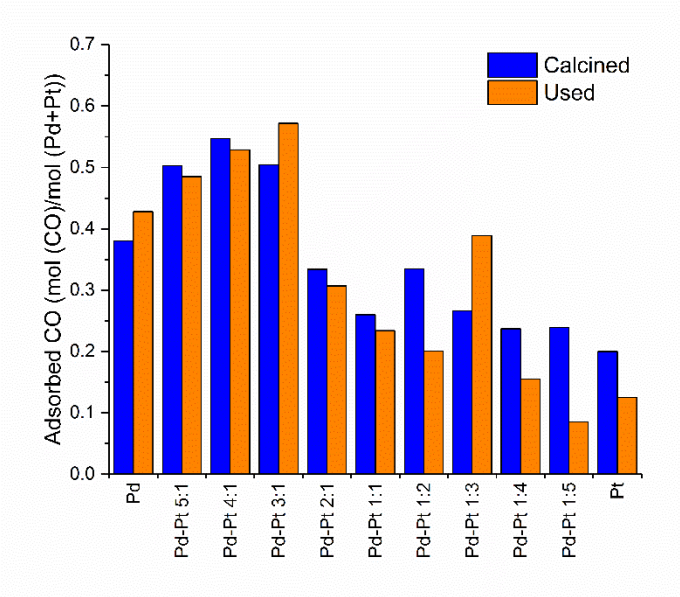

Figure 5.2 Surface sites on the calcined and used catalysts as probed by CO chemisorption. The deviation is 0.07 $mol_{CO}/mol_{(Pd+Pt)}$.

As seen from Figure 5.1 (c), there is a trade-off between high activity but low stability of Pd-rich compositions and low activity but high stability of the Pt-rich catalysts. Among the tested combinations, the most optimal performance from the viewpoint of both activity and stability at the conditions of the strongest water influence (400ºC, as opposed to 550ºC) is achieved for the Pd-Pt ratios from 1:1 to 4:1, which covers the range of different reported ratios by other groups

[17, 20, 21, 29, 30]. The post-HTA ignition-extinction experiments in the presence of water at the temperature range of 250-550ºC confirmed that these ratios require lower temperatures for methane combustion (Figure 5.3 (a)). No significant hysteresis was observed between the ignition and extinction curves on the catalysts after HTA.

Figure 5.3 (b) summarizes initial turnover frequencies that were calculated from post-HTA ignition curves (wet conditions). To conform to the condition of the differential reactor performance (< 15% methane conversion), the TOFs are reported at 340ºC for the Pd-rich catalysts and 360ºC for the Pt-rich catalysts. The number of surface atoms was found from CO chemisorption of used catalysts (Figure 5.2) assuming 1:1 stoichiometry. Interesting that for Pd-rich catalysts, TOFs calculated based on the total surface atoms are almost constant for the Pd-Pt ratios 4:1 to 1:1, but they drop significantly with further Pt enrichment. When TOFs were calculated per surface Pd only assuming the same bulk and surface composition, the peak activities belong to the catalysts with Pd-Pt ratios between 2:1 and 1:2. The latter assumption is not necessarily correct because PdO segregation to the surface of Pd-Pt catalysts is known to occur at hydrothermal ageing [29], which makes our calculated values of TOF per only Pd overpredicted. However, the trends in both Figures 5.3(a) and (b) show that Pt addition to the Pd-rich catalysts is crucial to maintain the high activity in the wet feed, but the Pt enrichment beyond 1:3 Pd:Pt ratio is not recommended.

Our earlier in situ X-ray absorption spectroscopy study performed on the 2:1 Pd-Pt catalyst [53] suggested that water causes oxygen deficit, which suppresses the amount of active PdO sites but activates Pt for methane activation, that is not active in the presence of oxygen. Dianat et al. [62] concluded that the higher the Pd content in the surface layer of Pd-Pt catalysts, the higher oxygen adsorption energy. Thus, in wet feed on Pd-Pt catalysts, Pt is responsible for methane activation but it also affects the oxygen binding energy. Apparently, at excessive Pt amounts for the ratios exceeding 3:1 Pt:Pd, there is a deficit of oxygen required for the combustion. Such Pt effect of promoting metallic state of Pd was reported even for the dry methane combustion [54].

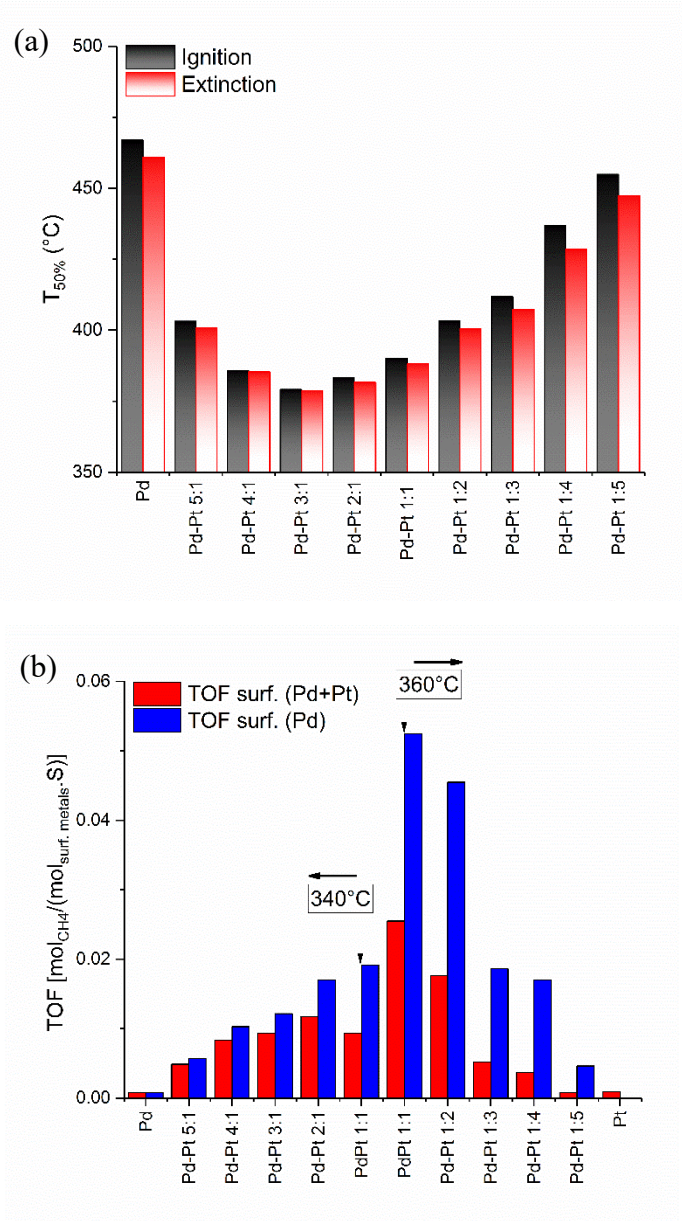

Figure 5.3 Catalytic activity during post-HTA ignition and extinction in the wet feed: (a) temperature of 50% methane conversion (Pt is omitted because it did not reach 50% conversion even at 550ºC); (b) initial ignition turnover frequencies.

5.3.2 Structural evolution of Pd, Pt and Pd-Pt nanoparticles

Figure 5.1 (b) for HTA of Pt-rich catalysts reveals an interesting trend at constant 400ºC, which is the activity increase during ageing. Spontaneous surface segregation and adsorbate-induced restructuring at elevated temperature and under oxidative atmosphere of the reaction could be the

reasons of this phenomenon [63-71], such as in situ PdO segregation to the surface of Pd-Pt particles [29] or to the support [34]. Our earlier X-ray absorption spectroscopy study of Pd(core)-Ru(shell) and Pd-Ru mixed alloy nanoparticles showed that after oxidative ageing at 550ºC they transformed into one structure with Pd-rich shells and demonstrated the same performance in methane combustion [72]. The restructuring is caused by differences in surface energies of constituent atoms, adsorption energies of reactants or dissociated species, and diffusion barriers [67-70]. In Pd-Pt nanoparticles, Pd with lower cohesive energy than Pt is expected to segregate to the surface producing Pd-rich shells and Pt-rich core [63, 65-67, 71], but the degree of segregation depends on the temperature and composition of the alloy [65, 66, 70]. Based on Monte Carlo simulation, Duan et al. [67] investigated surface segregation of random alloys Pd-Pt 1:1, 3:1, and 1:3 and showed that surface segregation causes about 15-20% lower Pt concentrations in the shell.

Is it thus possible that the original location of Pd and Pt atoms in bimetallic Pd-Pt nanoparticles actually does not matter and they will transform in situ into the most stable structure only depending on their metal ratio? To verify this hypothesis, we used a controlled synthesis of metal nanoparticles and produced two samples with the same Pd-Pt ratio of 1:1, but one was synthesized as a mixed alloy (Pd-Pt 1:1), another as a Pd(core)-Pt(shell) nanoparticles (Pd-Pt 1:1 C-S). Figure 5.4 shows the original structures of the Pd-Pt nanoparticles, confirming the Pt enrichment of the shells in the as-synthesized core-shell nanoparticles. After the use in the wet methane combustion at temperatures not exceeding 550ºC, the original core-shell structure was lost: the EDX mapping reveals nearly constant Pd-Pt ratio throughout the particle after the use. The catalytic results were concomitant with the structure change: the activity of 1:1 originally alloy and core-shell structures are similar (with a longer stabilization period for the core-shell sample, Figure 5.5). Moreover, another sample prepared by mixing the individual colloidal dispersion of Pd and Pt nanoparticles followed by deposition on the support and calcination (referred to as “mixed colloids” MC) at the same 1:1 Pd-to-Pt ratio, demonstrated the same stable behavior and a similar activity as the alloyed Pd-Pt catalyst (Figure 5.5). Thus, it appears that it does not matter how the bimetallic particles were synthesized as soon as the overall metal ratio is maintained.

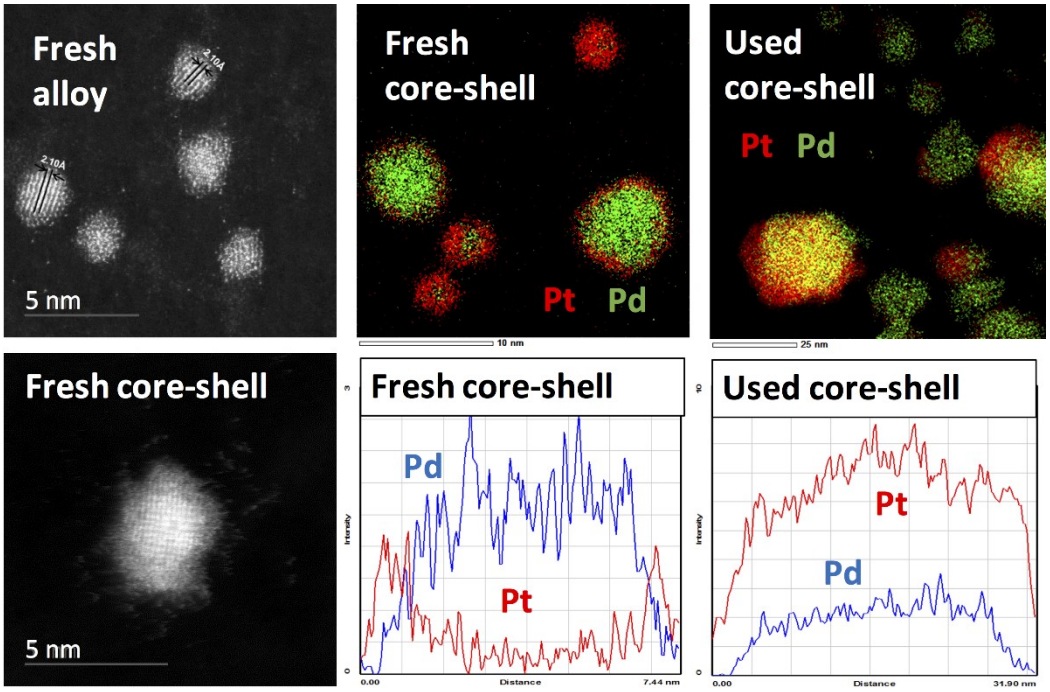

Figure 5.4 TEM and EDX mapping of as-synthesized (fresh) 1:1 Pd-Pt alloy and fresh and used in HTA Pd(core)-Pt(shell) nanoparticles.

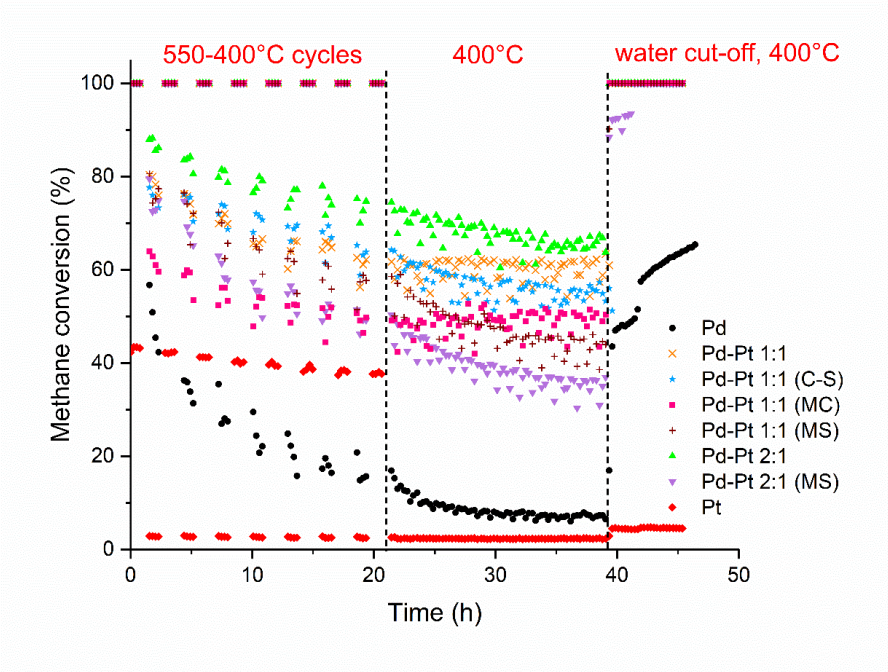

Figure 5.5 Hydrothermal ageing tests for alloyed, core-shell (C-S), mixed colloids (MC) and mixed supported catalysts (MS). Pd and Pd-Pt catalyst amounts correspond to the same Pd loading in the reactor (1.2 mg). Pt catalyst loading corresponds to 1.2 mg of Pt.

There is also another phenomenon described for Pd-Pt catalysts in high-temperature oxidative applications, which is the trapping of mobile Pt species by PdO nanoparticles [73]. In general, Pt sintering in oxidizing conditions is mediated by surface migration of Pt species or through gas-phase PtO_2 [59, 73]. The latter mechanism has been gaining more evidence in the recent literature by means of theoretical predictions [73] and experimental observations [74]. The abrupt changes in sintering kinetics via volatile PtO_2 were found to occur at 450ºC, with lower oxygen coverage leading to a higher sticking coefficient of $PtO_2(g)$ and increased sintering [73]. The most significant decrease in sintering rate was observed in the presence of excess PdO which serves to trap mobile Pt species [74]. Evaporation of Pt as an oxide is known to be inhibited by the presence of Pd, and growth of crystallites in slower for alloys than for pure Pt metal [32]. When physical mixtures of monometallic Pd and Pt catalysts were aged in air, formation of bimetallic Pd-Pt particles was observed [60, 75]. Smaller PdO were more effective in trapping efficiency for Pt and led to smaller size of Pd-Pt nanoparticles [75]. Such changes are described for the temperatures above the typical NGV exhaust temperature [25], but the lower oxygen concentration leads to the decreased temperature of phase transformations [25, 59]. Water may also reduce the reconstruction temperature [35]. In the present case, water causes lower active oxygen surface concentration, as evidenced by in situ X-ray absorption spectroscopy study [53], which thus may promote the Pd-Pt phase transformations at the low temperatures of interest.

To verify this hypothesis, we mixed monometallic supported ("MS") Pt and Pd catalysts (Pd-Pt 2:1 MS and Pd-Pt 1:1 MS) and tested them in methane combustion (Figure 5.5). Both mechanical combinations showed significantly higher activity and stability than practically inactive monometallic counterparts. Note that the reactions were performed at the same Pd loading in the reactor (1.2 mg). The activities at the end of 400ºC ageing followed the trend of 2:1 (alloy) ~ 1:1 (alloy) ~ 1:1 (C-S) > 1:1 (MS) > 2:1 (MS) >> monometallic Pd or Pt. Such a dramatic synergism can be explained only by formation of Pd-Pt bimetallic particles in situ at the temperature intervals of 400-550ºC in the presence of water. The EDX mapping of the mixed monometallic Pd and Pt catalyst after the hydrothermal ageing (Figure 5.6) confirms the collocation of the metal species. Such rearrangements are indicative of relatively insignificant effect of where Pd and Pt are located in the fresh catalysts in comparison with the effect of the metal ratio (Figures 5.1 (a) and (b)). Figure 5.5 also shows that the mixed supported catalysts deactivate in a similarly manner as

Pd-rich 2:1 catalyst. The performance of the Pd-Pt 2:1 MS catalyst is rather close to the HTA of the Pd-Pt 5:1 alloyed catalyst (Figure 5.1 (a)), which shows that Pt relocation has not been completed. As the catalyst was prepared by mixing the monometallic already supported catalysts, the restructurization is only possible via vapor-phase PtO_2 [73], which happens in situ in the wet combustion at temperatures not exceeding 550ºC. The present study thus demonstrates the significance of structural rearrangements and Pt vaporization at the NGV exhaust conditions, but a further study is warranted to investigate if at longer times on stream all catalysts achieve one stable structure depending only on the metal ratio.

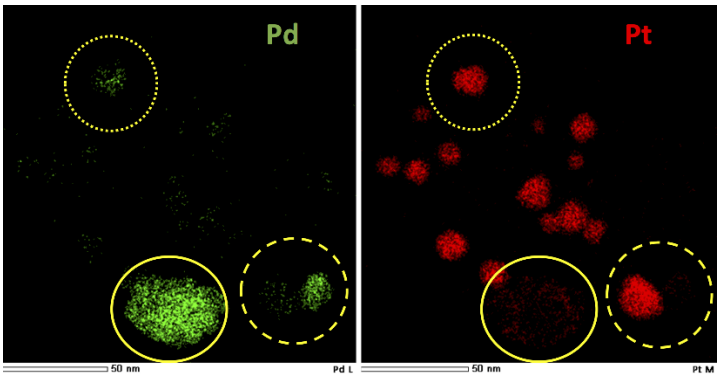

Figure 5.6 TEM-EDX mapping of the used mixed supported catalyst Pd-Pt 2:1 MS (after the reaction shown in Figure 5.5). No similar Pd-Pt association was detected in the fresh catalyst.

5.4 Conclusions

Monometallic Pd, Pt and bimetallic "alloyed" Pd-Pt alumina-supported catalysts (with the Pd-Pt atomic ratios of 1:5 to 5:1) were studied in lean methane combustion with 5% water in the feed. The ageing tests were performed for 40 h at temperatures of 400-550ºC. Platinum presence at Pd-Pt 1:1 to 4:1 ratios was found the most optimal from the viewpoint of activity, with the most stable formulation being 1:1 Pd-Pt catalyst. Platinum excess above 1:1 ratio prevented deactivation but at lower activity levels. The effect was found not to be affected significantly by the particle size, but by the ratio of Pd/Pt that affects the methane and oxygen activation pathways in the wet feed, as we suggested earlier by in situ X-ray absorptions study [53].

The activity and stability of the "alloyed" Pd-Pt 1:1 and 2:1 catalysts were also compared with the activity of core-shell nanoparticles, co-deposited monometallic particles and monometallic mixed supported catalysts. The activity tests and EDX mapping of the used catalysts suggest significant

structural changes in the metal nanoparticles. Even the mechanically mixed monometallic supported catalysts progressively transformed into intrinsic bimetallic structures with activity and stability approaching those of the alloyed nanoparticles. The results suggest that platinum vaporization (most likely as PtO_2 [73]) is significant in the wet feed at low surface oxygen concentrations even at the temperature interval of 400-550ºC. It appears that the proper Pd-Pt metal ratio has a governing effect on the activity and stable behavior in wet low-temperature methane combustion rather than the catalyst preparation method.

Acknowledgments

Financial support from NSERC (Strategic grants STPGP 430108-12 and STPGP 478979-15), CFI (Leaders' Opportunity Fund, grant 24766) is appreciated. The TEM-EDX work was performed at the nanoFAB (University of Alberta). We thank Dr. John Duke for NAA and Dr. Jing Shen for TEM-EDX analyses.

5.5 References

[1] B. Coq, F. Figueras, J. Mol. Catal. A: Chem. 173 (2001) 117-134.

[2] A. Chen, P. Holt-Hindle, Chem. Rev. 110 (2010) 3767-3804.

[3] Y.C. Weng, C.T. Hsieh, Electrochim. Acta. 56 (2011) 1932-1940.

[4] H. Zhang, M. Jin, Y. Xia, Chem. Soc. Rev. 41 (2012) 8035-8049.

[5] S. Limpattayanate, M. Hunsom, Renew. Energy 63 (2014) 205-211.

[6] S. Thanasilp, M. Hunsom, Renew. Energy 36 (2011) 1795-1801.

[7] H.X. Zhang, C. Wang, J.Y. Wang, J.J. Zhai, W.B. Cai, J. Phys. Chem. C. 114 (2010) 6446-6451.

[8] K. Wu, Q. Zhang, D. Sun, X. Zhu, Y. Chen, T. Lu, Y. Tang, Int. J. Hydrogen Energy 40 (2015) 6530-6537.

[9] F. Zhan, T. Bian, W. Zhao, H. Zhang, M. Jin, D. Yang, CrystEngComm. 16 (2014) 2411-2416.

[10] Y. Kim, Y. Noh, E.J. Lim, S. Lee, S.M. Choi, W.B. Kim, J. Mater. Chem. A 2 (2014) 6979-6986.

[11] C. Zhu, S. Guo, S. Dong, Adv. Mater. 24 (2012) 2326-2331.

[12] M. Rana, P.K. Patil, M. Chhetri, K. Dileep, R. Datta, U.K. Gautam, J. Colloid. Interf. Sci. 463 (2016) 99-106.
[13] Y. Liu, M. Chi, V. Mazumder, K.L. More, S. Soled, J.D. Henao, S. Sun, Chem. Mater. 23 (2011) 4199-4203.
[14] A.T. Gremmiger, H.W.P.d. Carvalho, R. Popescu, J.-D. Grunwaldt, O. Deutschmann, Catal. Today 258 (2015) 470-480.
[15] N.M. Kinnunen, J.T. Hirvi, M. Suvanto, T.A. Pakkanen, J. Mol. Catal. A: Chem. 356 (2012) 20-28.
[16] A. Ersson, H. Kušar, R. Carroni, T. Griffin, S. Järås, Catal. Today 83 (2003) 265-277.
[17] G. Lapisardi, L. Urfels, P. Gélin, M. Primet, A. Kaddouri, E. Garbowski, S. Toppi, E. Tena, Catal. Today 117 (2006) 564-568.
[18] R. Strobel, J.-D. Grunwaldt, A. Camenzind, S.E. Pratsinis, A. Baiker, Catal. Lett. 104 (2005) 9-16.
[19] C. Micheaud, P. Marécot, M. Guérin, J. Barbier, Appl. Catal. A: Gen. 171 (1998) 229-239.
[20] K. Persson, A. Ersson, K. Jansson, N. Iverlund, S. Järås, J. Catal. 231 (2005) 139-150.
[21] H. Yamamoto, H. Uchida, Catal. Today 45 (1998) 147-151.
[22] K. Narui, H. Yata, K. Furuta, A. Nishida, Y. Kohtoku, T. Matsuzaki, Appl. Catal. A: Gen. 179 (1999) 165-173.
[23] Y. Deng, T.G. Nevell, Catal. Today 47 (1999) 279-286.
[24] R. Abbasi, L. Wu, S.E. Wanke, R.E. Hayes, Chem. Eng. Res. Des. 90 (2012) 1930-1942.
[25] M. Honkanen, T.W. Hansen, H. Jiang, M. Kärkkäinen, M. Huuhtanen, O. Heikkinen, K. Kallinen, J. Lahtinen, R.L. Keiski, J.B. Wagner, M. Vippola, J. Catal. 349 (2017) 19-29.
[26] M. Honkanen, M. Kärkkäinen, T. Kolli, O. Heikkinen, V. Viitanen, L. Zeng, H. Jiang, K. Kallinen, M. Huuhtanen, R.L. Keiski, J. Lahtinen, E. Olsson, M. Vippola, Appl. Catal. B: Environ. 182 (2016) 439-448.
[27] K. Persson, A. Ersson, S. Colussi, A. Trovarelli, S.G. Järås, Appl. Catal. B: Environ. 66 (2006) 175-185.
[28] Y. Ozawa, Y. Tochihara, A. Watanabe, M. Nagai, S. Omi, Appl. Catal. A: Gen. 259 (2004) 1-7.
[29] E.D. Goodman, S. Dai, A.-C. Yang, C.J. Wrasman, A. Gallo, S.R. Bare, A.S. Hoffman, T.F. Jaramillo, G.W. Graham, X. Pan, M. Cargnello, ACS Catal. 7 (2017) 4372-4380.

[30] K. Persson, A. Ersson, K. Jansson, J.L.G. Fierro, S.G. Järås, J. Catal. 243 (2006) 14-24.
[31] K. Persson, L.D. Pfefferle, W. Schwartz, A. Ersson, S.G. Järås, Appl. Catal. B: Environ. 74 (2007) 242-250.
[32] M. Chen, L.D. Schmidt, J. Catal. 56 (1979) 198-218.
[33] A. Morlang, U. Neuhausen, K.V. Klementiev, F.-W. Schütze, G. Miehe, H. Fuess, E.S. Lox, appl. Catal. B: Environ. 60 (2005) 191-199.
[34] T.R. Johns, J.R. Gaudet, E.J. Peterson, J.T. Miller, E.A. Stach, C.H. Kim, M.P. Balogh, A.K. Datye, ChemCatChem 5 (2013) 2636-2645.
[35] C.H. Bartholomew, Appl. Catal. A: Gen. 212 (2001) 17-60.
[36] D. Ciuparu, M.R. Lyubovsky, E. Altman, L.D. Pfefferle, A. Datye, Catal. Rev. 44 (2002) 593-649.
[37] T.V. Choudhary, S. Banerjee, V.R. Choudhary, Appl. Catal. A: Gen. 234 (2002) 1-23.
[38] R. Gholami, M. Alyani, K.J. Smith, Catalysts 5 (2015) 561-594.
[39] Z. Wu, J. Deng, Y. Liu, S. Xie, Y. Jiang, X. Zhao, J. Yang, A. Arandiyan, G. Guo, H. Dai, J. Catal. 332 (2015) 13-24.
[40] R.J. Farrauto, Science 337 (2012) 659-660.
[41] G. Li, W. Hu, F. Huang, J. Chen, M. Gong, S. Yuan, Y. Chen, L. Zhong, Can. J. Chem. Eng. 95 (2017) 1117-1123.
[42] M. Monai, T. Montini, C. Chen, E. Fonda, R.J. Gorte, P. Fornasiero, ChemCatChem 7 (2015) 2038-2046.
[43] D. Pi, W.Z. Li, Q.Z. Lin, Q.F. Huang, H.Q. Hu, C.Y. Shao, Energy Technol. 4 (2016) 943-949.
[44] C.F. Cullis, T.G. Nevell, D.L. Trimm, J. Chem. Soc., Faraday Trans. 1 68 (1972) 1406-1412.
[45] R. Burch, F.J. Urbano, P.K. Loader, Appl. Catal. A: Gen. 123 (1995) 173-184.
[46] R. Burch, P.K. Loader, F.J. Urbano, Catal. Today 27 (1996) 243-248.
[47] D. Roth, P. Gelin, M. Primet, E. Tena, Appl. Catal. A: Gen. 203 (2000) 37-45.
[48] F.H. Ribeiro, M. Chow, R.A. Dalla, J. Catal. 146 (1994) 537-544.
[49] K.I. Fujimoto, F.H. Ribeiro, M. Abalos-Borja, E. Iglesia, J. Catal. 179 (1998) 431-442.
[50] R. Burch, M.J. Hayes, J. Mol. Catal. A: Chem. 100 (1995) 13-33.
[51] W.R. Schwartz, L.D. Pfefferle, J. Phys. Chem. C 116 (2012) 8571-8578.
[52] W.R. Schwartz, D. Ciuparu, L.D. Pfefferle, J. Phys. Chem. C 116 (2012) 8587-8593.

[53] H. Nassiri, K.-E. Lee, Y. Hu, R.E. Hayes, R.W.J. Scott, N. Semagina, J. Catal. 352 (2017) 649-656.
[54] H. Nassiri, K.-E. Lee, Y. Hu, R.E. Hayes, R.W.J. Scott, N. Semagina, ChemPhysChem 18 (2017) 238-244.
[55] J. Shen, R.E. Hayes, X. Wu, N. Semagina, ACS Catal. 5 (2015) 2916-2920.
[56] D. Ciuparu, R. Altman, L. Pfefferle, J. Catal. 203 (2001) 64-74.
[57] C.F. Cullis, B.M. Willatt, J. Catal. 83 (1983) 267-285.
[58] C.H. Bartholomew, Studies in Surface Science and Catalysis, in: B. Delmon, G.F. Froment (Eds.), Catalyst Deactivation 1994, Esevier1994, p. 1.
[59] C. Carrillo, T.R. Johns, H. Xiong, A. DeLaRiva, S.R. Challa, R.S. Goeke, K. Artyushkova, W. Li, C.H. Kim, A.K. Datye, J. Phys. Chem. Lett. 5 (2014) 2089-2093.
[60] G.W. Graham, H.-W. Jen, O. Ezekoye, R.J. Kudla, W. Chun, X.Q. Pan, R.W. McCabe, Catal. Lett. 116 (2007) 1-8.
[61] M.-A. Ha, J. Dadras, A. Alexandrova, ACS Catal. 4 (2014) 3570-3580.
[62] A. Dianat, J. Zimmermann, N. Seriani, M. Bobeth, W. Pompe, L.C. Ciacchi, Suf. Sci. 602 (2008) 876-884.
[63] Y. Yu, B. Fonfé, A. Jentys, G.L. Haller, J.A.R.v. Veen, O.Y. Gutiérrez, J.A. Lercher, J. Catal. 292 (2012) 1-12.
[64] L.C.A.v.d. Oetelaar, O.W. Nooij, S. Oerlemans, A.W.D.v.d. Gon, H.H. Brongersma, J. Phys. Chem. B 102 (1998) 3445-3455.
[65] R. Huang, Y.-H. Wen, Z.-Z. Zhu, S.-G. Sun, J. Phys. Chem. C 116 (2012) 8664-8671.
[66] C. Massen, T.V. Mortimer-Jones, R.L. Johnston, J. Chem. Soc., Dalton Trans. (2002) 4375-4388.
[67] Z. Duan, G. Wang, J. Phys.: Condens. Matter 23 (2011) 475301.
[68] J.R. Kitchin, S.D. Miller, D.S. Sholl, Chem. Modell. 5 (2008) 150-181.
[69] F. Tao, S. Zhang, L. Nguyen, X. Zhang, Chem. Soc. Rev. 41 (2012) 7980-7993.
[70] S. Zafeiratos, S. Piccinin, S. Piccinin, Catal. Sci. Technol. 2 (2012) 1787-1801.
[71] C.M. Celis-Cornejo, J.L. Gómez-Ballesteros, S.A. Giraldo, Revista Ion 26 (2013) 65-72.
[72] J. Shen, R.W.J. Scott, R.E. Hayes, N. Semagina, Appl. Catal. A: Gen. 502 (2015) 350-360.
[73] P.N. Plessow, F. Abild-Pedersen, ACS Catal. 6 (2016) 7098-7108.

[74] C. Carrillo, A. DeLaRiva, H. Xiong, E.J. Peterson, M.N. Spilde, D. Kunwar, R.S. Goeke, M. Wiebenga, S.H. Oh, G. Qi, S.R. Challa, A.K. Datye, Appl. Catal. B: Environ. 218 (2017) 581-590.
[75] H. Xiong, E. Peterson, G. Qi, A.K. Datye, Catal. Today 272 (2016) 80-86.

5.6 Supporting Information

Table 5S.1 Actual metal loadings in the calcined supported catalysts as determined by NAA.

Sample	Pd, wt.%	Pt, wt.%
Mono Pd	0.2550	-
Pd-Pt 5:1	0.2110	0.0640
Pd-Pt 4:1	0.1780	0.0772
Pd-Pt 3:1	0.1490	0.0816
Pd-Pt 2:1	0.1520	0.1240
Pd-Pt 1:1	0.0875	0.1700
Pd-Pt 1:2	0.0659	0.1910
Pd-Pt 1:3	0.0456	0.2170
Pd-Pt 1:4	0.0328	0.2150
Pd-Pt 1:5	0.0245	0.2140
Mono Pt	-	0.295
Pd-Pt 1:1 (C-S)	0.1060	0.1800
Pd-Pt 1:1 (MC)	0.1010	0.1750
Pd-Pt 1:1 (MS)	0.1070	0.1740
Pd-Pt 2:1 (MS)	0.1460	0.1250

Chapter 6. Tin dioxide as a potential replacement of Pt in wet lean methane combustion catalysts[5]

6.1 Introduction

Catalytic oxidation of methane has been extensively studied for pollution emission control and supported palladium catalyst is known as the most active catalyst for this reaction [1-3], with the performance strictly related to the nature of the support through the Pd crystallite size and morphology [4-6], dispersion on the support [7, 8], and Pd-support interaction effects [8-10]. Alumina support has been conventionally used for Pd-catalyzed methane combustion due to its high surface area and low cost. The rate of catalytic deactivation in methane combustion reaction and the water inhibition effect through hydroxyl coverage on the surface [11], as well as the kinetics of surface dihydroxylation [12] are strongly dependent on the nature of the support. The reaction order with respect to water, considering the dependence of its inhibitory effect on the support materials, was reported as being between -0.25 and -1.3 [13-16]. It is also reported that the support materials influence the oxygen adsorption property of Pd and the stability of Pd oxide [17].

A few research groups studied the catalytic performance of Pd catalyst supported on various metal oxides (MO_x; M = Al, Ga, In, Nb, Si, Sn, Ti, Y, Zr, Ni) for methane combustion reaction, and Pd/Al_2O_3-36NiO and Pd/SnO_2 achieved the highest activity [8, 18-24]. SnO_2 is an n-type oxide that is widely used in semiconductor and gas sensor technology [25-27]. It is mostly employed as a support for Pd and Pt catalysts in CO oxidation reaction as it is known to enhance catalytic performance in the combustion of CO due to the beneficial effect of CO spillover [7, 26, 28-31]. For methane combustion reaction, Roth et al. [22] did not observe any beneficial effect of using

[5] Chapter 6 of the thesis is under submission as "Tin dioxide as a potential replacement of Pt in wet lean methane combustion catalysts" H. Nassiri, R.E. Hayes, N. Semagina (2018). The reaction setup for methane oxidation was originally designed and built by Dr. Long Wu and Dr. Robert E. Hayes. The lab view program to communicate with the reaction setup was written by Les Dean. The NAA analysis was performed by Dr. John Duke at the University of Alberta and Becquerel Laboratories Inc.; Maxxam Analytics, Ontario. HRTEM and TEM-EDX mapping were performed by Dr. Jing Shen at the University of Alberta Nanofabrication and Characterization Facility (nanoFAB). SEM analysis was performed by Dr. Shihong Xu at the University of Alberta Nanofabrication and Characterization Facility (nanoFAB). Dr. Shihong Xu and Dr. Anqiang He performed XPS analyses at the University of Alberta Nanofabrication and Characterization Facility (nanoFAB). The author performed all the syntheses, catalytic reactions, analyses and other characterizations. Manuscript preparation and writing were conducted by the author under the supervision and final approval of Dr. Natalia Semagina and Dr. Robert E. Hayes.

SnO_2 support for mono Pd, which could be the reason for using a chlorine-containing precursor for making mono Pd catalyst which is known to have a strong inhibitory effect. Yoshida et al. [17] studied the catalytic activity of Pd and Pt supported on different supports based on the acidic/basic properties of the supports. Less activity was obtained via basic supports due to the higher degree of the stabilization of Pd on them rather than on acidic supports; however, the oxidation state of Pd was higher on the basic supports. In fact, the relationship of activity with the acidic/basic properties of the support may not be applicable to SnO_2, which is a metal oxide intermediate between acidic and basic metal oxides [32]. Widjaja et al. [8] observed high catalytic activity by using 1 wt.% Pd/SnO_2, but their attempt to add other metals, such as Al, Ce, Fe, Mn, Ni, and Zr into the support and to create a SnO_2-MO_x mixed-oxides support with a 1:1 ratio for Pd led to lower activity. They claimed that the high exposure of Pd active centers as a result of making an egg-shell structure around SnO_2 fragments, the interaction of Pd and SnO_2, the adsorption state of oxygen on Pd/SnO_2, and the slow reduction rate of Pd on SnO_2 as a result of strong metal-support interaction (SMSI) are the reasons for the higher activity of Pd/SnO_2 in methane combustion reaction. Sekizawa et al. [20] studied the effect of various Pd precursors, such as $Pd(CH_3COO)_2$, $Pd(C_5H_7OO)_2$, $PdCl_2$, $Pd(NH_3)_4Cl_2$, $Pd(NO_3)_2$, and $PdSO_4$., for impregnated Pd/SnO_2. The highest activity was obtained through the aqueous solution of palladium (II) acetate ($Pd(CH_3COO)_2$). Sekizawa et al. [20] and Zhao et al. [24] also investigated the effect of SnO_2 pretreatment condition. Both groups found that the activity was higher on the well-crystallized SnO_2 surface at 1200ºC due to the higher and better Pd distribution and stability [20], and also the lattice match of PdO and SnO_2 with a higher calcination temperature [24]. They observed a lower amount of oxygen desorption from the SnO_2 surface at a lower pretreatment temperature than 800ºC. Takeguchi et al. [18] studied the effect of the catalytic preparation procedure for Pd/SnO_2 via co-precipitation and impregnation methods with the various metal loadings of 1.1, 5.7, 11, and 22 wt.%. The results revealed that an 11 wt.% Pd loading on SnO_2 prepared via the impregnation method had better performance than did PdO-SnO_2 alloy catalyst (co-precipitation method) with the same loading. Eguchi et al. [19] and Kikuchi et al. [21] followed the research of their group [8, 18, 20] with the investigation of water effect on Pd/SnO_2 by increasing the amount of water from 0 to 20%. The activity dropped with an increase in the water, but Pd/SnO_2 still maintained a good $T_{30\%}$ of 365ºC compared with Pd/Al_2O_3 with $T_{30\%}$ of 510ºC at the 20% water amount. Gholami [23] studied ~ 6 wt.% Pd/SnO_2 for methane combustion reaction in part of his thesis. Its activity

was the same as that of Pd/α-Al_2O_3, which was another low-surface area support, but not higher than a high-surface area support such as Pd/γ-Al_2O_3 and Pd/SiO_2. He also investigated the effect of the hydrothermal aging (HTA) time (0, 16, and 65 h) prior to the reaction with 6.5 vol% water. Pd/SnO_2 demonstrated the same activity after HTAs of 0 and 16 h but failed after an HTA of 65 h. The sintering of Pd particles on SnO_2 at high temperatures and also the transformation of PdO to Pd^0 were mentioned as the reasons.

A previous in situ X-ray absorption study from our group indicated that bimetallic PdPt supported on alumina is a promising catalyst in terms of activity and stability for wet methane combustion. The presence of water leads to the increased fraction of metallic Pd due to the lack of surface oxygen, and this results in Pt atoms to be available for methane dissociation. This does not occur in the dry methane-lean feed in which oxygen poisons Pt [33, 34]. The aim of this study was to assess SnO_2 as a substitute for an expensive and rare second noble metal, for example, Pt, as a promoter through studying of low-loading (~ 0.2-0.3 wt.%) monometallic Pd and bimetallic PdPt catalysts on Al_2O_3 and SnO_2 supports prepared via the colloidal solution technique in both dry and wet conditions.

6.2 Experimental

6.2.1 Materials

Hexachloroplatinic (IV) acid (H_2PtCl_6, 8% w/v solution in water, Sigma-Aldrich), palladium (II) acetate ($Pd(AcO)_2$, Sigma-Aldrich), palladium (II) nitrate dehydrate ($Pd(NO_3)_2.2H_2O$, ~40% Pd basis, Sigma-Aldrich), 1,4-Dioxane (>99.9% Sigma-Aldrich), tin (II) oxalate (SnC_2O_4, 98%, Sigma-Aldrich), poly N-vinylpyrrolidone (PVP, average molecular weight 40,000, Sigma-Aldrich), Ethylene glycol (>99.9%, Fischer Scientific), gamma alumina (γ-Al_2O_3, average pore size 58 Å, SAA 155 m^2/g, Sigma-Aldrich), and tin dioxide (SnO_2, −325 mesh, 99.9% trace metals basis, Sigma-Aldrich) were used as received. Milli-Q water (18.2 MΩ.cm) was used throughout the study.

6.2.2 Catalyst preparation

Pd and Pt monometallic nanoparticles were synthesized via the one-step alcohol reduction method on the basis of 0.2 mmol metal. To synthesize Pt nanoparticles, H_2PtCl_6 and PVP with a molar ratio of $\frac{\text{PVP}}{\text{Metal}} = 40$ were added to a 500-ml flask and were mixed with 80 vol.% ethylene glycol in water solution. In the case of Pd nanoparticles synthesis, $Pd(AcO)_2$ was first dissolved in 10 ml of dioxane and was then mixed with the aforementioned amount of PVP and solvent solution. The resulting mixture was stirred and heated until it boiled and then was refluxed in air under vigorous stirring for 3 h to complete the synthesis of PVP-protected nanoparticles. SnC_2O_4 was used as the Sn precursor in making a bimetallic catalyst with Pd. Bimetallic PdPt and PdSn nanoparticles were synthesized with the co-reduction of metal precursors with the desired molar ratio. The rest of the process was exactly the same as that used for monometallic nanoparticles. A dark colloidal dispersion of nanoparticles was obtained at the end of all syntheses without any precipitates. Nanoparticles were supported on γ-Al_2O_3 and SnO_2 via acetone precipitation to obtain 0.3 wt.% metal loading. High-loading Pd/SnO_2 was achieved through the dry impregnation of 1 ml of an aqueous solution of $Pd(NO_3)_2.2H_2O$ on SnO_2 support followed by drying at 60ºC for 24 h. After drying, all samples were calcined in air at 550°C for 16 h. Hereafter, the catalyst after calcination, which was ready for the reaction, is referred to as a calcined catalyst.

6.2.3 Catalyst characterizations

The metal loading on the catalysts was determined through neutron activation analysis (NAA). Samples were irradiated for 110 s in the Cd shielded, epithermal site of the reactor core. They were counted for 30 min each on an Aptec CS11-A31C gamma detector, approximately 12 h after irradiation.

Transmission electron microscopy (TEM) photographs were taken by using a JEOL-2100 for 50-nm resolution images and JEOL JEM-ARM200CF for scanning transmission electron microscopy (STEM) and energy-dispersive X-ray spectroscopy (EDX) mapping. They were operating at 200 kV. The JEOL JEM-ARM200CF was an atomic resolution S/TEM with a probe Cs-corrected cold field emission gun (cFEG), equipped with a large-collection-angle SDD EDX detector that enabled fast elemental mapping. Specimens were prepared by placing a couple of drops of the colloidal

dispersion of nanoparticles on a copper grid covered with a perforated carbon film and then evaporating the solvent.

Scanning electron microscopy (SEM) was completed with the Zeiss Sigma FE-SEM which is equipped with an Everhart-Thornley Secondary Electron Detector (ET-SE) operating at 20 kV.

Hydrogen temperature-programmed reduction (H_2-TPR) was performed using an AutoChem 2920 instrument (Micromeritics, USA) under atmospheric pressure. About 300 mg of the catalysts was used for the analysis. Before the TPR spectra were collected, samples were initially degassed in 25 ml/min He up to 120ºC with a rate of 10ºC /min and kept at 120°C for 1 h. After cooling down to room temperature under inert atmosphere, they were oxidized in 25 ml/min of 10% O_2 in He up to 550ºC at a rate of 20ºC/min, and then, they were cooled down to room temperature under a mixture of 10% O_2 in He. The TPR spectra were collected in 10% H_2 in Ar from room temperature to 550ºC at a rate of 10 ml/min. After this, the samples were allowed to cool down to ambient temperature under He. Due to the relative thermal conductivities of Ar and H_2 gases, the TCD signals in TPR spectra were reported as inverted signals. Then, negative and positive peaks refer to the release and consumption of hydrogen, respectively.

CO pulse chemisorption analysis was performed with an AutoChem 2920 instrument (Micromeritics, USA). Prior to this analysis, about 100-300 mg of the samples were reduced in 25 ml/min of 10% H_2 in Ar from room temperature to 250ºC for Sn containing samples and to 550ºC for other samples with a rate of 20ºC/min. Then pulse chemisorption was performed by dosing 3% CO in He at room temperature. The volumetric flow rates of CO in He loop gas and He carrier gas were adjusted to 25 mL/min. The deviation of CO chemisorption results for selected catalysts was 0.07 $mol_{CO}/mol_{surface\ metals}$.

X-ray photoelectron spectroscopy (XPS) was performed on calcined samples using a Kratos Axis 165 X-ray photoelectron spectrometer with a mono Al Ka source operated at 15 mA and 14 kV. The survey spectrum and the high-resolution spectrum were scanned with pass energies of 160 eV and 20 eV, respectively. During the acquisition of a spectrum, charge neutralization was applied to compensate for the sample's insulating problem. CasaXPS software was used for the data processing. Core-level binding energies were corrected using the C 1s peak at 284.8 eV as a charge reference.

The Brunauer-Emmett-Teller (BET) surface area and pore size distribution were measured via N_2 adsorption at the liquid nitrogen temperature using Quantachrome Autosorb-iQ analyzer.

6.2.4 Catalytic performance in methane combustion reaction

Wet methane combustion reaction was studied in a conventional tubular reactor over the monometallic Pd and bimetallic PdPt and PdSn nanocatalysts. The detail of the reaction set-up could be found in the previous studies of our group [35, 36]. The reactor tube was packed with pre-calcined catalyst corresponding to 1.2 mg of active Pd. Then, a gas mixture of 10 vol.% CH_4 in nitrogen along with dry air were fed to the reactor at a flow rate of 8.5 ml/min and 205 ml/min, respectively, to produce a CH_4 concentration of about 4000 ppm in the reactor. Next, 5 vol.% water vapor was added to the feed stream by a Series II Legacy HPLC pump to evaluate the effect of water vapor on the catalytic activity. The composition of the product gas was analyzed with an on-line Agilent 7890A gas chromatograph equipped with thermal conductivity (TCD) and flame ionization (FID) detectors. In an ignition-extinction (I-E) test the temperature was increased 50ºC step-wise from 250ºC to 550ºC, decreased vice versa at a rate of 5ºC/min, and kept at each temperature for 45 min to investigate the catalytic performance in a heating or cooling cycle. The I-E test was followed by a hydrothermal aging (HTA) test as follows: In 22 h, the catalyst was cycled between the end-cycle temperature, which was 550ºC, and 400ºC and was kept at each temperature for 1 h. After 22 h, the temperature held constant at 400ºC for about 18 h. Then, the activity recovery at 400ºC was also checked by cutting off the water vapor from the feed stream 6 h after the HTA test. Finally, the catalytic test was terminated with another I-E test to check the catalytic activity after a 40-hour HTA test. The catalyst sample after all of these steps of the reaction was referred to as the used catalyst. Selected catalysts were repeated and methane combustion results reproduced within 2% error. Negligible conversion was obtained for the neat Al_2O_3 support up to 550ºC.

6.3 Results and discussions

The sample information along with metal loadings, amount of CO uptake, and BET surface area are in Table 6.1. CO uptake per gram of pure supports was also evaluated; it was subtracted from

the values for the supported catalysts. The BET surface area of SnO_2 was so low compared with Al_2O_3 that we can refer to it as a non-porous support. It did not change much after five days of reaction, including the first I-E test in the dry condition, the 40-hour HTA test with 5 vol% water, and the second I-E test with 5 vol% water. The pore size distribution did not changed much after the reaction (not shown here).

Table 6.1 The metal loadings, CO uptake, and BET surface area of different catalysts

Samples	Metal loadings (wt.%)[a]		CO uptake (mol/mol $_{metals}$)		BET surface area (m^2/g)	
	Pd	Pt	Calcined	Used	Calcined	Used
Pd/Al_2O_3	0.2550	-	0.380	0.428	-	-
$PdPt/Al_2O_3$	0.0659	0.1910	0.335	0.201	144	-
Pd/SnO_2	0.1910	-	0.164	0.110	6	6
$PdPt/SnO_2$	0.0760	0.2410	0.075	0.103	6	6
Pd/SnO_2 (IMP)[b]	1.0770	-	0.002	0.005	-	-
$PdSn/Al_2O_3$	0.0820	-	0.027	0.023	-	-

[a] determined by NAA.
[b] impregnated catalyst

The catalytic activity of the monometallic Pd and bimetallic PdPt catalysts on γ-Al_2O_3 and SnO_2 supports during the combustion of methane is shown through the first and second I-E tests in Figure 6.1. In both I-E tests, regardless of the presence of water, the mono Pd and bimetallic PdPt on the SnO_2 support are more active than their counter-parts on the Al_2O_3 support are. Water had a lot less of an effect on deactivating the catalysts on the SnO_2 support. The surface area of SnO_2 is much lower than that of alumina; therefore, contrary to some studies [37], the requisite of a support with a high surface area to have greater Pd dispersion for higher catalytic activity is not necessary with low-temperature methane combustion. As shown, the hysteresis effect is strongly dependent on the nature of the support materials. The high oxygen mobility of SnO_2 as a result of forming oxygen vacancies plays a major role in eliminating the hysteresis effect of PdO phase transformation in the extinction cycles, especially in a dry condition [9]. On the other hand, the strong ionic interatomic bonding of alumina makes it less capable of forming surface oxygen

vacancies [38]; this results in less activity in methane oxidation reaction and also makes it more susceptible to hysteresis.

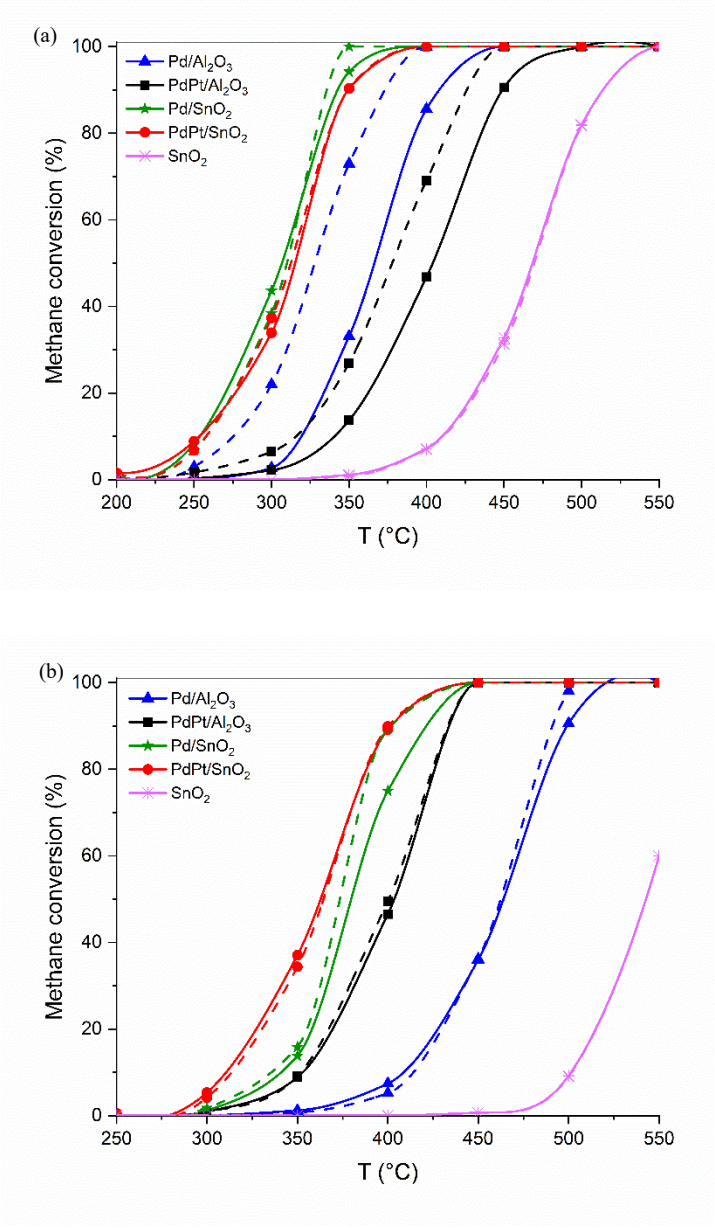

Figure 6.1 I-E (I) (a) and I-E (II) (b) of different catalysts. Catalyst loading in the reactor corresponds to 1.2 mg of active Pd. Solid line (—) indicates the ignition curve, and dashed line (--) indicates the extinction curve.

The degree of stability was tested with HTA for 40 h (Figure 6.2). The bulk non-stoichiometry of SnO_2 within the oxygen lattice makes it able to donate electron density to the adsorbed oxygen molecules with the mobility of electrons from Sn^{2+} to Sn^{4+} sites [26, 39]. However, the use of neat SnO_2 by itself for methane oxidation revealed only 65% activity at 550ºC, and it was not active at 400ºC. SnO_2 contains a low number of active centers on the surface to stabilize electrophilic adsorbed oxygen from the gas phase on the surface. It is highly dependent on the surface defects of SnO_2 that make the surface oxygen vacancies possible [40]. However, in the presence of water, and with the formation of more Sn-OH groups and the accumulation of hydroxyl groups, even fewer active centers for adsorbing oxygen will be present. Therefore, the multivalent oxidation states of the SnO_2 may be beneficial at higher temperatures, at which the thermal desorption of chemisorbed hydroxyl groups occurs, by giving up lattice oxygen for methane oxidation and then reoxidizing with gas-phase oxygen. This would be the same for dry methane oxidation on SnO_2 [41].

The low activity and fast exponential deactivation of Pd/Al_2O_3 with time on stream could be significantly improved with Pt addition. Remarkably, Pd-only catalyst supported on SnO_2 revealed higher activity compared with $PdPt/Al_2O_3$. The further addition of Pt as $PdPt/SnO_2$ did not result in conversion enhancement; it simply made it a bit more stable. It is likely that the beneficial role of SnO_2 in enhancing the activity of PdO sites overrides the Pt-promoting role in bimetallic $PdPt/Al_2O_3$ catalyst.

The activity enhancement of the Pd or PdPt noble metals over the SnO_2 support compared with the alumina, other than the effective exposure of active sites to the reactants [42], can be explained by the electronic and chemical effects that occur over SnO_2 [9, 26, 43]. In a charge transfer or electronic mechanism, a depletion layer is formed at the interface of the noble metal oxide and the SnO_2 surface due to the electron transfer from SnO_2 to PdO. According to our last finding, Pt remains in its metallic form during the reaction [34]; thus PdO is the only active metal oxide. The concept of chemical effect is focused on the oxygen spillover effect, where Pd particles act as portholes for exchanging oxygen between the gas phase and the support and then reoxidize through a reaction with O_2 from the gas phase or through the reverse spillover of O atoms from the SnO_2 support to induce more stability by preventing catalyst deactivation [9, 10, 43, 44]. It is also

believed that chemical effects lead to the better performance of doped SnO_2 more than electronic effects do [43].

The mechanism of water adsorption and its effect on SnO_2 is crucial for finding out the reasons behind the stability of the catalysts in the HTA test. Water adsorption on neat SnO_2 has been investigated via temperature-programmed desorption (TPD), IR, thermal desorption (TDS), and ultraviolet photoelectron spectroscopy (UPS) [45-49]. The results indicated that water is adsorbed in the two states of molecular and surface hydroxyl groups and that the former is easily desorbed at a temperature lower than 150ºC. Meanwhile, the latter are not completely desorbed even at 500ºC [45, 47-49] and the amount of desorption is limited with increasing the density of in-plane surface oxygen vacancies [46, 47]. Nevertheless, the stability of Pd on SnO_2 toward water is related to the associative adsorption of water on tin dioxide under a fully oxidized surface that leads to the electron enrichment of the support surface, which causes less cross-sensitivity to humidity [25]. In other words, water dissociatively adsorbs on neat SnO_2 via adsorbed O^- species on the surface. However, based on the finding of Ma et al. [30], the adsorbed oxygen species on the SnO_2 surface is changed to O^{2-} by just loading small amount Pd on the surface. Therefore, in the presence of water, the electronic effect in the interface of metal-support seems to impede the dissociative adsorption of water on SnO_2 and the O^{2-} on the SnO_2 surface seems to facilitate Pd oxidation during the reaction. On the other hand, Großmann et al. [50] suggested another mechanism of water adsorption for doped SnO_2 in which water vapors react with the surface lattice oxygen to form Sn-OH groups and beneficially create oxygen vacancies on the surface. It is also considered that depending on the catalyst preparation method, the reaction pathway for the adsorption sites in the presence of water might be competitive between the oxygen and the water [19, 51]. Apart from the mechanism, what seems to be dominated in agreement with some studies [10-12] is the higher surface oxygen mobility of the SnO_2 support that induces higher water inhibition resistance. This was also demonstrated in the calculation of the enthalpy of water adsorption for Pd/Al_2O_3 and Pd/SnO_2 catalysts, which was more negative for Pd/Al_2O_3 compared with Pd/SnO_2 catalyst, implying the greater susceptibility of Pd/Al_2O_3 to hydroxyl adsorption on the surface [21]. Activity recovery without the presence of water in the feed stream happened very quickly for the catalysts on SnO_2 and $PdPt/Al_2O_3$ but not for the Pd/Al_2O_3 and SnO_2 by itself.

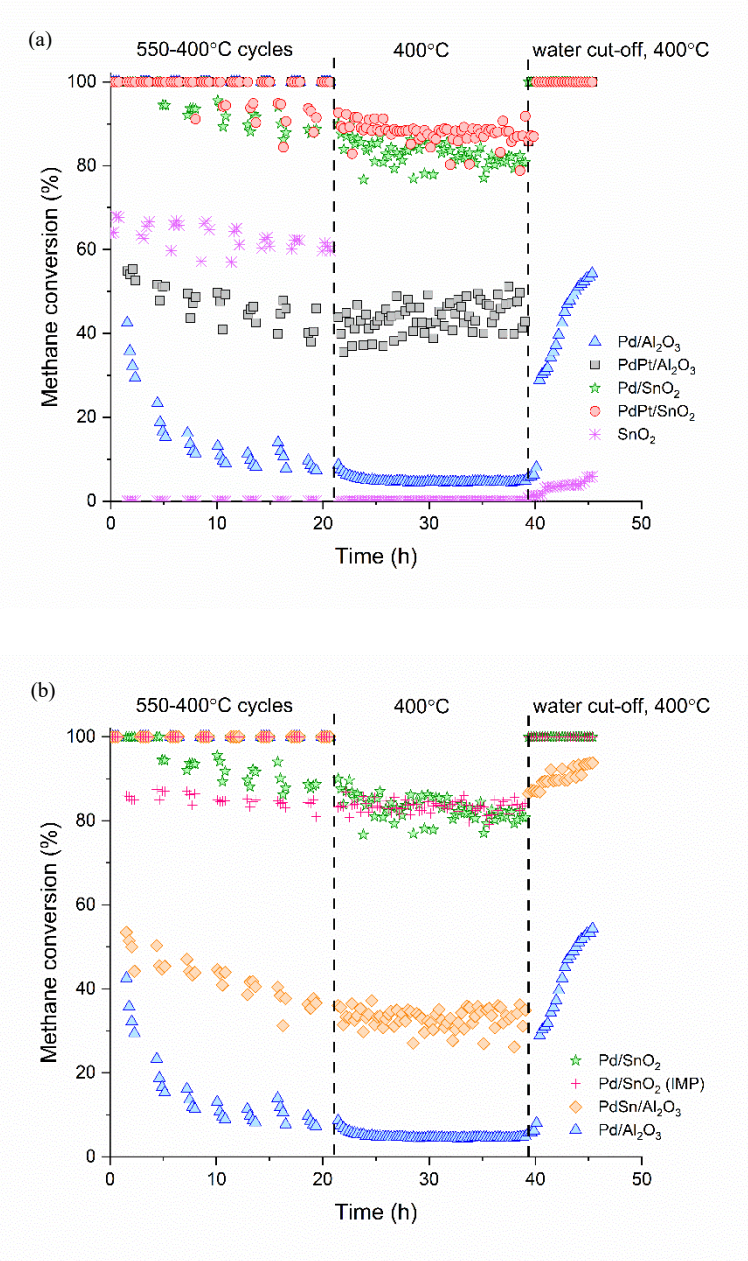

Figure 6.2 HTA test of various catalysts

It is believed that the reoxidation rate of small Pd particles is faster than that of larger particles [8]. However, does it support the relationship of the Pd cluster size and the amount of electron density transferred to Pd from a semiconductor, such as SnO_2, in metal-semiconductor contact theory [52]? Theoretically, the smaller the metal clusters, the more that electrons are transferred, and the more prominent SMSI is on the surface compared with the larger Pd clusters, in which the active centers

are farther away from the metal-support interface and thus cannot easily be affected by the SMSI phenomenon [52, 53]. Therefore, we tried the dry-impregnated high-loading Pd/SnO_2 (IMP) in the reaction. As it is shown in Figure 6.2 (b), surprisingly, no difference in the performance of ca. 0.2 wt.% Pd/SnO_2 prepared via the colloidal solution technique and ca. 1.1 wt.% dry-impregnated Pd/SnO_2 was found. We also increased the amount of water to 10 vol.% after the second I-E test with 5 vol.% water. The biggest activity drop, compared with the 5 vol.% water, happened at 300 and 350ºC with almost a 20-30% drop. At other temperatures, the drop was below 10% (Figure 6.3 (a)). Even after increasing the amount of water, the results of activity recovery with two further I-E tests in the dry condition were the same as that of the first I-E test (Figure 6.3 (b)). However, the results of the first and last I-E tests in the dry condition for the catalysts on Al_2O_3 were totally different. Therefore, the particles benefit from SMSI with SnO_2 support, and no matter what preparation method is used, according to Ma et al. [7], the Pd particle size does not affect the adsorbed oxygen state on the SnO_2 surface.

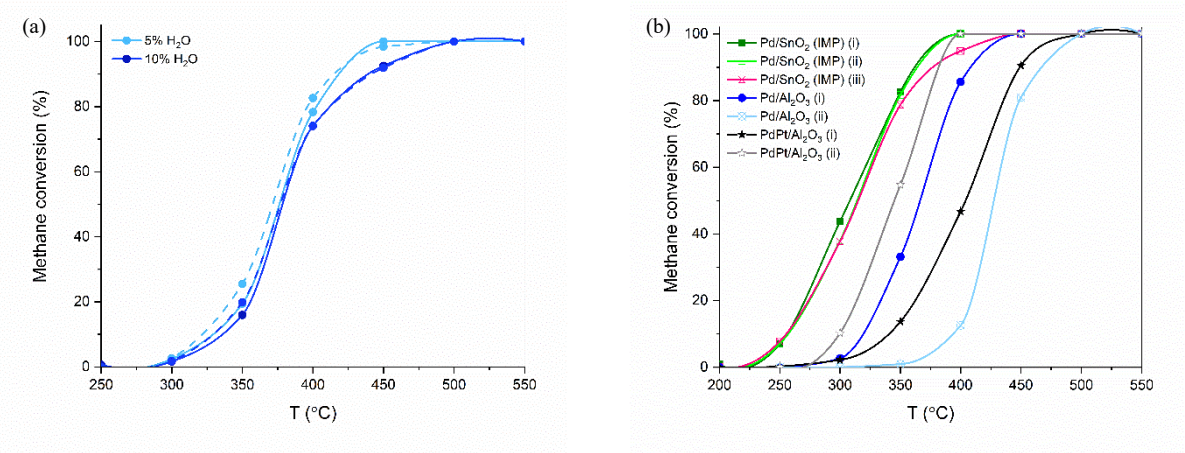

Figure 6.3 (a) Water effect on Pd/SnO_2 (IMP). (b) Activity recovery of Pd/SnO_2 (IMP) in comparison with Pd/Al_2O_3 and $PdPt/Al_2O_3$. Catalyst loading in the reactor corresponds to 1.2 mg of active Pd. Solid line (—) indicates the ignition curve and dashed line (--) indicates the extinction curve.

The attempt to decrease SnO_2 loading by making bimetallic PdSn and having that as $PdSn/Al_2O_3$ did not lead to the aforementioned improvement with Pd/SnO_2 as it relates to the total Pd-mass-based activity (Figure 6.2 (b)). However, TOFs calculated from post-HTA ignition curves (wet

conditions) at 340ºC with the assumption of a differential reactor performance (conversion 4-13%) were found similar for $PdSn/Al_2O_3$ as 128 mmol/($mol_{surface\ Pd}$·s) and Pd/SnO_2 (IMP) as 120 mmol/($mol_{surface\ Pd}$·s). These TOFs are significantly higher than TOF is for the SnO_2 impregnated with preformed 2-nm Pd nanoparticles Pd/SnO_2 (29 mmol/($mol_{surface\ Pd}$·s)) and Pd/Al_2O_3 (1.5 mmol/($mol_{surface\ Pd}$·s)) [34]. This indicates the existence of SMSI, which are enhanced when Pd is atomically dispersed as a molecular precursor with Sn or on SnO_2, but they are not as significant when Pd nanoparticles are deposited on SnO_2.

Willis et al. [54] recently claimed that with $PdSn/Al_2O_3$, an amorphous shell of SnO_2 layers, covers the Pd surface completely and prevents the penetration of methane and oxygen to the catalyst surface at a temperature as high as 500ºC. Metals with high surface energy, such as Pd and Pt, favor encapsulation for minimizing the free surface energy [55]. In addition, oxide with low surface energy, such as SnO_2, tends to contribute to SMSI more than oxides with high surface energy, such as Al_2O_3, do [56]. However, the encapsulation of Pd particles via SnO_2 layers is reversible in the oxidative environment and leads to the re-exposure of catalytic active centers to the reactants [53, 57]. On the other hand, Kim et al. [28] believed that the lower performance of having Pd in the SnO_2 bulk as PdSn is due to the fact that it just benefits from the electronic effects. However, a better interpretation has been achieved via an in situ XAS analysis of methanol oxidation reaction: that alloying Pd with Sn inhibits hydrocarbon adsorption and the dissociation of the C-H bond through the occupation of Pd d-orbitals and by shifting the d-band center down; however, it promotes the dissociative adsorption of oxygen [58, 59]. Therefore, it seems that as a result of the better adsorption of oxygen species, the activity of $PdSn/Al_2O_3$ is higher than that of Pd/Al_2O_3, but it is not a good candidate due to the inhibition of methane dissociation.

SnO_2, can therefore be considered a potential replacement of Pt in a TWC for a NGV. In addition, the high oxygen mobility of SnO_2 preserves it for a longer period of time in the probable perturbation of the feed condition to the oxygen-deficient condition and makes it more desirable in a TWC application. Low-oxygen mobility supports, such as alumina, have less of a chance of surviving the feed mal-condition.

Catalytic activity is also dependent on the Pd oxidation state as seen in TPR profiles (Figure 6.4). TPR experiments indicated the complex behavior of the reduction depending on the support and adsorption state of oxygen to Pd. Samples containing SnO_2 as a support revealed the up-right tail

at 550ºC. It seemed that a large peak would occur after the maximum reaction temperature. In fact, the reduction of bulk SnO_2, for example, the decomposition of SnO_2 to metallic Sn, happens at about 750ºC [60]. Therefore, the assignment of low temperature peaks of SnO_2 at around 280-460ºC is controversial and can be assigned to dissociatively adsorbed oxygen species that participate in CH_4 oxidation [61, 62]. Alternatively, according to Yamaura et al. [63], these three low temperature peaks, from the lowest to the highest temperature, can be assigned to the reduction of anionic oxygen species adsorbed on the SnO_2 surface, near the surface lattice oxygen of SnO_2, and amorphous SnO_2. The small peak at round 130ºC was also assigned to anionic oxygen [45]. Therefore, at lower temperatures, we had a reduction of surface Sn^{4+} to Sn^{2+}, whereas at higher temperatures than 500ºC, we had a reduction of bulk Sn^{4+} to Sn^{2+} and also surface Sn^{2+} to Sn^0 [64]. On the other hand, Pd/SnO_2 revealed a higher reducibility of the Pd-O bond through two large and broad peaks at 150 and 250°C in addition to the negative peak at the lowest temperature, which was due to the releasing adsorbed hydrogen. Additionally, a gentle small peak was also seen at around 350°C, at which PdO reduction was completely achieved [65]. It is concluded that more than one type of oxygen species exists in relation to Pd on SnO_2; O^- and O^{2-}. The latter one could be from O^{2-} adsorbed on PdO [30] or PdO_2 as revealed in XPS data analysis (Table 6.2 and Figure 6.5). In addition, it can be interpreted that the addition of Pd on SnO_2 shifts the reduction of SnO_2 to the lower temperatures. The overlapping of the $PdPt/SnO_2$ TPR profile with Pd/SnO_2 indicates that with both Pd and Pt on the support, the broad band centered at 160ºC is a relatively strong indication of the reduction of a significant amount of SnO_2 at lower temperatures. The TPR profiles of Pd and PdPt on Al_2O_3 revealed completely different trends for the reduction of adsorbed oxygen on the metals, which happened at higher temperatures of around 380 and 430ºC, respectively. On the other hand, $PdSn/Al_2O_3$ demonstrated the intermediate behavior of SnO_2- and Al_2O_3-supported samples by having two peaks at 230 and 320ºC, which could be assigned to the reduction of surface oxygen adsorbed on Sn, and one peak at 490ºC that could be assigned to the reduction of Pd^{2+}.Therefore, at the expense of SnO_2 support in reduction reaction and in participation in oxygen delivery to the metals, Pd and PdPt catalysts on SnO_2 support demonstrated superior activity and stability in methane combustion reaction.

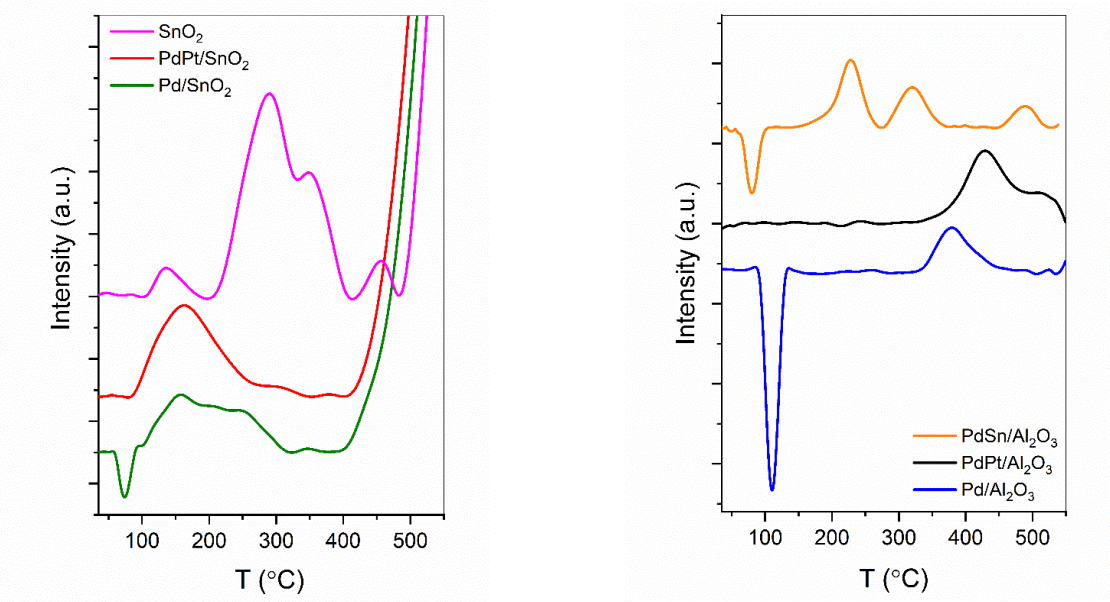

Figure 6.4 TPR profiles of calcined catalysts

The electronic state of supported catalysts were investigated via XPS analysis as depicted in Figure 6.5, along with the binding energy (BE) of Pd and Sn species in Table 6.2 and 6.3. The values of BEs are in accordance with literature. The deconvolution of Pd $3d_{5/2}$ revealed the presence of a Pd^{4+} peak on Sn-containing samples. Highly oxidized Pd^{4+} species may occur due to a reaction with hydroxyl groups on the SnO_2 surface [66]. Although, PdO_2 is unstable in its anhydrous form, it is stabilized by the matrix of other oxides, such as SnO_2 [67]. The presence of the Pd(0) state on $PdSn/Al_2O_3$ may be another reason for its lower activity compared with Pd/SnO_2. The alloy formation of Pd with Sn on $PdSn/Al_2O_3$ was proved through XPS characterization analyses.

Table 6.2 Binding energies values of Sn $3d_{5/2}$

	Calcined	Used
Samples	Sn^{4+} BE (eV)	Sn^{4+} BE (eV)
$PdSn/Al_2O_3$	486.6 [68]	486.2 [69]
Pd/SnO_2	486.7 [70]	486.6 [68]
$PdPt/SnO_2$	486.7 [70]	486.6 [68]

Table 6.3 Binding energies values and area percentage of different states of Pd $3d_{5/2}$

Samples	Calcined						Used					
	Pd^0		Pd^{2+}		Pd^{4+}		Pd^0		Pd^{2+}		Pd^{4+}	
	BE (eV)	Area (%)	BE (eV)	Area (%)	BE (eV)	Area (%)	BE (eV)	Area (%)	BE (eV)	Area (%)	BE (eV)	Area (%)
Pd/Al_2O_3			336.7 [71]	100					336.6 [72]	100		
$PdSn/Al_2O_3$	334.7 [73]	4	336.6 [72]	83	337.7 [73]	13	334.7 [73]	4	336.3 [74]	78	337.5 [75]	18
Pd/SnO_2			336.5 [76]	77	337.4 [77]	23			336.5 [76]	93	337.4 [77]	7
$PdPt/SnO_2$			336.7 [71]	66	337.6 [73]	34			336.5 [76]	75	337.7 [73]	25

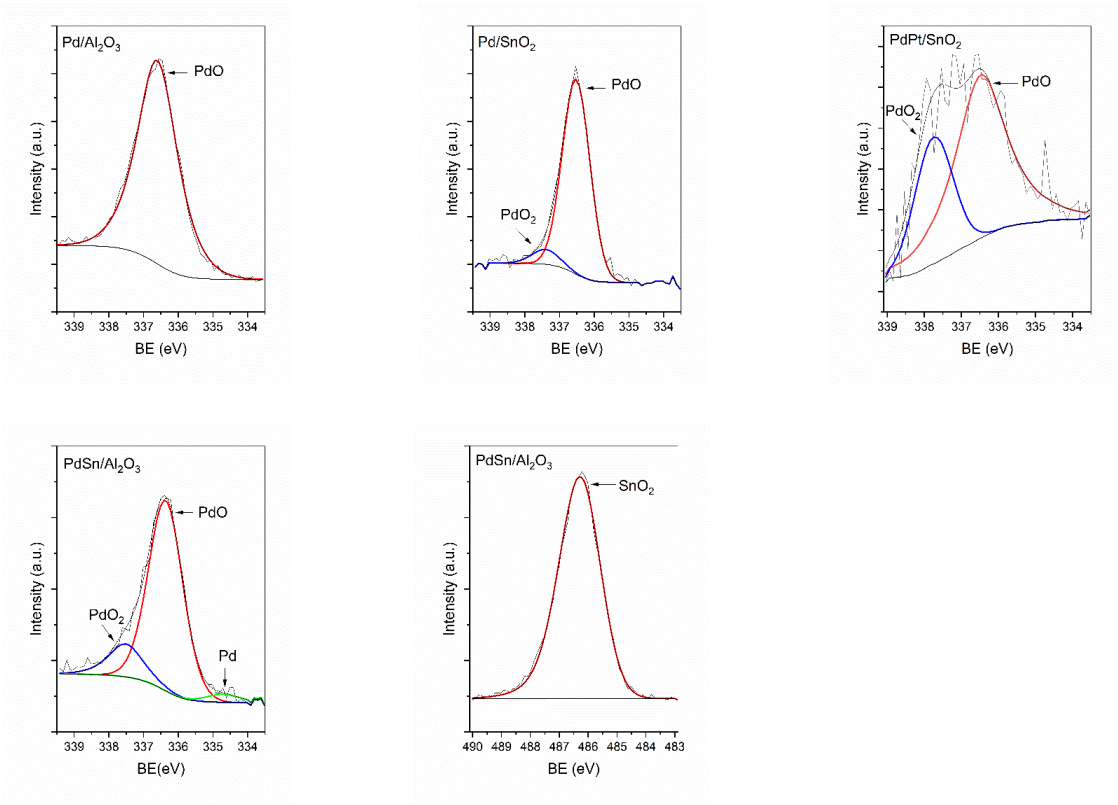

Figure 6.5 XPS spectra of used catalysts

SnO_2 displayed a large particle size and thick chunks due to the low surface area in the SEM and TEM images (Figure 6.6). Some Pd clusters were seen along with partially amorphous SnO_2 support (on the edges) as a result of the low-temperature pretreatment condition of SnO_2 before the deposition of noble metals on SnO_2 (Figure 6.7 (a)). EDX mapping was also used to trace the particles of the used samples (Figure 6.7 (b), (c)). It revealed Pd in clusters over the SnO_2, which implies the perfect exposure of catalytic sites to adsorbed oxygen and for dissociation of methane. This is in agreement with the previous study [8].

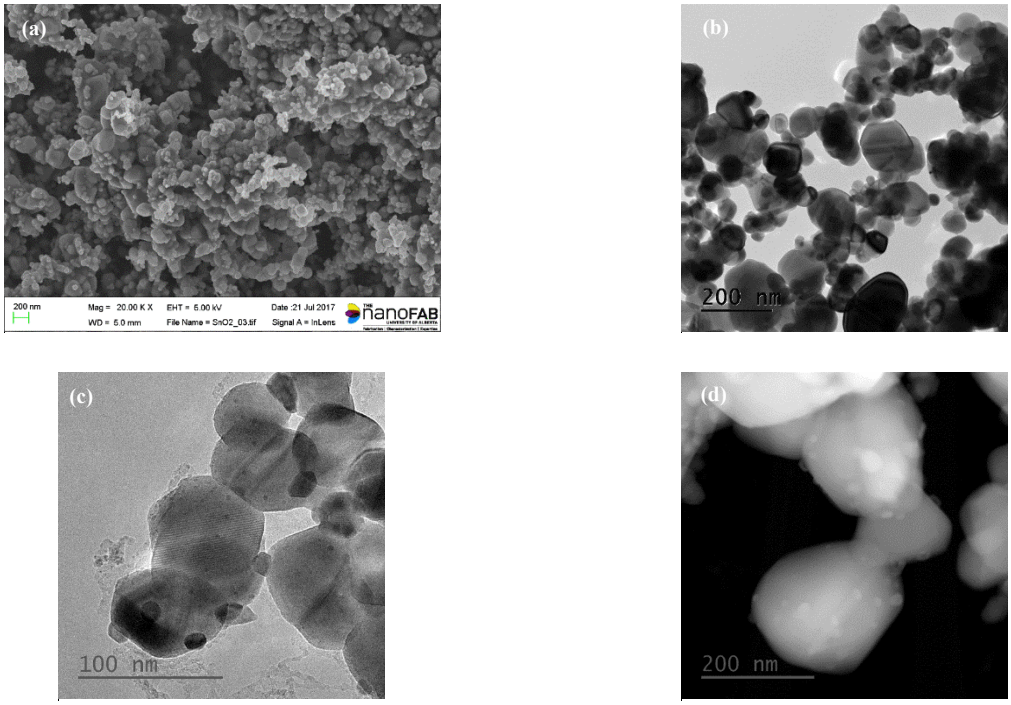

Figure 6.6 (a) SEM and (b) TEM images of SnO_2 support. (c) HRTEM and (d) dark field images of used Pd/SnO_2

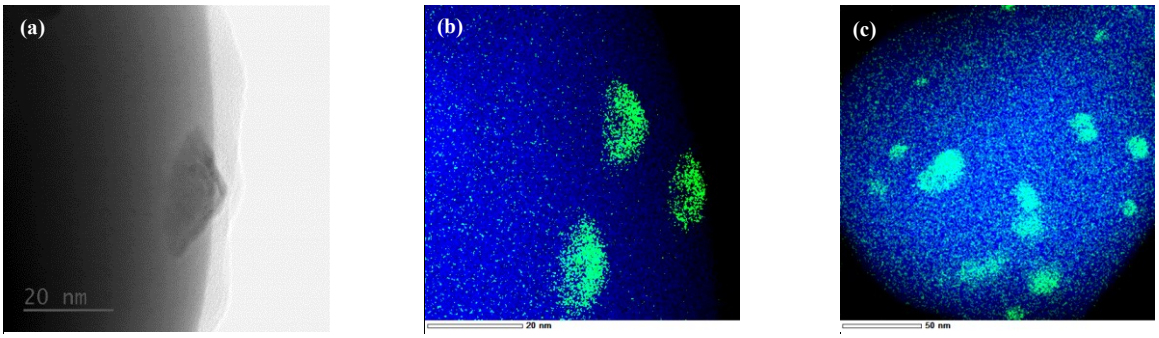

Figure 6.7 STEM-EDX mapping of used Pd/SnO_2. Green is Pd and blue is SnO_2

6.4 Conclusions

The use of SnO_2 support for active Pd metal increases methane conversion in the presence of water to an even higher extent than the addition of Pt to Al_2O_3-supported Pd. The further addition of Pt as $PdPt/SnO_2$ simply led to a bit more stability but no enhancement in activity. The activity and stability enhancement over SnO_2 compared with the conventional alumina support can be explained by SMSI and the mechanism of water adsorption over SnO_2. The expense of SnO_2 in the reduction reaction and in participation in oxygen delivery to Pd was demostrated through the TPR experiments. The deconvolution of Pd $3d_{5/2}$ also revealed the higher oxidation state of Pd (Pd^{4+} peak) on Sn-containing samples. The potential of SnO_2 as a replacement of Pt in wet lean methane combustion decreases the price of the catalytic converter and eliminates the need for scarce Pt.

6.5 References

[1] T. Zhang, Y. Xin, Z. Ren, F. Qi, C.K. Law, Combust. Flame 160 (2013) 149-154.

[2] T. Shimizu, A.D. Abid, G. Poskrebyshev, H. Wang, J. Nabity, J. Engel, J. Yu, D. Wickham, B.V. Devener, S.L. Anderson, S. Williams, Combust. Flame 157 (2010) 421-435.

[3] Y. Xin, H. Wang, C.K. Law, Combust. Flame 161 (2014) 1048-1054.

[4] J.B. Miller, M. Malatpure, Appl. Catal. A: Gen. 495 (2015) 54-62.

[5] B. Yue, R. Zhou, Y. Wang, X. Zheng, Appl. Catal. A: Gen. 295 (2005) 31-39.

[6] B. Yue, R. Zhou, Y. Wang, X. Zheng, J. Mol. Catal. A: Chem. 238 (2005) 241-249.

[7] N. Ma, K. Suematsu, M. Yuasa, K. Shimanoe, ACS Appl. Mater. Interfaces 7 (2015) 15618-15625.

[8] H. Widjaja, K. Sekizawa, K. Eguchi, Bull. Chem. Soc. Jpn. 72 (1999) 313-320.

[9] D. Ciuparu, F. Bozon-Verduraz, L. Pfefferle, J. Phys. Chem. B 106 (2002) 3434-3442.

[10] W.R. Schwartz, L.D. Pfefferle, J. Phys. Chem. C 116 (2012) 8571-8578.

[11] W.R. Schwartz, D. Ciuparu, L.D. Pfefferle, J. Phys. Chem. C 116 (2012) 8587-8593.

[12] D. Ciuparu, E. Perkins, L. Pfefferle, Appl. Catal. A: Gen. 263 (2004) 145-153.

[13] G. Zhu, J. Han, D.Y. Zemlyanov, F.H. Ribeiro, J. Am. Chem. Soc. 126 (2004) 9896-9897.

[14] P. Araya, S. Guerrero, J. Robertson, F.J. Gracia, Appl. Catal. A: Gen. 283 (2005) 225-233.

[15] P. Hurtado, S. Ordóñez, H. Sastre, F.V. Díez, Appl. Catal. B: Environ. 51 (2004) 229-238.
[16] J.-H. Park, B. Kim, C.-H. Shin, G. Seo, S.H. Kim, S.B. Hong, Top. Catal. 52 (2009) 27-34.
[17] H. Yoshida, T. Nakajima, Y. Yazawa, T. Hattori, Appl. Catal. B: Environ. 71 (2007) 70-79.
[18] T. Takeguchi, O. Takeoh, S. Aoyama, J. Ueda, R. Kikuchi, K. Eguchi, Appl. Catal. A: Gen. 252 (2003) 205-214.
[19] K. Eguchi, H. Arai, Appl. Catal. A: Gen. 222 (2001) 359-367.
[20] K. Sekizawa, H. Widjaja, S. Maeda, Y. Ozawa, K. Eguchi, Appl. Catal. A: Gen. 200 (2000) 211-217.
[21] R. Kikuchi, S. Maeda, K. Sasaki, S. Wennerström, K. Eguchi, Appl. Catal. A: Gen. 232 (2002) 23-28.
[22] D. Roth, P. Gelin, E. Tena, M. Primet, Top. Catal. 16/17 (2001) 77-82.
[23] R.G. Shahrestani, Kinetic and deactivation studies of methane oxidation over palladium catalysts in the presence of water, University of British Colombia, Vancouver, Canada, 2015.
[24] Z. Zhao, B. Wang, J. Ma, W. Zhan, L. Wang, Y. Guo, Y. Guo, G. Lu, Chinese J. Catal. 38 (2017) 1322-1329.
[25] G. Santarossa, K. Hahn, A. Baiker, Langmuir 29 (2013) 5487-5499.
[26] N. Murata, T. Suzuki, M. Kobayashi, F. Togoh, K. Asakura, Phys. Chem. Chem. Phys. 15 (2013) 17938-17946.
[27] S. Das, V. Jayaraman, Prog. Mater. Sci. 66 (2014) 112-255.
[28] S.H. Kim, K.T. Lee, S. Lee, J.H. Moon, B.-T. Lee, Jpn. J. Appl. Phys. 41 (2002) L 1002- L 1005.
[29] T. Okanishi, T. Toshiaki, T. Takeguchi, R. Kikuchi, K. Eguchi, Appl. Catal. A: Gen. 298 (2006) 181-187.
[30] N. Ma, K. Suematsu, M. Yuasa, T. Kida, K. Shimanoe, ACS Appl. Mater. Interfaces 7 (2015) 5863-5869.
[31] D. Koziej, M. Hübner, N. Barsan, U. Weimar, M. Sikora, J.-D. Grunwaldt, Phys. Chem. Chem. Phys. 11 (2009) 8620-8625.
[32] M. Ai, J. Catal. 40 (1975) 318-326.
[33] H. Nassiri, K.-E. Lee, Y. Hu, R.E. Hayes, R.W.J. Scott, N. Semagina, ChemPhysChem 18 (2017) 238-244.

[34] H. Nassiri, K.-E. Lee, Y. Hu, R.E. Hayes, R.W.J. Scott, N. Semagina, J. Catal. 352 (2017) 649-656.
[35] R. Abbasi, L. Wu, S.E. Wanke, R.E. Hayes, Chem. Eng. Res. Des. 90 (2012) 1930-1942.
[36] J. Shen, R.E. Hayes, X. Wu, N. Semagina, ACS Catal. 5 (2015) 2916-2920.
[37] K. Persson, A. Ersson, S. Colussi, A. Trovarelli, S.G. Järås, Appl. Catal. B: Environ. 66 (2006) 175-185.
[38] X. Xu, X. Wang, Y. Li, J. Tian, W. Liu, Z. Gao, Z. Phys. Chem. 228 (2014) 27-48.
[39] S.-N. Hong, Y.-H. Kye, C.-J. Yu, U.G. Jong, G.-C. Ri, C.-S. Choe, K.-H. Kim, J.-M. Han, Phys. Chem. Chem. Phys. 18 (2016) 31566-31578.
[40] V. Krivetskiy, M. Rumyntseva, A. Gaskov, in: M.A. Carpenter, S. Mathur, A. Kolmakov (Eds.), Metal oxide nanomaterials for chemical sensors, Springer Science & Business Media, New York, 2013, pp. 76-80.
[41] I. Brown, W.R. Patterson, J. Chem. SOC. Faraday Trans. I 79 (1983) 1431-1449.
[42] H. Widjaja, K. Sekizawa, K. Eguchi, H. Arai, Catal. Today 35 (1997) 197-202.
[43] O.V. Safonova, T. Neisius, A. Ryzhikov, B. Chenevier, A.M. Gaskov, M. Labeau, Chem. Commun. (2005) 5202-5204.
[44] C. Descorme, D. Duprez, Appl. Catal. A: Gen. 202 (2000) 231-241.
[45] N. Yamazoe, J. Fuchigami, M. Kishikawa, T. Seiyama, Surf. Sci. 86 (1979) 335-344.
[46] V.A. Gercher, D.F. Cox, Surf. Sci. 322 (1995) 177-184.
[47] J. Tamaki, M. Nagaishi, Y. Teraoka, N. Miura, N. Yamazoe, Suf. Sci. 221 (1989) 183-196.
[48] M. Egashira, m. Nakashima, S. Kawasumi, T. Seiyama, J. Phys. Chem. 85 (1981) 4125-4130.
[49] E.W. Thornton, P.G. Harrison, J. Chem. SOC. Faraday Trans. I 71 (1975) 461-472.
[50] K. Großmann, S. Wicker, U. Weimar, N. Barsan, Phys. Chem. Chem. Phys. 15 (2013) 19151-19158.
[51] D. Koziej, B. Bârsan, K. Shimanoe, N. Yamazoe, J. Szuber, U. Weimar, Sensors and Actuators B 118 (2006) 98-104.
[52] T. Ioannides, X.E. Verykios, J. Catal. 161 (1996) 560-569.
[53] C.-J. Pan, M.-C. Tsai, W.-N. Su, J. Rick, N.G. Akalework, A.K. Agegnehu, S.-Y. Cheng, B.-J. Hwang, J. Taiwan Inst. Chem. Eng. 74 (2017) 154-186.
[54] J.J. Willis, E.D. Goodman, L. Wu, A.R. Riscoe, P. Martins, C.J. Tassone, M. Cargnello, J. Am. Chem. Soc. 139 (2017) 11989-11997.

[55] S. Labich, E. Taglauer, H. Knözinger, Top. Catal. 14 (2001) 153-161.
[56] Q. Fu, T. Wagner, Suf. Sci. Reports 62 (2007) 431-498.
[57] M. Ahmadi, H. Mistry, B.R. Cuenya, J. Phys. Chem. Lett. 7 (2016) 3519-3533.
[58] J. Salvador–Pascuala, J.A. Chávez–Carvayar, O. Solorza–Feria, ECS Trans. 15 (2008) 3-9.
[59] S. Mukerjee, J. McBreen, J. Electrochem. Soc. 146 (1999) 600-606.
[60] P.W. Park, H.H. Kung, D.-W. Kim, M.C. Kung, J. Catal. 184 (1999) 440-454.
[61] X. Wang, Y.-C. Xie, Catal. Lett. 75 (2001) 73-80.
[62] X. Wang, Y.-C. Xie, New J. Chem. 25 (2001) 1621-1626.
[63] H. Yamaura, S. Hirao, S. Yamaguchi, H. Yahiro, Sensors and Materials 28 (2016) 1203-1210.
[64] S. Chai, X. Bai, J. Li, C. Liu, T. Ding, Y. Tian, C. Liu, H. Xian, W. Mi, X. Li, Appl. Surf. Sci. 402 (2017) 12-20.
[65] A. Baylet, P. Marécot, D. Duprez, P. Castellazzi, G. Groppi, P. Forzatti, Phys. Chem. Chem. Phys. 13 (2011) 4607-4613.
[66] G. Collins, M. Blömker, M. Osiak, J.D. Holmes, M. Bredol, C. O'Dwyer, Chem. Mater. 25 (2013) 4312-4320.
[67] S. Shao, H. Wu, S. Wang, Q. Hong, R. Koehn, T. Wu, W.-F. Rao, J. Mater. Chem. C 3 (2015) 10819-10829.
[68] M. Batzill, U. Diebold, Prog. Surf. Sci. 79 (2005) 47-154.
[69] M.S. Setty, A.P.B. Sinha, Thin Solid Films 144 (1986) 7-19.
[70] W.E. Morgan, J.R.V. Wazer, J. Phys. Chem. 77 (1973) 964-969.
[71] L.P. Haack, K. Otto, Catal. Lett. 34 (1195) 31-40.
[72] K. Noack, H. Zbinden, Catal. Lett. 4 (1990) 145-156.
[73] N. Barsan, M. Schweizer-Berberich, W. Göpel, Fresenius J. Anal. Chem. 365 (1999) 287-304.
[74] K.S. Kim, A.F. Gossmann, N. Winograd, Anal. Chem. 46 (1974) 197-200.
[75] M.K.S. Barr, L. Assaud, N. Brazeau, M. Hanbücken, S. Ntais, L. Santinacci, E.A. Baranova, J. Phys. Chem. C 121 (2017) 17727-17736.
[76] L.S. Kibis, A.I. Stadnichenko, S.V. Koscheev, V.I. Zaikovskii, A.I. Boronin, J. Phys. Chem. C 116 (2012) 19342-19348.
[77] A.M. Venezia, G.D. Carlo, L.F. Liotta, G. Pantaleo, M. Kantcheva, Appl. Catal. B: Environ. 106 (2011) 529-539.

Chapter 7. Conclusions and future work

7.1 Conclusions

The current thesis focused on rational, size-controlled monometallic and bimetallic Pd, Pt, and PdPt catalyst design to develop methane combustion catalysts with high activity and hydrothermal stability using advances in nanotechnology such as the colloidal solution technique. Contrary to the conventional bimetallic catalysts obtained via support impregnation with metal precursors followed by heat treatment, rational catalyst design leads to intrinsic bimetallicity and allows elucidation of structure-property relationships and understanding of the interaction and role of different metallic phases, promoters, and supports in a heterogeneous catalytic reaction. Therefore, the first step was the investigation of the nanoparticles synthesis method and evaluation of influencing parameters. Pd and Pt nanoparticles can be synthesized by an alcohol reduction method in the presence of PVP as a stabilizer. The effect of different metal precursors such as $PdCl_2$, $Pd(AcO)_2$, andH_2PtCl_6 and their concentrations (0.25-1.00 mM) along with different reductants like ethanol and EG on nanoparticle size, size distribution, agglomeration in the systems, and superstructure formation were analyzed and confirmed by the TEM characterization method. It has also been revealed that EG is a better reductant for H_2PtCl_6 and $Pd(AcO)_2$ precursors, while ethanol is successful for $PdCl_2$ to get isolated and monodispersed nanoparticles. Additionally, in the optimal systems monodispersed nanoparticles of ~2 nm were obtained. Thus, synthesis of PVP-protected particles is sensitive to a metal precursor and a solvent, and also the isolated nanoparticles or superstructures of Pd and Pt can be tailored by synthesis conditions.

After developing the synthesis method, in situ XAS analyses in two separate dry and wet conditions were performed to understand the role of Pt in bimetallic PdPt catalysts on γ-Al_2O_3 during methane combustion reactions. It was found that in dry lean methane combustion, a bimetallic PdPt catalyst has lower activity than a monometallic Pd catalyst. Activity suppression by Pt addition to the catalytic system could not be explained by the decrease in dispersion or the reaction structure-sensitivity. According to the in situ XANES and EXAFS spectroscopy measurements on monometallic Pd, Pt and PdPt 2:1 catalysts, the addition of Pt resulted in a reduced Pd phase under an oxidative reaction environment, which has lower activity for the

dissociation of methane compared to the oxidized Pd phase. However, monometallic Pd is fully oxidized in the full temperature range. During the reaction, the Pd/PdO weight ratio in bimetallic PdPt 2:1 catalysts decreases from 98/2 to 10/90 in the 200-500ºC temperature range. The presence of water also led to an increased fraction of metallic Pd due to the lack of surface oxygen. Therefore, the reason behind the improved performance of the bimetallic PdPt catalyst over the monometallic Pd catalyst in the presence of water is that Pt addition hinders the water inhibition effect since the surface oxygen deficit results in Pt atoms available for methane dissociation in the bimetallic PdPt catalyst, which does not occur in the dry condition where oxygen poisons the Pt. Additionally, the pre-reduced Pd catalyst that showed the same activity as the calcined Pd in the dry feed was less active than the calcined Pd in the wet feed. The reason was different Pd oxidation trends in dry and wet feed: in dry feed the pre-reduced Pd catalyst was in an oxidized state at the whole reaction temperature range of 200-600ºC. However, in wet feed the oxidation of Pd(0) happened progressively with the temperature increase. The decreased Pd(0) fraction with increasing temperature was also shown by the thermodynamic analysis, since water renders the surface oxygen deficient at lower temperatures. The fractions of metallic Pd were similar for the monometallic and bimetallic catalysts in the wet feed.

Although role of Pt in PdPt/γ-Al_2O_3 catalysts was clarified via in situ XAS study, understanding the influence of Pt amount on activity and hydrothermal stability of the PdPt catalysts was also crucial. Thus, the effect of the Pd:Pt ratio (from 5:1, 4:1 … to 1:4, 1:5) on the catalytic stability during and after 40-hour in situ hydrothermal ageing at 400-550ºC (5% water) was evaluated. PdPt 1:1 to 4:1 ratios were found to be the most optimal from the viewpoint of activity, with the most stable formulation being a 1:1 Pd-Pt catalyst. A higher content of Pt above a 1:1 ratio leads to better hydrothermal stability, but at a lower activity level. The effect was not governed significantly by particle size, but by the ratio of Pd/Pt that affects the methane and oxygen activation pathways in the wet feed, as was suggested by the in situ XAS study. In the meanwhile, the comparative experiments performed on PdPt 1:1 and 2:1 ratios with Pd core-Pt shell nanoparticles, co-deposited monometallic particles, and monometallic mixed supported catalysts (along with EDX mapping of the used catalysts). It suggested significant structural changes when such particles progressively transformed into alloyed structures with activity and stability approaching those of the alloyed nanoparticles. Seemingly, platinum vaporization (most likely as

PtO_2) is significant in the wet feed at low surface oxygen concentrations even at the temperature interval of 400-550ºC. Therefore, a proper PdPt metal ratio also has a governing effect on the catalytic activity and hydrothermal stability of low-temperature methane combustion compared to the catalyst preparation method.

Platinum-group metal (PGM) depletion and the high costs of PGM in view of the needs of the automotive industry is a problem destined to get worse with time. Therefore, at the end, assessment of SnO_2 as a substitute for part of PGM in the catalytic converters was performed. The activity of various Pd and PdPt catalysts was compared on conventional alumina support and SnO_2 in wet lean methane combustion. Remarkably, Pd-only catalyst supported on SnO_2 revealed higher activity compared with $PdPt/Al_2O_3$. It is likely that the beneficial role of SnO_2 in facilitating oxygen delivery overrides the Pt-promoting role of bimetallic $PdPt/Al_2O_3$ catalyst. The activity and stability enhancement over SnO_2 compared with the conventional alumina support could be explained by SMSI and the mechanism of water adsorption over SnO_2. The expense of SnO_2 in the reduction reaction and in participation in oxygen delivery to Pd was demonstrated through the TPR experiments. Performing the XPS analyses and the deconvolution of Pd $3d_{5/2}$ also revealed the higher oxidation state of Pd (Pd^{4+} peak) on Sn-containing samples. SnO_2 can thus be considered a potential replacement of Pt in a TWC for a NGV. This potentially decreases the price of the catalytic converter and eliminates the need for scarce Pt

7.2 Future work

Important issues relevant to the oxidation catalyst of NGVs are generally associated with: (i) thermal deactivation at high temperature as a result of transformation of PdO to a Pd(0) state (which is less reactive), (ii) resistance level of catalytic systems to poisoning effects of especially sulfur compounds and water, and (iii) catalytic activity level at the lowest temperature typically during the engine cold start. Therefore, further research related to the current thesis could be as follows:

- An extended study of metal oxide supports or mixed-oxide supports for a monometallic Pd catalyst that can maintain Pd in its oxidation state while facilitating methane activation to enhance catalytic activity of the reaction.

- Addition of other material as a promoter or to modify the support to suppress cross-sensitivity of the catalyst to humidity in order to increase hydrothermal stability of the catalyst.
- Lower use of critical materials, especially expensive PGMs, could be considered by studying use of non-noble metal oxide catalysts.
- Further characterization of surface species like isotopic oxygen or Electron Paramagnetic Resonance (EPR) to assess the presence of the paramagnetic metal ion species, oxygen atoms in the form of superoxide (O_2^-), or other oxygen radicals on the surface of the catalyst along with in situ XAS analysis that will provide more information about electronic configuration of the metal ion species.

Bibliography

A. Baylet, P. Marécot, D. Duprez, P. Castellazzi, G. Groppi, P. Forzatti, Phys. Chem. Chem. Phys. 13 (2011) 4607-4613.

A. Chen, P. Holt-Hindle, Chem. Rev. 110 (2010) 3767-3804.

A. Dianat, J. Zimmermann, N. Seriani, M. Bobeth, W. Pompe, L.C. Ciacchi, Suf. Sci. 602 (2008) 876-884.

A. Dianat, N. Seriani, M. Bobeth, W. Pompe, L.C. Ciacchi, J. Phys. Chem. C 112 (2008) 13623-13628.

A. Ersson, H. Kušar, R. Carroni, T. Griffin, S. Järås, Catal. Today 83 (2003) 265-277.

A. Maione, F. André, P. Ruiz, Appl. Catal. B: Environ. 75 (2007) 59-70.

A. Miyazaki, I. Balint, Y. Nakano, J. Nanopart. Res. 5 (2003) 69-80.

A. Molnar, A. Sarkany, M. Varga, J. Mol. Catal. A: Chem. 173 (2001) 185-221.

A. Morlang, U. Neuhausen, K.V. Klementiev, F.-W. Schütze, G. Miehe, H. Fuess, E.S. Lox, Appl. Catal. B: Environ. 60 (2005) 191-199.

A.L. K. Stephan, J. Phys. Chem. Ref. Data 14 (1985) 227-234.

A.M. Venezia, G.D. Carlo, L.F. Liotta, G. Pantaleo, M. Kantcheva, Appl. Catal. B: Environ. 106 (2011) 529-539.

A.T. Gremmiger, H.W.P.d. Carvalho, R. Popescu, J.-D. Grunwaldt, O. Deutschmann, Catal. Today 258 (2015) 470-480.

A.Y. Stakheev, A.M. Batkin, N.S. Teleguina, G.O. Bragina, V.I. Zaikovsky, I.P. Prosvirin, A.K. Khudorozhkov, V.I. Bukhtiyarov, Top. Catal. 56 (2013) 306-310.

B. Coq, F. Figueras, J. Mol. Catal. A: Chem. 173 (2001) 117-134.

B. Ravel, M. Newville, J. Synchrotron Radiat. 12 (2005) 537-541.

B. Yue, R. Zhou, Y. Wang, X. Zheng, Appl. Catal. A: Gen. 295 (2005) 31-39.

B. Yue, R. Zhou, Y. Wang, X. Zheng, J. Mol. Catal. A: Chem. 238 (2005) 241-249.

B.E. Knox, H.B. Palmer, Chem. Rev. 61 (1961) 247-255.

BP Statistical Review of World Energy 2017, 2017. http://www.bp.com/en/global/corporate/energy-economics/statistical-review-of-world-energy.html. (Accessed 9/19/2017 2017).

C. Burda, X. Chen, R. Narayanan, M.A. El-Sayed, Chem. Rev. 105 (2005) 1025-1102.

C. Carrillo, A. DeLaRiva, H. Xiong, E.J. Peterson, M.N. Spilde, D. Kunwar, R.S. Goeke, M. Wiebenga, S.H. Oh, G. Qi, S.R. Challa, A.K. Datye, Appl. Catal. B: Environ. 218 (2017) 581-590.
C. Carrillo, T.R. Johns, H. Xiong, A. DeLaRiva, S.R. Challa, R.S. Goeke, K. Artyushkova, W. Li, C.H. Kim, A.K. Datye, J. Phys. Chem. Lett. 5 (2014) 2089-2093.
C. Descorme, D. Duprez, Appl. Catal. A: Gen. 202 (2000) 231-241.
C. Massen, T.V. Mortimer-Jones, R.L. Johnston, J. Chem. Soc., Dalton Trans. (2002) 4375-4388.
C. Micheaud, P. Marécot, M. Guérin, J. Barbier, Appl. Catal. A: Gen. 171 (1998) 229-239.
C. Zhu, S. Guo, S. Dong, Adv. Mater. 24 (2012) 2326-2331.
C.B. Alcock, G.W. Hooper, Proc. R. Soc. Lond. A 254 (1960) 551-561.
C.B. Y.-H. Chin, M. Neurock, E. Iglesia, J. Am. Chem. Soc. 135 (2013) 15425-15442.
C.F. Cullis, B.M. Willatt, J. Catal. 83 (1983) 267-285.
C.F. Cullis, T.G. Nevell, D.L. Trimm, J. Chem. Soc., Faraday Trans. 1 68 (1972) 1406-1412.
C.H. Bartholomew, Appl. Catal. A: Gen. 212 (2001) 17-60.
C.H. Bartholomew, R.J. Farrauto, Fundamentals of Industrial Catalytic Processes, John Wiely & Sons, Hoboken, New Jersey, 2011.
C.H. Bartholomew, Studies in Surface Science and Catalysis, in: B. Delmon, G.F. Froment (Eds.), Catalyst Deactivation 1994, Esevier 1994, p. 1.
C.-J. Pan, M.-C. Tsai, W.-N. Su, J. Rick, N.G. Akalework, A.K. Agegnehu, S.-Y. Cheng, B.-J. Hwang, J. Taiwan Inst. Chem. Eng. 74 (2017) 154-186.
C.L. Pieck, C.R. Vera, E.M. Peirotti, J.C. Yori, Appl. Catal. A: Gen. 226 (2002) 281-291.
C.M. Celis-Cornejo, J.L. Gómez-Ballesteros, S.A. Giraldo, Revista Ion 26 (2013) 65-72.
D. Ciuparu, E. Perkins, L. Pfefferle, Appl. Catal. A: Gen. 263 (2004) 145-153.
D. Ciuparu, F. Bozon-Verduraz, L. Pfefferle, J. Phys. Chem. B 106 (2002) 3434-3442.
D. Ciuparu, L. Pfefferle, Appli. Catal. A: Gen. 209 (2001) 415-428.
D. Ciuparu, M.R. Lyubovsky, E. Altman, L.D. Pfefferle, A. Datye, Catal. Rev. 44 (2002) 593-649.
D. Ciuparu, N. Katsikis, L. Pfefferle, Appl. Catal. A: Gen. 216 (2001) 209-215.
D. Ciuparu, R. Altman, L. Pfefferle, J. Catal. 203 (2001) 64-74.
D. Koziej, B. Bârsan, K. Shimanoe, N. Yamazoe, J. Szuber, U. Weimar, Sensors and Actuators B 118 (2006) 98-104.
D. Koziej, M. Hübner, N. Barsan, U. Weimar, M. Sikora, J.-D. Grunwaldt, Phys. Chem. Chem. Phys. 11 (2009) 8620-8625.

D. Pi, W.Z. Li, Q.Z. Lin, Q.F. Huang, H.Q. Hu, C.Y. Shao, Energy Technol. 4 (2016) 943-949.
D. Roth, P. Gelin, E. Tena, M. Primet, Top. Catal. 16/17 (2001) 77-82.
D. Roth, P. Gelin, M. Primet, E. Tena, Appl. Catal. A: Gen. 203 (2000) 37-45.
D.D. Wagman, W.H. Evans, V.B. Parker, R.H. Schumm, I.Halow, S.M.Bailey, K.L. Churney, R.L. Nutall, J. Phys. Chem. Ref. Data 11(suppl. 2) (1982) 1-392.
E. Becker, P.-A. Carlsson, H. Grönbeck, M. Skoglundh, J. Catal. 252 (2007) 11-17.
E.D. Goodman, S. Dai, A.-C. Yang, C.J. Wrasman, A. Gallo, S.R. Bare, A.S. Hoffman, T.F. Jaramillo, G.W. Graham, X. Pan, M. Cargnello, ACS Catal. 7 (2017) 4372-4380.
E.I. S. Kunz, J. Phys. Chem. C 118 (2014) 7468-7479.
E.N. Fuller, P.D. Schettler, J.C. Giddings, Ind. Eng. Chem. 58 (1966) 18-27.
E.W. Thornton, P.G. Harrison, J. Chem. SOC. Faraday Trans. I 71 (1975) 461-472.
F. Bonet, V. Delmas, S. Grugeon, R.H. Urbina, P.Y. Silvert, K. Tekaia-Elhsissen, Nanostructured Materials 11 (1999) 1277-1284.
F. Klingstedt, A.K. Neyestanaki, R. Byggningsbacka, L.E. Lindfors, M. Lundén, M. Petersson, P. Tengström, T. Ollonqvist, J. Väyrynen, Appl. Catal. A: Gen. 209 (2001) 301-316.
F. Tao, S. Zhang, L. Nguyen, X. Zhang, Chem. Soc. Rev. 41 (2012) 7980-7993.
F. Zaera, Prog. Surf. Sci. 69 (2001) 1-98.
F. Zhan, T. Bian, W. Zhao, H. Zhang, M. Jin, D. Yang, CrystEngComm. 16 (2014) 2411-2416.
F.H. Ribeiro, M. Chow, R.A. Dalla, J. Catal. 146 (1994) 537-544.
G. Collins, M. Blömker, M. Osiak, J.D. Holmes, M. Bredol, C. O'Dwyer, Chem. Mater. 25 (2013) 4312-4320.
G. Groppi, C. Cristiani, L. Lietti, P. Forzatti, Stud. Surf. Sci. Catal. 130 (2000) 3801-3806.
G. Lapisardi, L. Urfels, P. Gélin, M. Primet, A. Kaddouri, E. Garbowski, S. Toppi, E. Tena, Catal. Today 117 (2006) 564-568.
G. Li, W. Hu, F. Huang, J. Chen, M. Gong, S. Yuan, Y. Chen, L. Zhong, Can. J. Chem. Eng. 95 (2017) 1117-1123.
G. Santarossa, K. Hahn, A. Baiker, Langmuir 29 (2013) 5487-5499.
G. Zhu, J. Han, D.Y. Zemlyanov, F.H. Ribeiro, J. Am. Chem. Soc. 126 (2004) 9896-9897.
G.G.P. Castellazzi, P. Forzatti, Appl. Catal. B: Environ. 95 (2010) 303-311.
G.N. Vayssilov, Y. Lykhach, A. Migani, T. Staudt, G.P. Petrova, N. Tsud, T. Skála, A. Bruix, F. Illas, K.C. Prince, V. Matolín, K.M. Neyman, J. Libuda, Nature Mater. 10 (2011) 310-315.

G.P.W. Lyons, M. Lorenz, Standard handbook of petroleum and natural gas engineering, 3rd ed., Elsevier 2016.
G.W. Graham, H.-W. Jen, O. Ezekoye, R.J. Kudla, W. Chun, X.Q. Pan, R.W. McCabe, Catal. Lett. 116 (2007) 1-8.
H. Naohara, Y. Okamoto, N. Toshima, J. Power Sources 196 (2011) 7510-7513.
H. Nassiri, K.-E. Lee, Y. Hu, R.E. Hayes, R.W.J. Scott, N. Semagina, ChemPhysChem 18 (2017) 238-244.
H. Nassiri, K.-E. Lee, Y. Hu, R.E. Hayes, R.W.J. Scott, N. Semagina, J. Catal. 352 (2017) 649-656.
H. Widjaja, K. Sekizawa, K. Eguchi, Bull. Chem. Soc. Jpn. 72 (1999) 313-320.
H. Widjaja, K. Sekizawa, K. Eguchi, H. Arai, Catal. Today 35 (1997) 197-202.
H. Xiong, E. Peterson, G. Qi, A.K. Datye, Catal. Today 272 (2016) 80-86.
H. Yamamoto, H. Uchida, Catal. Today 45 (1998) 147-151.
H. Yamaura, S. Hirao, S. Yamaguchi, H. Yahiro, Sensors and Materials 28 (2016) 1203-1210.
H. Yoshida, T. Nakajima, Y. Yazawa, T. Hattori, appl. Catal. B: Environ. 71 (2007) 70-79.
H. Zhang, M. Jin, Y. Xia, Chem. Soc. Rev. 41 (2012) 8035-8049.
H.R. X. Weng, M. Chen, H. Wan, ACS Catal. 4 (2014) 2598-2604.
H.S. Fogler, Elements of chemical reaction engineering, 4th ed., Pearson Education Inc. 2006.
H.S. Fogler, Elements of chemical reaction engineering, 4th Ed., Prentice Hall, 2005.
H.X. Zhang, C. Wang, J.Y. Wang, J.J. Zhai, W.B. Cai, J. Phys. Chem. C. 114 (2010) 6446-6451.
I. Brown, W.R. Patterson, J. Chem. SOC. Faraday Trans. I 79 (1983) 1431-1449.
International Energy Outlook 2016, US energy information administration (EIA), 2016, pp. 1-276.
J. Au-Yeung, K. Chen, A.T. Bell, E. Iglesia, J. Catal. 188 (1999) 132-139.
J. Chen, B. Lim, E.P. Lee, Y. Xia, Nano Today 4 (2009) 81-95.
J. Perez-Ramirez, R.J. Berger, G. Mul, F. Kapteijn, J.A. Moulijn, Catal. Today 60 (2000) 93-109.
J. Salvador–Pascuala, J.A. Chávez–Carvayar, O. Solorza–Feria, ECS Trans. 15 (2008) 3-9.
J. Shen, N. Semagina, ACS Catal. 4 (2014) 268-279.
J. Shen, R.E. Hayes, X. Wu, N. Semagina, ACS Catal. 5 (2015) 2916-2920.
J. Shen, R.W.J. Scott, R.E. Hayes, N. Semagina, Appl. Catal. A: Gen. 502 (2015) 350-360.
J. Tamaki, M. Nagaishi, Y. Teraoka, N. Miura, N. Yamazoe, Suf. Sci. 221 (1989) 183-196.
J.A. Moulijn, A.E.v. Diepen, F. Kapteijn, Appl. Catal. A: Gen. 212 (2001) 3-16.

J.B. Miller, M. Malatpure, Appl. Catal. A: Gen. 495 (2015) 54-62.

J.-D. Grunwaldt, M. Maciejewski, A. Baiker, Phys. Chem. Chem. Phys. 5 (2003) 1481-1488.

J.F. Le Page, Applied heterogeneous catalysis: design, manufacture, use of solid catalysts, Technip, Paris, France, 1987.

J.G. McCarty, Catal. Today 26 (1995) 283-293.

J.-H. Park, B. Kim, C.-H. Shin, G. Seo, S.H. Kim, S.B. Hong, Top. Catal. 52 (2009) 27-34.

J.J. Willis, E.D. Goodman, L. Wu, A.R. Riscoe, P. Martins, C.J. Tassone, M. Cargnello, J. Am. Chem. Soc. 139 (2017) 11989-11997.

J.L. DuBois, P. Mukherjee, T.D.P. Stack, B. Hedman, E.I. Solomon, K.O. Hodgson, J. Am. Chem. Soc. 122 (2000) 5775-5787.

J.N. Armor, Appl. Catal. A: Gen. 194-195 (2000) 3-11.

J.R. Kitchin, S.D. Miller, D.S. Sholl, Chem. Modell. 5 (2008) 150-181.

J.S. Warner, J. Electrochem. Soc. 114 (1967) 68-71.

K. Eguchi, H. Arai, Appl. Catal. A: Gen. 222 (2001) 359-367.

K. Großmann, S. Wicker, U. Weimar, N. Barsan, Phys. Chem. Chem. Phys. 15 (2013) 19151-19158.

K. Murtezaoglu, E. Oray, T. Dogu, G. Dogu, N. Saracoglum C. Cabbar, J. Chem. Eng. Data 40 (1995) 720-725.

K. Narui, H. Yata, K. Furuta, A. Nishida, Y. Kohtoku, T. Matsuzaki, Appl. Catal. A: Gen. 179 (1999) 165-173.

K. Noack, H. Zbinden, Catal. Lett. 4 (1990) 145-156.

K. Nomura, K. Noro, Y. Nakamura, Y. Yazawa, H. Yoshida, A. Satsuma, T. Hattori, Catal. Lett. 53 (1998) 167-169.

K. Persson, A. Ersson, K. Jansson, J.L.G. Fierro, S.G. Järås, J. Catal. 243 (2006) 14-24.

K. Persson, A. Ersson, K. Jansson, N. Iverlund, S. Järås, J. Catal. 231 (2005) 139-150.

K. Persson, A. Ersson, S. Colussi, A. Trovarelli, S.G. Järås, Appl. Catal. B: Environ. 66 (2006) 175-185.

K. Persson, K. Jansson, S.G. Järås, J. Catal. 245 (2007) 401-414.

K. Persson, L.D. Pfefferle, W. Schwartz, A. Ersson, S.G. Järås, Appl. Catal. B: Environ. 74 (2007) 242-250.

K. Sekizawa, H. Widjaja, S. Maeda, Y. Ozawa, K. Eguchi, Appl. Catal. A: Gen. 200 (2000) 211-217.

K. Stephan, A. Laesecke, The thermal conductivity of fluid air, J. Phys. Chem. Ref. Data, 14 (1985) 227-234.

K. Wu, Q. Zhang, D. Sun, X. Zhu, Y. Chen, T. Lu, Y. Tang, Int. J. Hydrogen Energy 40 (2015) 6530-6537.

K.C. Taylor, Automobile Catalytic Converters, Springer-Verlag, Berlin, 1984.

K.I. Fujimoto, F.H. Ribeiro, M. Abalos-Borja, E. Iglesia, J. Catal. 179 (1998) 431-442.

K.M. Koczkur, S. Mourdikoudis, L. Polavarapu, S.E. Skrabalak, Dalton Trans. 44 (2015) 17883-17905.

K.S. Kim, A.F. Gossmann, N. Winograd, Anal. Chem. 46 (1974) 197-200.

L. Ma, D.L. Trimm, C. Jiang, Appl. Catal. A: Gen. 138 (1996) 275-283.

L.C.A. van den Oetelaar, O.W. Nooij, S. Oerlemans, A.W.D.v.d. Gon, H.H. Brongersma, J. Phys. Chem. B 102 (1998) 3445-3455.

L.P. Haack, K. Otto, Catal. Lett. 34 (1195) 31-40.

L.S. Escandón, D. Niño, E. Díaz, S. Ordóñez, F.V. Díez, Catal. Commun. 9 (2008) 2291-2296.

L.S. Kibis, A.I. Stadnichenko, S.V. Koscheev, V.I. Zaikovskii, A.I. Boronin, J. Phys. Chem. C 116 (2012) 19342-19348.

M. Ahmadi, H. Mistry, B.R. Cuenya, J. Phys. Chem. Lett. 7 (2016) 3519-3533.

M. Ai, J. Catal. 40 (1975) 318-326.

M. Aryafar, F. Zaera, Catal. Lett. 48 (1997) 173-183.

M. Batzill, U. Diebold, Prog. Surf. Sci. 79 (2005) 47-154.

M. Cargnello, J.J.D. Jaén, J.C.H. Garrido, K. Bakhmutsky, T. Montini, J.J.C. Gámez, R.J. Gorte, P. Fornasiero, Science 337 (2012) 713-717.

M. Chen, L.D. Schmidt, J. Catal. 56 (1979) 198-218.

M. Egashira, m. Nakashima, S. Kawasumi, T. Seiyama, J. Phys. Chem. 85 (1981) 4125-4130.

M. Honkanen, M. Kärkkäinen, T. Kolli, O. Heikkinen, V. Viitanen, L. Zeng, H. Jiang, K. Kallinen, M. Huuhtanen, R.L. Keiski, J. Lahtinen, E. Olsson, M. Vippola, Appl. Catal. B: Environ. 182 (2016) 439-448.

M. Honkanen, T.W. Hansen, H. Jiang, M. Kärkkäinen, M. Huuhtanen, O. Heikkinen, K. Kallinen, J. Lahtinen, R.L. Keiski, J.B. Wagner, M. Vippola, J. Catal. 349 (2017) 19-29.

M. Kumar, G. Rattan, R. Prasad, Canadian Chem. Trans. 3 (2015) 381-409.
M. Lyubovsky, L. Pfefferle, Appl. Catal. A: Gen. 173 (1998) 107-119.
M. Monai, T. Montini, C. Chen, E. Fonda, R.J. Gorte, P. Fornasiero, ChemCatChem 7 (2015) 2038-2046.
M. Montalti, A. Credi, L. Prodi, M.T. Gandolfi, Handbook of photochemistry, 3rd ed., Taylor & Francis Group LLC, USA, 2006.
M. Rana, P.K. Patil, M. Chhetri, K. Dileep, R. Datta, U.K. Gautam, J. Colloid. Interf. Sci. 463 (2016) 99-106.
M. Valden, N. Xiang, J. Pere, M. Pessa, Appl. Surf. Sci. 99 (1996) 83-89.
M.-A. Ha, J. Dadras, A. Alexandrova, ACS Catal. 4 (2014) 3570-3580.
M.A. Vannice, Kinetics of catalytic reactions, Springer, New York, 2005.
M.K.S. Barr, L. Assaud, N. Brazeau, M. Hanbücken, S. Ntais, L. Santinacci, E.A. Baranova, J. Phys. Chem. C 121 (2017) 17727-17736.
M.M. Khalasane, J. Info. Knowl. Res. Mec. Eng. 4 (2016) 668-674.
M.S. Setty, A.P.B. Sinha, Thin Solid Films 144 (1986) 7-19.
M.S. Spencer, M.V. Twigg, Annu. Rev. Mater. Res. 35 (2005) 427-464.
N. Barsan, M. Schweizer-Berberich, W. Göpel, Fresenius J. Anal. Chem. 365 (1999) 287-304.
N. Ma, K. Suematsu, M. Yuasa, K. Shimanoe, ACS Appl. Mater. Interfaces 7 (2015) 15618-15625.
N. Ma, K. Suematsu, M. Yuasa, T. Kida, K. Shimanoe, ACS Appl. Mater. Interfaces 7 (2015) 5863-5869.
N. Murata, T. Suzuki, M. Kobayashi, F. Togoh, K. Asakura, Phys. Chem. Chem. Phys. 15 (2013) 17938-17946.
N. Semagina, L. Kiwi-Minsker, Catal. Rev. 51 (2009) 147-217.
N. Toshima, H. Yan, Y. Shiraishi, Recent progress in bimetallic nanoparticles: their preparation, structures and functions, Elsevier, The Netherlands, 2008.
N. Toshima, Metal Nanoparticles Used as Catalysts, 2nd ed., CRC Press, New York, 2008.
N. Toshima, T. Yonezawa, K. Kushihashi, J. Chem. Soc. Faraday Trans. 89 (1993) 2537-2543.
N. Yamazoe, J. Fuchigami, M. Kishikawa, T. Seiyama, Surf. Sci. 86 (1979) 335-344.
N.M. Kinnunen, J.T. Hirvi, M. Suvanto, T.A. Pakkanen, J. Mol. Catal. A: Chem. 356 (2012) 20-28.

N.M. Kinnunen, J.T. Hirvi, T. Venäläinen, M. Suvanto, T.A. Pakkanen, Appl. Catal. A: Gen. 397 (2011) 54-61.

O. Demoulin, M. Navez, E.M. Gaigneaux, P. Ruiz, A.-S. Mamede, P. Granger, E. Payen, Phys. Chem. Chem. Phys. 5 (2003) 4394-4401.

O.M. Wilson, M.R. Knecht, J.C. Garcia-Martinez, R.M. Crooks, J. Am. Chem. Soc. 128 (2006) 4510-4511.

O.V. Safonova, T. Neisius, A. Ryzhikov, B. Chenevier, A.M. Gaskov, M. Labeau, Chem. Commun. 0 (2005) 5202-5204.

P. Araya, S. Guerrero, J. Robertson, F.J. Gracia, Appl. Catal. A: Gen. 283 (2005) 225-233.

P. Gelin, L. Urfels, M. Primet, E. Tena, Catal. Today 83 (2003) 45-57.

P. Gélin, M. Primet, Appl. Catal. B: Environ. 39 (2002) 1-37.

P. Hurtado, S. Ordonez, H. Sastre, F.V. Diez, Appl. Catal. B: Environ. 47 (2004) 85-93.

P. Hurtado, S. Ordóñez, H. Sastre, F.V. Díez, Appl. Catal. B: Environ. 51 (2004) 229-238.

P. Mäki-Arvela, D.Y. Murzin, Appl. Catal. A: Gen. 451 (2013) 251-281.

P.N. Plessow, F. Abild-Pedersen, ACS Catal. 6 (2016) 7098-7108.

P.W. Park, H.H. Kung, D.-W. Kim, M.C. Kung, J. Catal. 184 (1999) 440-454.

Q. Fu, T. Wagner, Suf. Sci. Reports 62 (2007) 431-498.

Q. Yuan, Z. Zhou, J. Zhuang, X. Wang, Chem. Commun. 46 (2010) 1491-1493.

R. Abbasi, L. Wu, S.E. Wanke, R.E. Hayes, Chem. Eng. Res. Des. 90 (2012) 1930-1942.

R. Burch, F.J. Urbano, Appl. Catal. A: Gen. 124 (1995) 121-138.

R. Burch, F.J. Urbano, P.K. Loader, Appl. Catal. A: Gen. 123 (1995) 173-184.

R. Burch, M.J. Hayes, J. Mol. Catal. A: Chem. 100 (1995) 13-33.

R. Burch, P.K. Loader, Appl. Catal. B: Environ. 5 (1994) 149-164.

R. Burch, P.K. Loader, F.J. Urbano, Catal. Today 27 (1996) 243-248.

R. Gholami, M. Alyani, K.J. Smith, Catalysts 5 (2015) 561-594.

R. Huang, Y.-H. Wen, Z.-Z. Zhu, S.-G. Sun, J. Phys. Chem. C 116 (2012) 8664-8671.

R. Kikuchi, S. Maeda, K. Sasaki, S. Wennerström, K. Eguchi, Appl. Catal. A: Gen. 232 (2002) 23-28.

R. Strobel, J.-D. Grunwaldt, A. Camenzind, S.E. Pratsinis, A. Baiker, Catal. Lett. 104 (2005) 9-16.

R.E. Hayes, Chem. Eng. Sci. 59 (2004) 4073-4080.

R.E. Hayes, J.P. Mmbaga, Introduction to chemical reactor analysis, 2nd ed., CRC Press, 2013.
R.E. Hayes, S.T. Kolaczkowski, Intoduction to Catalytic Combustion, 1st ed., Gordon and Breach Science Publisher, Amsterdam, 1997.
R.F. Hicks, H. Qi, M.L. Young, R.G. Lee, J. Catal. 122 (1990) 280-294.
R.G. Shahrestani, Kinetic and deactivation studies of methane oxidation over palladium catalysts in the presence of water, University of British Colombia, Vancouver, Canada, 2015.
R.I. Esparza, G. Rosas, E. Valenzuela, S.A. Gamboa, U. Pa, R. Pérez, Revista Matéria 13 (2008) 579-586.
R.J. Farrauto, M.C. Hobson, T. Kennelly, E.M. Waterman, Appl. Catal. A: Gen. 81 (1992) 227-237.
R.J. Farrauto, Science 337 (2012) 659-660.
S. Chai, X. Bai, J. Li, C. Liu, T. Ding, Y. Tian, C. Liu, H. Xian, W. Mi, X. Li, Appl. Surf. Sci. 402 (2017) 12-20.
S. Das, V. Jayaraman, Prog. Mater. Sci. 66 (2014) 112-255.
S. Eriksson, M. Boutonnet, M. Boutonnet, Appl. Catal. A: Gen. 312 (2006) 95-101.
S. Guoa, E. Wang, Nano Today 6 (2011) 240-264.
S. Labich, E. Taglauer, H. Knözinger, Top. Catal. 14 (2001) 153-161.
S. Limpattayanate, M. Hunsom, Renew. Energy 63 (2014) 205-211.
S. Mukerjee, J. McBreen, J. Electrochem. Soc. 146 (1999) 600-606.
S. Shao, H. Wu, S. Wang, Q. Hong, R. Koehn, T. Wu, W.-F. Rao, J. Mater. Chem. C 3 (2015) 10819-10829.
S. Su, J. Agnew, Fuel 85 (2006) 1201-1210.
S. Thanasilp, M. Hunsom, Renew. Energy 36 (2011) 1795-1801.
S. Wang, W.J. Tseng, J. Nanopart. Res. 11 (2009) 947-953.
S. Zafeiratos, S. Piccinin, S. Piccinin, Catal. Sci. Technol. 2 (2012) 1787-1801.
S.H. Kim, K.T. Lee, S. Lee, J.H. Moon, B.-T. Lee, Jpn. J. Appl. Phys. 41 (2002) L 1002- L 1005.
S.H. Oh, P.J. Mitchell, R.M. Siewert, J. Catal. 132 (1991) 287-301.
S.-N. Hong, Y.-H. Kye, C.-J. Yu, U.G. Jong, G.-C. Ri, C.-S. Choe, K.-H. Kim, J.-M. Han, Phys. Chem. Chem. Phys. 18 (2016) 31566-31578.
Standard handbook of petroleum and natural gas engineering, Eds.: W. Lyons, G. Plisga, M. Lorenz, 3rd Ed., Elsevier, 2016.

T. Ioannides, X.E. Verykios, J. Catal. 161 (1996) 560-569.
T. Okanishi, T. Toshiaki, T. Takeguchi, R. Kikuchi, K. Eguchi, Appl. Catal. A: Gen. 298 (2006) 181-187.
T. Otto, J.M. Ramallo-Lopez, L.J. Ciovanetti, F.G. Requejo, S.I. Zones, E. Iglesia, J. Catal. 342 (2016) 125-137.
T. Schalow, M. Laurin, B. Brandt, S. Schauermann, S. Guimond, H. Kuhlenbeck, D.E. Starr, S.K. Shaikhutdinov, J. Libuda, H.J. Freund, Angew. Chem. Int. Ed. 44 (2005) 7601-7605.
T. Shimizu, A.D. Abid, G. Poskrebyshev, H. Wang, J. Nabity, J. Engel, J. Yu, D. Wickham, B.V. Devener, S.L. Anderson, S. Williams, Combust. Flame 157 (2010) 421-435.
T. Takeguchi, O. Takeoh, S. Aoyama, J. Ueda, R. Kikuchi, K. Eguchi, Appl. Catal. A: Gen. 252 (2003) 205-214.
T. Teranishi, M. Hosoe, J. Phys. Chem. B 103 (1999) 3818-3827.
T. Teranishi, M. Miyake, Chem. Mater. 10 (1998) 594-600.
T. Tran, T. Nguyen, Colloids and Surfaces B: Biointerfaces 88 (2011) 1-22.
T. Zhang, Y. Xin, Z. Ren, F. Qi, C.K. Law, Combust. Flame 160 (2013) 149-154.
T.E. Hoost, K. Otto, Appl. Catal. A: Gen. 92 (1992) 39-58.
T.R. Johns, J.R. Gaudet, E.J. Peterson, J.T. Miller, E.A. Stach, C.H. Kim, M.P. Balogh, A.K. Datye, ChemCatChem 5 (2013) 2636-2645.
T.R. Johns, R.S. Goeke, V. Ashbacher, P.C.Thune, J.W. Niemantsverdriet, B. Kiefer, C.H. Kim, M.P. Balogh, A.K. Datye, J. Catal. 328 (2015) 151-164.
T.V. Choudhary, S. Banerjee, V.R. Choudhary, Appl. Catal. A: Gen. 234 (2002) 1-23.
V. Krivetskiy, M. Rumyntseva, A. Gaskov, in: M.A. Carpenter, S. Mathur, A. Kolmakov (Eds.), Metal oxide nanomaterials for chemical sensors, Springer Science & Business Media, New York, 2013, pp. 76-80.
V. Meeyoo, D.L. Trimm, N.W. Cant, Appl. Catal. B: Environ. 16 (1998) L101-L104.
V.A. Gercher, D.F. Cox, Surf. Sci. 322 (1995) 177-184.
W. Qi, J. Ran, R. Wang, X. Du, J. Shi, J. Niu, P. Zhang, M. Ran, RSC Adv. 6 (2016) 109834-109845.
W.C. Conner, J.L. Falconer, Chem. Rev. 95 (1995) 759-788.
W.E. Morgan, J.R.V. Wazer, J. Phys. Chem. 77 (1973) 964-969.
W.R. Schwartz, D. Ciuparu, L.D. Pfefferle, J. Phys. Chem. C 116 (2012) 8587-8593.

W.R. Schwartz, L.D. Pfefferle, J. Phys. Chem. C 116 (2012) 8571-8578.
X. Li, W.X. Chen, J. Zhao, W. Xing, Z.D. Xu, Carbon 43 (2005) 2168-2174.
X. Wang, Y.-C. Xie, Catal. Lett. 75 (2001) 73-80.
X. Wang, Y.-C. Xie, New J. Chem. 25 (2001) 1621-1626.
X. Xu, X. Wang, Y. Li, J. Tian, W. Liu, Z. Gao, Z. Phys. Chem. 228 (2014) 27-48.
Y. Deng, T.G. Nevell, Catal. Today 47 (1999) 279-286.
Y. Kim, Y. Noh, E.J. Lim, S. Lee, S.M. Choi, W.B. Kim, J. Mater. Chem. A 2 (2014) 6979-6986.
Y. Liu, M. Chi, V. Mazumder, K.L. More, S. Soled, J.D. Henao, S. Sun, Chem. Mater. 23 (2011) 4199-4203.
Y. Ozawa, Y. Tochihara, A. Watanabe, M. Nagai, S. Omi, Appl. Catal. A: Gen. 259 (2004) 1-7.
Y. Shiraishi, M. Nakayama, E. Takagi, T. Tominaga, N. Toshima, Inorganica Chimica Acta 300-302 (2000) 964-969.
Y. Wang, J. Ren, K. Deng, L. Gui, Y. Tang, Chem. Mater. 12 (2000) 1622-1627.
Y. Wang, S. Xie, J. Liu, J. Park, C.Z. Huang, Y. Xia, Nano Lett. 13 (2013) 2276-2281.
Y. Wang, X. Wang, Solvent and simple ion-stabilized metal nanoclusters: chemical synthesis and application, Elsevier, Amsterdam, 2007.
Y. Xin, H. Wang, C.K. Law, Combust. Flame 161 (2014) 1048-1054.
Y. Yu, B. Fonfé, A. Jentys, G.L. Haller, J.A.R.v. Veen, O.Y. Gutiérrez, J.A. Lercher, J. Catal. 292 (2012) 1-12.
Y.C. Weng, C.T. Hsieh, Electrochim. Acta. 56 (2011) 1932-1940.
Y.-H. Chin, D.E. Resasco, Catalysis 14 (1999) 1-39.
Y.-H. Chin, M. Garcia-Dieguez, E. Iglesia, J. Phys. Chem. C 120 (2016) 1446-1460.
Y.-N. Wang, R.G. Herman, K. Klier, Surf. Sci. 279 (1992) 33-48.
Z. Duan, G. Wang, J. Phys.: Condens. Matter 23 (2011) 475301.
Z. Li, G.B. Hoflund, J. Nat. Gas Chem. 12 (2003) 153-160.
Z. Peng, H. Yang, Nano Today 4 (2009) 143-164.
Z. Wu, J. Deng, Y. Liu, S. Xie, Y. Jiang, X. Zhao, J. Yang, A. Arandiyan, G. Guo, H. Dai, J. Catal. 332 (2015) 13-24.
Z. Zhao, B. Wang, J. Ma, W. Zhan, L. Wang, Y. Guo, Y. Guo, G. Lu, Chinese J. Catal. 38 (2017) 1322-1329.